Characterising the Interaction between Dynamics Wake Mixing Techniques and Floating Wind Turbines

van den Berg, D.G.

DOI
10.4233/uuid:94a2e920-0ae2-49e7-bbe5-c7736154e1ed

Publication date
2025

Document Version
Final published version

Citation (APA)
van den Berg, D. G. (2025). *Characterising the Interaction between Dynamics Wake Mixing Techniques and Floating Wind Turbines*. [Dissertation (TU Delft), Delft University of Technology]. https://doi.org/10.4233/uuid:94a2e920-0ae2-49e7-bbe5-c7736154e1ed

Characterising the Interaction between Dynamic Wake Mixing Techniques and Floating Wind Turbines

Dissertation

for the purpose of obtaining the degree of doctor
at Delft University of Technology
by the authority of the Rector Magnificus prof. dr. ir. T.H.J.J. van der Hagen,
Chair of the Board for Doctorates
to be defended publicly on
Friday 4, April 2025 at 10:00 o'clock.

by

Daniel Graham VAN DEN BERG

Master of Science in Systems and Control,
Delft University of Technology, The Netherlands,
born in Zwijndrecht, The Netherlands.

This dissertation has been approved by the promotors.

Composition of the doctoral committee:

Rector Magnificus,	Chairperson
Prof. dr. ir. J.W. van Wingerden,	Technische Universiteit Delft, promotor
Dr. ir. D.A.M. De Tavernier,	Technische Universiteit Delft, copromotor

Independent Members:

Prof. dr. ir. J. Hellendoorn,	Technische Universiteit Delft
Prof. dr. D.A. von Terzi,	Technische Universiteit Delft
Dr. ir. P.R. Wellens,	Technische Universiteit Delft
Prof. dr. M. Belloli,	Politecnico di Milano, Italy
Prof. dr. P.W. Cheng,	Universität Stuttgart, Germany

Keywords: Floating Wind Turbine, Wind Farm Flow control, The Helix Wake Mixing Method, Wind Tunnel Experiments, Particle Image Velocimetry

Printed by: Gildeprint

Style: TU Delft House Style, with modifications by Moritz Beller
`https://github.com/Inventitech/phd-thesis-template`

Funding: This work in this thesis is part of the FLOATECH project. The research presented in this thesis has received funding from the European Union's Horizon 2020 research and innovation programme under grant agreement No. 101007142.

The author set this thesis in LaTeX using the Libertinus and Inconsolata fonts.

An electronic version of this dissertation is available at
`https://repository.tudelft.nl/`.

“There is nothing like looking, if you want to find something. You certainly usually find something, if you look, but it is not always quite the something you were after.”

Thorin Oakenshield in ‘The Hobbit’ by J.R.R. Tolkien

Contents

Summary

Wind energy has the potential to accelerate the transition from a carbon-based to a carbon-free energy supply system. This transition is essential in the ongoing global effort to combat the growing impacts of climate change. Due to the availability, as well as the increasingly competitive cost, the wind energy industry has enjoyed rapid growth in terms of installed wind capacity. Where the first onshore wind farm was composed of nearly 5000 turbines in 1980, with a capacity of 576 MW the current largest offshore wind farm in development has a design capacity of 1400 MW with only 100 turbines. Almost all offshore wind farms currently in operation, under construction, or in the planning phase are designed with bottom-fixed turbines and are in relatively shallow water.

The total available wind energy capacity increases significantly when deeper waters can also be accessed by wind turbines and wind farms. For these areas, floating wind turbine technology will play an essential role. When they are deployed in similarly sized wind farms as bottom-fixed wind farms they will also encounter challenges currently faced by these bottom-fixed farms. One of these challenges is the wake interaction between turbines, a cause of significant efficiency losses for a wind farm. The field of wind farm flow control aims to develop a control solution that can alleviate the negative effects of the wake interaction between turbines.

Wind farm flow control solutions can be divided into static solutions like induction control and wake steering or dynamic solutions like dynamic induction control ('The Pulse Method') or dynamic individual pitch control ('The Helix Method'). All methods rely on altering the thrust of the turbine in some way to impact the wake behind the turbine. Dynamic wind farm flow control solutions are often referred to as wake mixing methods. These methods use the blade pitch degree-of-freedom to alter the turbine's thrust in a time-varying manner, resulting in a time-varying wind field behind the turbine. When excited at the right frequency the wake will break up and start mixing with the outside flow reenergizing the wake.

When wind farm flow controllers and, in general, wind turbine controllers are applied to floating turbines the performance of the controller can change significantly. This is mainly because when applied on a floating wind turbine these control solutions will couple with the hydrodynamics of the floating turbine. The magnitude and type of motion are heavily dependent on the floating turbine dynamics, which is directly correlated to the design of the floating turbine. The goal of this thesis is to investigate this interaction and can be formulated as: *Can the dynamics of a floating turbine be used to enhance dynamic wake mixing techniques and if so can a floating turbine be optimised such that it promotes wake mixing?*

To answer this research question it is important first to understand and quantify the interaction between the two wake mixing methods and floating turbines. In this thesis, a simulation suite (QBlade) is used to model both the hydrodynamics and aerodynamics as well as the wake dynamics of a floating turbine. By carefully designing frequency identification experiments frequency response functions could be constructed which provide insight into the types of motion that get excited. Performing the same experiments for different floaters allows us to pair a wake mixing technique to a floating turbine foundation that exhibits significant motions. Using the same simulation setup wake dynamics can be analysed. The wake is modelled using a free-vortex wake method to represent the wake dynamics. Although this wake modelling method loses accuracy as the wake breakdown process has started it provided enough insight to quantify the effect of floating turbine motion on the wake mixing method.

In the case of the Pulse method, the changing magnitude of the thrust force creates a fore-aft motion at the nacelle of the turbine. Especially for single spar-type floaters the magnitude of this motion is of such degree that the time-varying thrust of dynamic induction control is reduced, diminishing the effectiveness of the wake mixing technique. The coupling between the control method and fore-aft motion is such that when motion is excited it will invariably reduce the effectiveness of the wake mixing method. The interaction between the Helix method and a floating turbine can be characterised by its yaw motion. Especially floating turbines mounted on a semi-submersible type foundation are subject to yaw motion as they typically have an eigenfrequency in yaw motion at a similar frequency with which the Helix method is applied. Simulation results show that depending on the phase offset between yaw motion and the Helix method this interaction can either lead to an increase or decrease in wake mixing performance.

Because a small change in dynamics yielded significant difference in wake recovery within the simulation environment, it was decided to carry out wind tunnel experiments. This was done for two reasons, one, to verify the results found in the simulation and, two, to gain a deeper understanding of the coupling between the Helix method and the dynamic yaw motion. Using tomographic particle image velocimetry the three-dimensional wake dynamics are measured, allowing analysis of the dynamics of the wake and interaction between the Helix method and dynamic yaw motion. When the turbine is yawing in motion it was observed that the interaction between the hub and tip vortex is accelerated. The wake mixing process is therefore accelerated or decelerated depending on whether the yawing motion is, respectively, in-phase or out-of-phase with the yaw motion, thereby confirming the preliminary results found in the simulation environment.

This thesis, therefore, contributes to the development of floating wind turbines. In its rapid development, floating wind has faced several challenges that need to be overcome for this technology to become more readily available. Adapting wind turbine controllers to be suited for floating turbines is one such challenge. However, as the work in this thesis shows, the interaction between floating turbines and control solutions can also be used to further enhance controller performance by coupling it smartly. This notion, where control solution and system dynamics are designed together, often referred to as ‘control co-design’, is a solution that can be used to advance floating wind turbine technology.

Samenvatting

Windenergie heeft de potentie om de transitie van fossiele energiebronnen naar hernieuwbare energiebronnen te versnellen. Deze transitie is essentieel om het steeds groter wordende effect van klimaatverandering te keren. In termen van opgesteld vermogen is de windenergieindustrie sterk gegroeid mede dankzij het feit dat windenergie breed beschikbaar is en steeds kostenefficiënter wordt. Waar, in 1980, een van de eerste windparken uit bijna 5000 windturbines bestond, goed voor een vermogen van 576 MW, bestaat het huidige grootste windpark dat in ontwikkeling is uit 'maar' 100 turbines goed voor een vermogen van 1400 MW. Bijna alle windparken die in zee geplaats zijn, of in aanbouw en of planning zijn, zijn ontworpen met windturbines die in de zeebodem zijn geplaatst en staan in relatief ondiep water.

Het totaal beschikbare opgestelde vermogen van windenergie neemt drastisch toe als windturbines en windparken ook in diepere wateren geplaatst kunnen worden. Drijvende windturbines zullen een essentiële rol spelen in dit soort gebieden. Wanneer drijvende windturbines in windparken van soortgelijke grootte als de huidige windparken worden geplaatst zullen dezelfde uitdagingen opgelost moeten worden voor deze drijvende windparken. Een van deze uitdagingen is de zoginteractie tussen verschillende windturbines in een windpark, een interactie die voor een significantie reductie van de efficiëntie zorgt. Het onderzoeksveld van windparkzogregelingen probeert door middel van het ontwerpen van verschillende regeltechnieken oplossingen hiervoor te vinden.

Windparkzogregelingen kunnen onderverdeeld worden in statische oplossingen zoals statische inductieregeling en zogsturing en dynamische oplossingen zoals periodiek dynamische inductieregeling (de 'Puls' methode) of periodiek dynamische individuele bladhoekregeling (de 'Helix' methode). Alle regeltechnieken gebruiken de stuwkracht van de turbine om op een bepaalde manier het zog achter de turbine te beïnvloeden. Dynamische zogregeltechnieken worden ook vaak zogmengmethodes genoemd. Deze methodes gebruiken de bladhoek vrijheidsgraad van de turbine om de stuwkracht van de turbine tijds variërend te laten veranderen, wat er toe lijdt dat het snelheidsprofiel achter de turbine ook tijdsvariërend wordt. Als dit op de juiste frequentie wordt gedaan, dan zal het zog zich gaan opbreken en mengen met de vrije luchtstroom waardoor de energie erin toeneemt.

Wanneer zogregeltechnieken, en in het algemeen turbineregelaars, worden toegepast op drijvende windturbines dan kan de effectiviteit van de regelaar significant veranderen. Als regelaars worden toegepast op een drijvende turbine zullen ze koppelen met de hydrodynamica van de drijven turbine. De type en grootte van de gekoppelde beweging zijn sterk gecorreleerd aan het ontwerp van de drijvende turbine. Het doel van dit proefschrift is om deze interactie te onderzoeken en de hoofdonderzoeksvraag in dit proefschrift wordt geformuleerd als: *Kan de dynamica van een drijvende wind turbine gebruikt worden om dynamische zogregeltechnieken te versterken en als dit mogelijk is kan een drijvende turbine zo geoptimaliseerd worden dat zogmenging wordt versterkt.*

Om deze onderzoeksvraag te beantwoorden is het belangrijk om eerst de interactie tussen de twee dynamische zogregeltechnieken en drijvende turbines te begrijpen en kwantificeren. In dit proefschrift wordt er gebruikt gemaakt van een simulatie omgeving waarin zowel de hydrodynamica, aerodynamica en zogdynamica worden gemodelleerd. Door het zorgvuldig uitvoeren van frequentie-identificatie-experimenten kunnen frequentieresponsfuncties worden geconstrueerd die inzicht verschaffen in de soorten bewegingen die worden geactiveerd. Door dezelfde experimenten voor verschillende drijvende platformen uit te voeren, kunnen we identificeren bij welke combinatie van zogregeltechniek en drijvend platform we significante beweging kunnen verwachten. Binnen dezelfde simulatieomgeving is het ook mogelijk om de zogdynamica te analyseren. Het zog wordt gemodelleerd met een vrije-wervel-methode. Ondanks het feit dat deze methode minder representatief wordt zodra het zog begint op te breken is het accuraat genoeg om inzicht te geven over de impact van de drijvende turbine bewegingen op de dynamische zogregeltechnieken.

Bij de Puls methode zorgt de tijdsvariërende stuwkracht voor een voor-achter beweging van de windturbine gondel. Specifiek voor de drijvende turbine van het enkele spartype ontwerp is de grootte van de voor-achter beweging dusdanig dat de grootte van tijdsvariërende stuwkracht afneemt, wat resulteert in een afname van de effectiviteit van de Puls methode. De koppeling tussen de regeltechniek en de voor-achterwaartse beweging is zodanig dat wanneer beweging wordt opgewekt, dit onveranderlijk de effectiviteit van de zogmengmethode zal verminderen. De interactie tussen de Helix methode en een drijvende turbine wordt gekarakteriseerd door de gierbeweging van de drijvende turbine. Vooral drijvende turbines die op een semi-onderdompelbaar type fundering zijn gemonteerd, zijn onderhevig aan gierbeweging, omdat ze doorgaans een eigenfrequentie in gierbeweging hebben op een vergelijkbare frequentie als waarmee de Helix methode wordt toegepast. Simulatieresultaten tonen aan dat afhankelijk van de faseverschuiving tussen de gierbeweging en de Helix methode deze interactie kan leiden tot een toename of afname van de zogmenging, afhankelijk van de faseverschuiving tussen de Helix-methode en de gierbeweging.

Omdat een kleine verandering in dynamica aanzienlijk verschillende resultaten opleverde in de simulatieomgeving, werd besloten om windtunnelexperimenten uit te voeren. Dit werd gedaan om twee redenen, ten eerste om de resultaten van de simulatie te verifiëren en ten tweede om een dieper begrip te krijgen van de koppeling tussen de Helix methode en de dynamische gierbeweging. Met behulp van tomografische deeltjesbeeldsnelheidsmetingen wordt de 3-dimensionale zogdynamica gemeten, waardoor analyse van de dynamiek in het zog en de interactie tussen de Helix-methode en de dynamische gierbeweging mogelijk is. Wanneer de turbine in fase giert met de Helix methode, werd waargenomen dat de interactie tussen de gondelwerveling en bladtipwerveling wordt versneld, waardoor de zogmenging wordt versneld. Deze wordt vertraagd wanneer de gierbeweging uit fase is met de Helix methode, wat overeenkomt met de resultaten die in de simulatieomgeving zijn gevonden.

Dit proefschrift draagt bij aan de ontwikkeling van drijvende windturbines. In zijn snelle ontwikkeling heeft drijvende wind te maken gehad met verschillende uitdagingen die overwonnen moeten worden om deze technologie gemakkelijker beschikbaar te maken. Het aanpassen van windturbineregelaars om geschikt te zijn voor drijvende turbines is zo een uitdaging. Zoals het werk in dit proefschrift echter laat zien, kan de interactie tussen drijvende turbines en regeloplossingen ook worden gebruikt om de presetatie verder te verbeteren door deze slim te koppelen. Dit idee, waarbij regeloplossing en systeemdynamiek samen worden ontworpen, vaak aangeduid als ‘co-design van regelingen’, is een oplossing die kan worden gebruikt om drijvende windturbinetechnologie te verbeteren.

Acknowledgments

The year is 2019 and on numerous occasions, I have proclaimed to *'never ever want to be involved with academia ever again after my thesis'*. Although this sounds quite definitive I have always followed that saying with a disclaimer. If a PhD position were to open that had an almost tangible connection to a real-world application I would consider it. When 2020 rolled along and I graduated during the height of the first COVID lockdowns it was a challenge to find work. After a search of nearly six months, I stumbled upon a PhD position on floating wind farm flow control. Now, four years later, I'm writing these acknowledgements while looking back at four remarkable, educational and most of all enjoyable years.

This in large part is thanks to Jan-Willem. I still remember attending your inauguration speech back in 2019 where you talked about the Helix method. The enthusiasm and energy I saw there prompted me to react to this PhD vacancy. To this day I'm astonished at how you manage to guide so many PhDs with such enthusiasm and at how you can latch on to results quickly and based on those propose new ideas or directions to explore it. Keep doing what you are doing and we will see each other on the Coolsingel Sunday 13th of April, 2025.

Special thanks also have to go to Delphine. Your feedback has proven invaluable and I'm extremely grateful for all the insights and for forcing me to be more precise in my work. The growth in terms of quality of my work over these 4 years can mainly be attributed to your feedback. I will also miss our weekly meetings, especially those of the last few months where the topics discussed have been everything except work.

These four years have been so enjoyable also due to the wind energy group, may it never stop growing. Daan, in your acknowledgements you wrote about the bleak nature of doing wind tunnel tests at the OJF. I am (extremely) grateful for all the help you provided during the not one but in the end, two wind tunnel campaigns and subsequent post-processing and I'm also grateful for making it a much more enjoyable experience (I believe that one day you will get a LEGO Rivendell and/or Barad-Dur set). Maarten, at the start of my PhD I was amazed that someone would even conceive the idea of running from work to home. I guess your enthusiasm is infectious because not only did I also start running home (albeit for only a brief period), I even ran the Rotterdam Marathon, something which I would have never guessed before starting my PhD. I hope to meet you in many more races. Marcus, I hope you enjoyed squatting at **my** office desk before the renovation started. Thank you very much for the many discussions we had. Furthermore, I couldn't have wished for a better dance partner in Glasgow...

Atin, we seemed to have a special connection when it came to taking the train to Delft because without any coordination more often than not we ended up on the same train. I enjoyed the many discussions we had during our travels. Livia, when you start missing the Netherlands you can always come back and we can start a QBlade consultancy company. Keep promoting our amazing guide (and this amazing piece of software) to all your new

Vestas colleagues. Furthermore, many thanks to everyone else in the wind energy group: Emanuel, Jonas (and your van), Claudia, Rogier, Mees, Amr, Bert, Marion, Guido, David, Matteo, Unai, Jesse, Tim for making it such a great experience. Using the term colleagues to refer to everyone wouldn't do justice looking back to all the things we have done together (Celebrating a Moroccan wedding until 6 in the morning for example...). Finally, many thanks to everyone else at DCSC for the many fruitful discussions during lunch and many a coffee break.

Thanks also have to go to all the people in the FLOATECH project. Working together on this quite expansive project has been a very educational and fun experience. Special mention has to go to Joe, David and Robert, working together using QBlade and visiting you in Berlin (with Livia!) is one of the highlights of this project. Wherever I go I will try to promote QBlade ;). Guido, I'm happy that the impression the TU Delft team left on you was so positive you decided to join our group.

Further mention has to go to Bernard, Koen, Yorrick, Damian, Thomas Oscar, Jonas, Gert, Chris, Len and everyone else from DUT15 and DUT16. The years at Formula Student are for sure the highlight of my 12 years at the TU Delft. I hope that we can keep getting together at Formula Student Germany to reminiscence about the days when everything was #better.

Finally, this PhD wouldn't have been possible without the unwavering support from my parents which goes way further back than the last four years. Furthermore, the support from my brother Erik, Floris, Michelle, Kees and Elma has been a great help in during both the ups and downs. The last and most important thanks go to Sara. Looking back to 4 years ago the things that have changed during that period are quite crazy. From getting married to moving from Delft to The Hague, to buying a house in Beautiful Barendrecht (#BTown), to getting a three-legged cat to adventuring through Canada etc., thank you for being by my side throughout this journey that has seen many ups and downs. I'm extremely grateful to have been able to share these experiences with you and hope to make many many more over the years to come.

Daniel van den Berg
Delft, September 2024

1

Introduction

1.1 The Race to Net Zero

On December 12th 2015 196 parties signed the Paris Agreement spelling out a global effort to combat the ever-increasing impact of climate change [1]. The overarching goal spelt out by the Paris Agreement is to hold

> "the increase in the global average temperature to well below 2.0°C above pre-industrial levels" and pursue efforts "to limit the temperature increase to 1.5°C above pre-industrial levels."

If temperatures are maintained below these target values, the impact on Earth will not be irreversible [2]. In 2023, the average global surface temperature was measured to be 1.17°C above the pre-industrial average with the last decade (2010-2019) being, on average, 0.81°C higher than the pre-industrial average [3]. As a consequence, the last 10 years are the warmest on record. Furthermore, the temperature anomaly is still trending upward as shown in Figure 1.1, which shows the average surface temperature of the Earth since measurements began in 1880 and have been tracked ever since [3]. However, climate change is not only responsible for an increase in temperature but also indirectly for an increase in severe weather events like droughts, flooding etc. These extreme weather events have a direct impact on food and water security, human life in terms of health and economics and damage to nature [4]. It is therefore of vital importance that the upward trend in global temperature is halted.

The stark increase in global temperature since 1950 can almost fully be attributed to human causes. Rapid industrialisation has led to a substantial increase in the emission of greenhouse gases of which CO_2 and methane (CH_4) have the most impact on climate change. Figure 1.1 also shows the global CO_2 and methane levels since their respective measurements began [3]. As with the global temperature, there is still a steady increase in the emission of the two most prevalent greenhouse gases. Preventing the global temperature from increasing above 1.5°C requires a drastic reduction in the emission of greenhouse gases. It is therefore also specified within the Paris Agreement that

> ...To limit global warming to 1.5°C, greenhouse gas emissions must peak before 2025 at the latest and decline 43% by 2030.

1

Both the impact of and remedy to climate change are well understood and it is generally agreed upon that drastic change is required. Over 50% of all greenhouse gases are emitted by industry and energy systems [5] of which 34% is emitted by burning fossil fuels for heat and electricity. Fully decarbonising the energy supply will therefore go a long way toward achieving the goal of 'net-zero' emissions. Earth has abundant low-carbon renewable energy sources to replace its fossil-based energy supply with sources such as solar, wind and hydropower. As of 2024, approximately 14% of the energy mix is from renewable sources [6]. Of this 14%, hydropower is responsible for 47% of the renewable energy production worldwide, followed by wind energy at 26%, solar energy at 18% and the remaining 9% other alternative renewable sources.

Given its abundant availability, wind energy alone is capable of providing enough energy to meet the world's demand several times over [7]. This is one of the reasons wind energy plays an essential role in the transition to a net-zero energy supply. In 2023, wind energy was responsible for 17% of the total energy production within Europe and its share within the renewable net generation was 37% [8]. The ambition of the European Union is to further expand this share by growing the current installed capacity of 204 GW to more than 500 GW in 2030 [9] requiring a rapid growth in installed wind energy capacity.

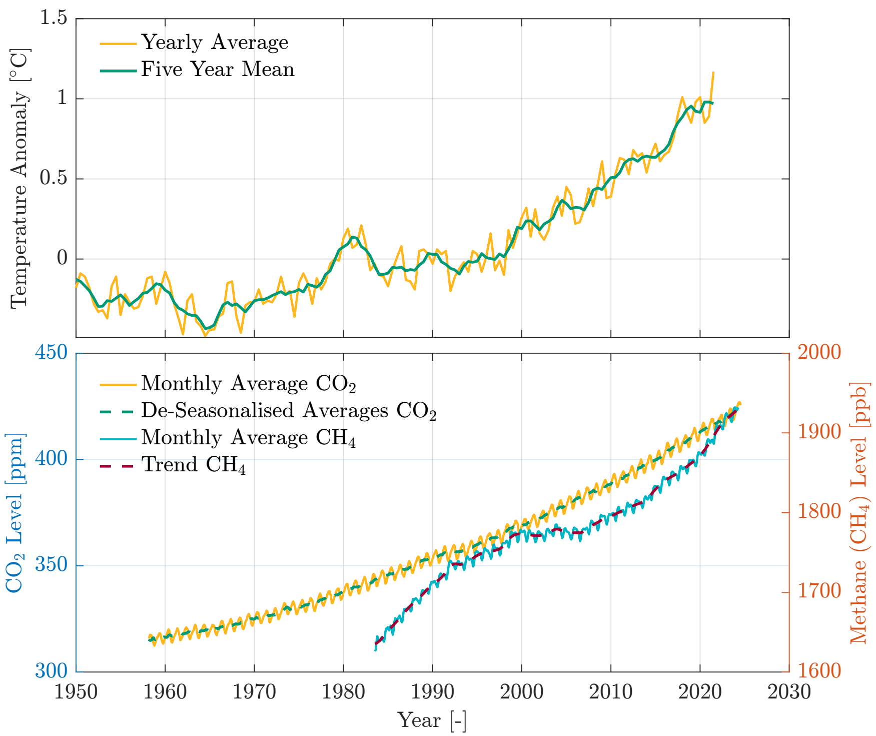

Figure 1.1: Top Figure: Global temperature anomaly since measurements started in 1880. Bottom Figure: Global CO_2 and methane (CH_4) levels since measurements started in 1953 and 1983, respectively. Data provided by NASA's Goddard Institute for Space Studies (GISS) [3].

1.2 The Growth of Wind Energy

Human beings have been relying on wind-assisted devices for over several millennia, with the first windmills dating back to 200 BC. These were used for pumping water and milling grain. The first wind turbines used to generate electricity were built between the years 1880 and 1890 [10, 11]. However, it wasn't until the oil crisis in the 1970s that there was renewed interest in wind energy. It was also the first time wind turbines were deployed in larger wind farms such as the Altamont Pass wind farm in the United States. As the oil crisis subsided so too did the interest in wind energy only to enjoy renewed interest in the past two decades as a viable renewable low-carbon energy source. The accelerated growth in wind energy can be seen by looking at, for example, the installed wind capacity in Europe. Figure 1.2 shows the growth of installed wind capacity within the European continent from 2000 to 2023 and its projected growth till 2030 [12]. In a similar period, the percentage of renewable energy production grew from 10% in 2005 to 23% in 2022 in the EU [13]. The

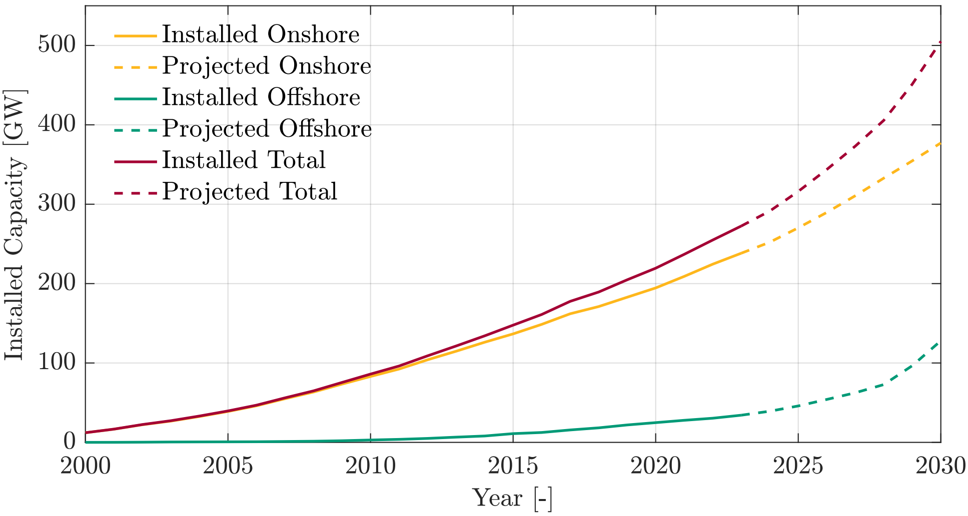

Figure 1.2: Total installed wind energy capacity within the European Union. The dashed lines indicate the projected growth until 2030. Data from [12].

rapid expansion of the installed wind energy capacity also comes with further challenges for the entire energy infrastructure. For example, the European energy network is designed around centralised power-producing nodes where the majority of power is produced and then distributed over the continent. However, the onset of a more distributed network where wind and solar farms act as small energy-producing nodes is causing grid congestion slowing down the deployment of wind and solar farms [14]. Within the European Union the plans to expand the electricity grid lag that of the renewable expansion targets [14].

A further challenge is the variability of energy production. Current fossil-fuel driven powerplants are capable of quickly responding to variations in the demand on the energy network. For renewable energy sources like wind and solar, this cannot be guaranteed given their dependency on weather conditions. To remedy this, some form of energy backup is required to ensure the availability of energy even when generation cannot meet demand. In recognition of this challenge, the year 2023 saw the launch of the Energy Storage Coalition in the European Union. Their primary goal is accelerating the deployment of sustainable and clean energy storage solutions in support of renewable energy sources [15].

Finally, aside from the technical challenges there is also a large socioeconomic question that needs to be answered. The growing size of wind turbines and wind farms has been met with resistance from local communities and industries. To expand the total wind capacity wind farm planning needs to consider stakeholders like the existing oil and gas, fishing and shipping industries as well as, arguably the most important, the natural environment itself [16–18]. The desire to decarbonise our energy supply whilst at the same time being restricted in the useable area is a key motivator for the work presented in this thesis. Expanding the wind energy capacity can be achieved by increasing turbine sizes and wind farm sizes but also by increasing the efficiency of current and future (floating) wind farms.

1.3 Wind Turbines and Wind Farms

Current generations of wind turbines are capable of operating close to their theoretical Betz limit [19, 20]. The aerodynamic power a turbine can extract from the flow is calculated as

$$P = \frac{1}{2} C_p \rho A U_\infty^3, \tag{1.1}$$

in which C_p is the dimensionless power coefficient, ρ the air density in kg/m^2, A the rotor swept area in m^2 and U_∞ the free stream wind speed in m/s. Since C_p is close to its theoretical maximum, increasing the individual power output of turbines can therefore either be achieved by increasing the rotor diameter, or by placing wind turbines in areas of higher wind speed. Especially the latter can have profound impacts on the power output given the cubic scaling of aerodynamic power with wind speed. This is one of the reasons that the share of offshore wind energy is growing more rapidly than that of onshore wind in the projections for 2030. At offshore locations, wind speeds are generally higher and more consistent than comparable onshore locations [21]. Furthermore, generally speaking, offshore locations provide more available area than onshore locations allowing for larger wind farms to be deployed.

Individual wind turbines are capable of running near their theoretical maximum efficiency, but wind farms still exhibit efficiency losses due to interactions between individual turbines. When wind turbines extract energy from the flow they leave behind an area of turbulent, low-velocity airflow behind them, an area often referred to as the wake of a wind turbine. When these wakes interact with other turbines in the wind farm the affected wind turbine will have a reduced power output, resulting in an efficiency loss on the wind farm. It is reported that the so-called *wake effect* in extreme cases can lead to a reduction of power production of up to 40% compared to the same wind farm without the wake effect but typically sits around 5-10% dependent on wind direction and wind farm lay-out [23–25].

This interaction between turbines is perfectly captured in Figure 1.3, which shows the Horns Rev wind farm in Denmark. When this photo was taken the atmospheric conditions were such that the wakes are clearly visible. Aside from optimising the layout of a wind farm to reduce the wake impact, typical wind turbine control aims at maximising power production per turbine and currently disregards the wake effect. With products like 'Wake-Adapt' from Siemens Gamesa Renewable Energy and 'PowerUp' from GE Renewable

Figure 1.3: Visualization of wind turbine wakes for the Horns Rev wind farm. Atmospheric conditions were such that water vapour condensed due to the pressure change behind the wind turbines resulting in visible wakes. Image courtesy of Vattenfall, distributed under the CC BY-ND 2.0 license [22].

Energy wake steering is already a commercially provided solution for reducing the turbine-to-turbine interaction [26, 27]. Although solutions are commercially available, mitigating the wake interaction between turbines remains an area of extensive research referred to as wind farm flow control [28, 29].

1.4 Wind Farm Flow Control

Currently, three different forms of wind farm flow control are actively being pursued. The most researched wake mitigation method is wake steering whereby the yaw degree of freedom of a turbine is used to divert the wake from any downstream turbine [23, 24, 30–34]. Using fast computation models like FLORIS, [35], or FLORIDyn [36], wake steering controllers can be developed that alter the yaw angles of turbines within a wind farm given certain wind conditions. Research indicates that wake steering controllers can uplift a wind farm's power production by 1 to 2% [37], percentages that can easily equate to the yearly energy demand of several thousands of households for larger wind farms. The second method that has gained interest is static induction control [38–41] whereby the thrust of the upstream turbine is lowered at the benefit of the downstream turbine. However, wind tunnel experiments and full-scale experiments have shown that the gain of induction

1

control is negligible [40, 42].

The third and final category of wind farm flow control methods can be classified as wake mixing methods. Wake mixing control can be categorised as control methods that use existing, or novel, actuators on a wind turbine to excite aerodynamic instabilities within the wake to promote wake mixing. Wake mixing differs from wake steering and static induction control, in the fact that it aims at dissipating the wake before it reaches the downstream turbine rather than deflecting (for wake steering control) or weakening (for static induction control) it. When the wake is destabilised, it will entrain energy from the outside flow into itself resulting in higher wind speeds within the wake.

Two notable wake mixing methods are collective pitch control (often referred to as 'The Pulse Method') [43] and dynamic individual pitch control(often referred to as 'The Helix Method') [44]. The working principle behind both the Pulse method is based on the work in [45]. In [45], an optimal control solution is sought to maximise wind farm power. The optimisation variable was chosen to be the coefficient of thrust of the turbines. The resulting control input was of a periodic time-varying nature and led to an increase of 6% energy extraction for the analysed wind farm. Both collective and dynamic individual pitch control mimic this behaviour by actively pitching the blades thereby varying the induction factor of the turbine. The resulting wake structures when these techniques are applied are illustrated in Figure 1.4.

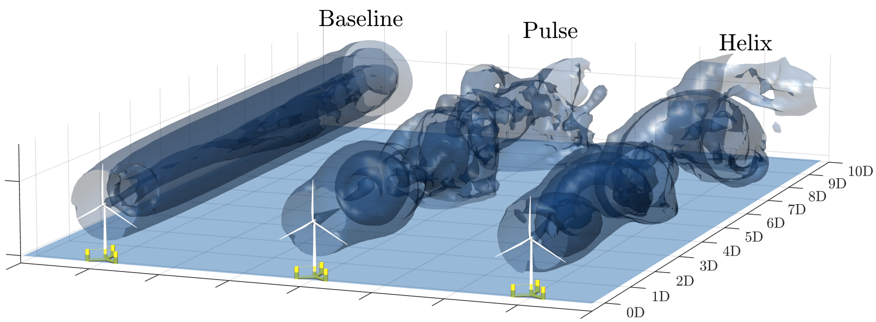

Figure 1.4: Wakes of three turbines each with different control methods. The turbine on the left is set to what is called 'greedy' control as it aims to extract the most amount of energy from the wake. This creates a long uniform wake of low wind speed, represented by the darker colour. The middle turbine and the rightmost turbine use the Pulse and Helix, respectively.

In Figure 1.4, the leftmost wake is the result of using greedy control, a control method whereby energy production is maximised per turbine. The middle and rightmost wakes are the result of using the Pulse and Helix methods respectively. With the Pulse method, collective blade pitch is used to dynamically alter the magnitude of the induction factor, resulting in a time-varying wind speed in the wake. The variation between high and low induction leads to the pulsating effect seen in the wake. For the Helix method, the magnitude of the induction factor remains relatively constant. The Helix method, however, displaces the thrust vector and moves it over the rotor plane in a circular fashion. This creates the characteristic helical shape that can be seen in the wake when the Helix method is enabled. Chapter 2 will provide a deeper analysis of the Pulse method whereas

Chapters 3, 4 and 5 focus on the Helix method and provide a detailed background on this method.

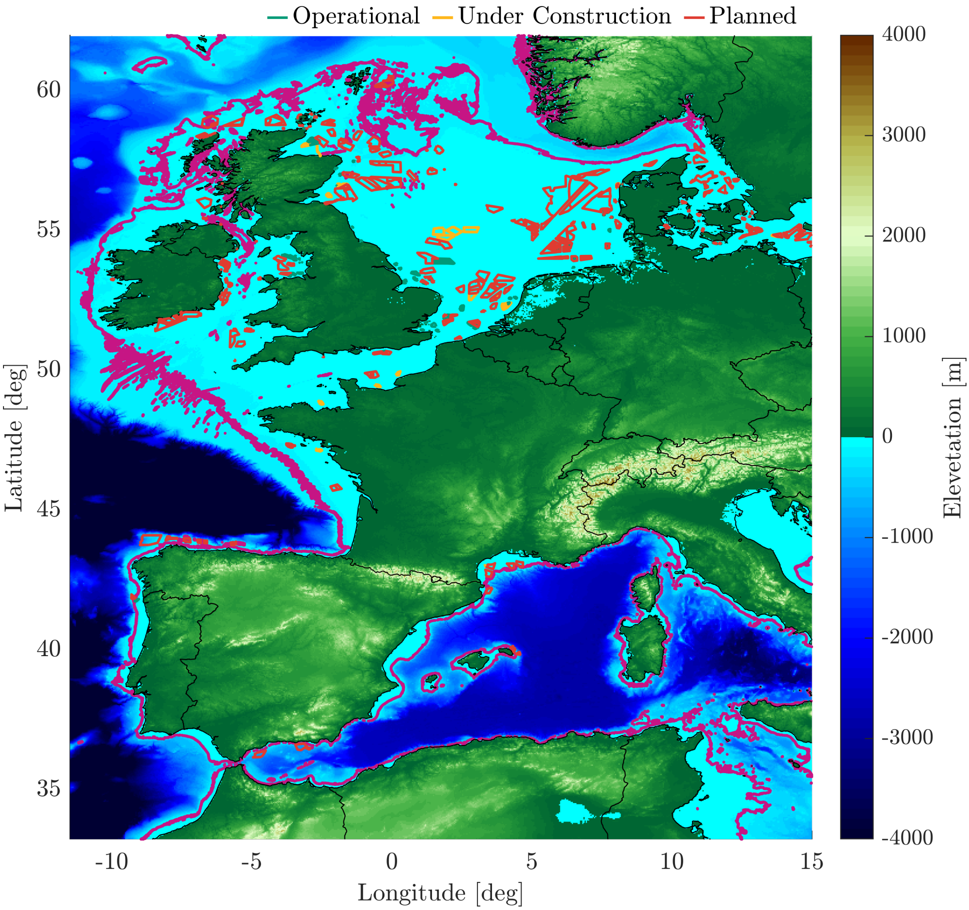

Figure 1.5: Overview of operational, under construction and planned offshore wind farms in western Europe projected onto a height map of the same area. The purple lines indicate a border where the water depth is between 120 and 125 metres. In general, going further into the sea equates to an increasing water depth. Height data from [46] and wind farm data from [47]

1.5 From Bottom-Fixed to Floating Wind Turbines

Figure 1.5 shows an overview of all offshore wind farms that are either operational, under construction or planned for the western part of Europe. The data is overlaid on a height map of the same area with the purple dotted line indicating the border where the water depth starts to exceed 120 to 125 metres. Almost all of the current wind farms that fall under one of the three aforementioned categories of operation are, or are destined to be, in locations where the water depth is less than 125 metres. Especially the North Sea, as well as parts of the Baltic Sea, are prime locations for large wind farms given the shallow

1

water and favourable wind conditions. The primary reason for these expansive plans is the economic feasibility of offshore wind in these areas; increasing the depth at which a wind farm is placed equates to increasing costs when it comes to the installation of an offshore wind farm. For bottom-fixed wind turbines, the often quoted maximum depth at which it remains economically viable is between 40 to 60 metres [48, 49].

Here lies an opportunity for the floating wind turbine. For Europe, the United States and the Sea of Japan area, over 80% of all the accessible wind energy resources can be found at depths of 60 metres or deeper [48, 50]. If Europe is to reach its net-zero goals it will need to access these deeper regions using floating wind turbines placed in large floating farms. Furthermore, for certain countries, especially around the Mediterranean Sea, there is (too) little access to shallow waters for their respective wind energy targets. These countries will need to rely on floating wind farms for their transition towards a carbon-free energy supply. As such, the floating wind market is rapidly growing with Europe aiming to have 4 GW of floating wind installed by 2030, up from the 0.18 GW currently installed [51]. However, unlike bottom-fixed turbines, floating wind turbines are still an emerging technology facing technological as well as logistical challenges. For example, currently over 50 different foundations for floating wind turbine designs are being developed [52] showing that there is not yet convergence on the 'ideal' floating wind turbine design.

Almost all foundation designs can be categorised as a variant of one of 5 archetypes depicted in Figure 1.6. Each variant has its advantages and disadvantages in terms of water depth, stability properties and complexity of design. For example, a spar-type floater is a relatively simple design suited for deeper waters due to its large draft. Most of the ballast is located deep down resulting in a centre of gravity lower than its centre of buoyancy providing it stability. The large draft requirement does provide challenges during assembly, transportation and installation as it requires a port suitable to such a structure. The suspended counterweight design aims to overcome these downsides by splitting the structure into two independent parts connected by chains. The semi-submersible and barge foundation types use a large foundation to create stability through buoyancy. Its shallower draft compared to the spar type makes construction and assembly easier. Finally, the tension leg platform creates stability by having taut mooring lines reducing the material needed for the platform itself. However, without the taut mooring lines, the platform is inherently unstable making installation and transportation difficult [50, 53].

1.5.1 Control of Floating Wind Turbines

Floating turbines can, in general, move in all 6 degrees of freedom. These six degrees of freedom consist of three translational ones: surge, sway and heave, and three rotational ones: roll, platform pitch (or tilt) and yaw. The coupling between turbine controls and these extra six degrees of freedom provides new engineering challenges and opportunities. Bottom-fixed turbines typically only have one degree of freedom that can be accessed which is the yaw degree of freedom. The coupling of turbine controls and floating wind turbine dynamics is a well-established control challenge. The most well-known is the so-called right-half-plane zero (or negative damping) issue when using blade pitch controllers to regulate generator torque in above-rated wind conditions [54, 55]. When a floating turbine tilts forward the effective wind speed increases which, in above-rated wind conditions will

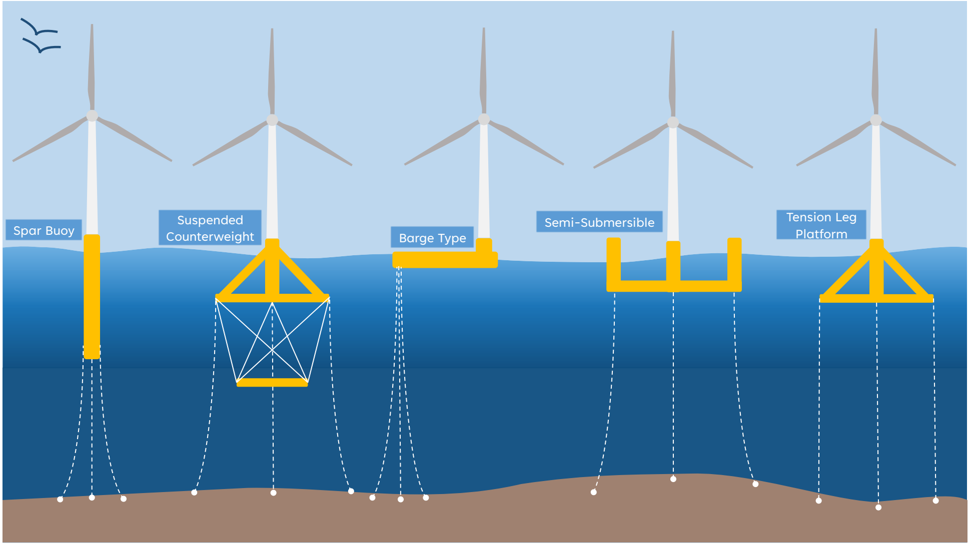

Figure 1.6: Representation of 5 different floating foundation types. Each type of foundation has its advantages and disadvantages when it comes to stability and ease of deployment.

result in a pitch action from the control system. This reduces the turbine thrust causing an increased tilt motion leading to further blade pitch action. When the floating turbine tilts backwards the opposite happens with the control system enhancing the turbine's fore-aft motion. When left unchecked, the floating turbine will become unstable in the fore-aft direction. Other instabilities include the roll-yaw lock instability [56]. At certain thrust levels, a floating wind turbine can enter a roll-yaw lock whereby a roll angle creates a yaw angle (or vice versa) which then reinforces the roll angle creating cyclic motion that alternates between the two.

It is expected that when floating wind technology matures through further development of new foundations and suitable control solutions, floating turbines will be deployed in large floating farms. The floating wind turbine dynamics can also be leveraged to mitigate the wake interaction in future floating wind farms. One such example is the ability to actively reposition wind turbines within a wind farm depending on the wind direction using the yaw degree of freedom of the turbine and by changing the thrust magnitude [57–59]. Another example is a variant of wake steering. Certain foundations use seawater as ballast which can be pumped in and out of the columns thereby altering the static roll or tilt angle of the floating turbine. In [60], this technique is used to tilt the floating turbine thereby deflecting the wake either upwards or downwards depending on tilt direction. Deflecting the wake into the ocean provided a noticeable uplift in wind farm power production.

1.6 This Thesis

Previous research has shown that in steady-state situations, the extra dynamics of a floating turbine can be leveraged for wind farm flow control. However, since the wake mixing methods use time-varying inputs the behaviour of the floating turbine will also become time-varying which will impact the wake behind the floating turbine. The work presented in this thesis investigates how wake mixing control methods like the Pulse and the Helix interact with a floating turbine. Given the growing interest in wake mixing methods, as well as the rapid development of floating wind turbines, the main research question this thesis answers is formulated as follows:

Research Question: Can the dynamics of a floating turbine be used to enhance dynamic wake mixing techniques and if so can a floating turbine be optimised such that it promotes wake mixing?

The first step to answering this research question is gaining an understanding of the dynamics of a floating turbine. There are different types of foundations, each having its advantages and disadvantages in terms of dynamics. Since wake mixing methods apply a time-varying input it will excite frequency-dependent dynamics which will be different for different foundations. The first contribution of this thesis is therefore:

> **Contribution 1:** Identification and characterisation of the dynamics for different types of floating turbines when they are excited using dynamic wake mixing techniques.

Movement of a floating turbine will result in a time-varying inflow to the turbine which, without rectification from a control system, will result in a time-varying thrust of the turbine. Using frequency domain analysis the coupling between the dynamic wake mixing method and the floating turbine can be characterised and analysed. The information acquired through the frequency analysis aids in pinpointing the combinations of floating turbine and wake mixing methods that show significant coupling effects. This also leads to the second contribution of this thesis which are simulations that quantify the effect of any potential movement on the effectiveness of the wake mixing method. The conclusions are based on wind speed measurements in the wake as well as measurements on the actuated turbine, hence, the second contribution reads:

> **Contribution 2:** Analysis and quantification of the effect of the coupled movement on the wake mixing method using fully coupled simulations of different floating turbines using both the Pulse and Helix wake mixing methods.

The first and second contributions of this thesis are staged as numerical studies in medium-fidelity simulations. However, the dynamics of a floating turbine and even more the dynamics of the wake are complex and non-linear, and the quality of the analysis is only as good as the simulation suite used. In this thesis, the wake is modelled using a free vortex model which is a method that can accurately model the wake close to the rotor but loses accuracy as the wake travels downstream. With the right settings, it is good enough to model wake dynamics triggered by the Helix and Pulse method but it might be unable to capture the more complex dynamics that stem from the combined platform motion and wake mixing method. The third contribution of this thesis is wind tunnel experiments that, firstly, validate the findings of the second contribution and, secondly, allow for deeper analysis of the wake dynamics and as such reads as:

> **Contribution 3:** Validation of simulation results through wind tunnel experiments using tomographic particle image velocimetry (or PIV) and analysis of wake dynamics when a floating turbine undergoes motion excited by the Helix wake mixing method.

1.6.1 Contents of this Thesis

This chapter has introduced the challenges posed to humanity by climate change. Wind energy provides a solution for the transition from a fossil-based energy system to a renewable one. The remaining content of this thesis provides detailed insight into the three main contributions. The chapters that form the main body of this thesis are all previously published articles with their own introduction and conclusions and can be read independently from one another. Figure 1.7 provides a visual overview of the main topic presented in each chapter.

Chapter 2 investigates how the Pulse wake mixing method couples to the movement of a spar-type floating wind turbine. The main finding is that extra movement is not necessarily beneficial for a wake mixing method. Using a frequency domain analysis the coupling between this type of floating turbine and the Pulse method is analysed and any loss in wake mixing performance is explained by it.

Chapter 3 conducts a similar investigation but then for the Helix wake mixing method and a semi-submersible type floater. Semi-submersible type floaters were found to exhibit significant yaw motion as a result of an eigenfrequency that is excited by the Helix method. The article that forms the content of this chapter shows that gains in wind speed can be achieved when the floating turbine is both yawing and using the Helix method.

Chapter 4 builds upon the results found in Chapter 3 and investigates two different floater types that have been optimised such that their yaw motion is enhanced. In this chapter, a significant difference was found in wake mixing performance between two different floating turbines whilst having a similar yaw amplitude. The main difference in dynamics was found to be within the phase coupling between yaw motion and Helix input.

Chapter 5 introduces unique wind tunnel experiments that are used to analyse the aerodynamics of the wake. The main motivation for the conducted experiments was the results presented in **Chapter 4**. Therefore the experiments focused on analysing and quantifying, within a wind tunnel setting, the impact a change in phase difference between yaw motion and Helix input can have on the wake mixing method. Using tomographic particle image velocimetry the wake could be reconstructed providing insight into the effect of phase offset and how the Helix method can be enhanced by exciting the yaw motion with the correct phase coupling.

Finally, **Chapter 6** will form the conclusion of this thesis that can be gathered from the contents of the preceding chapters ending with recommendations for improvements for this research and potential future research.

1

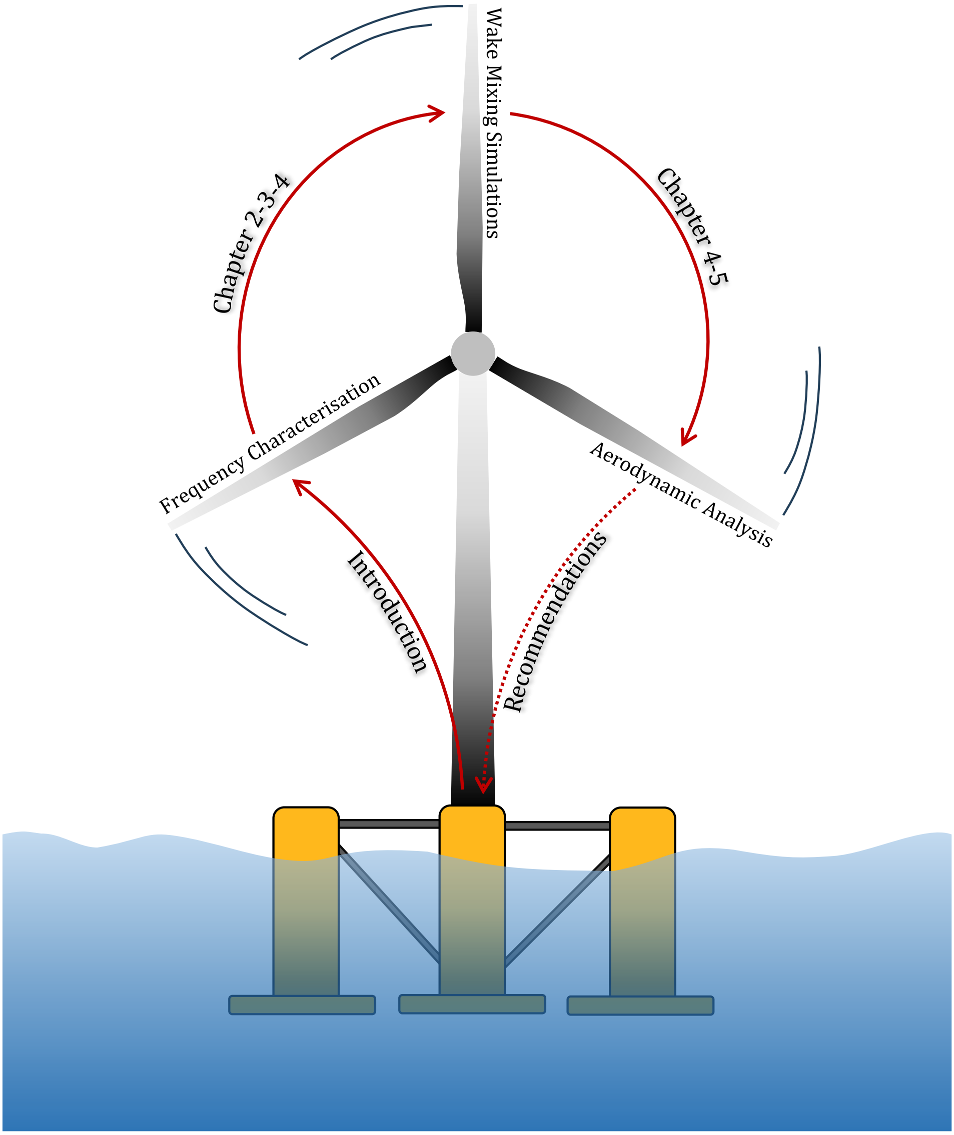

Figure 1.7: Schematic overview of main topics covered in different chapters of this thesis. The circular fashion is representative of the proposed design cycle based on the results presented in this thesis. As our understanding of wake dynamics increases we can start designing floating turbines that excite those dynamics. The effectiveness of this new optimal design can be analysed and quantified using analysis not unlike that presented in this work.

2

Investigating the Pulse Wake Mixing Method for Floating Turbines

In recent years control techniques such as dynamic induction control (often referred to as "The Pulse") have shown great potential in increasing wake mixing with the goal of minimizing turbine-to-turbine interaction within a wind farm. Dynamic induction control disturbs the wake by varying the thrust of the turbine over time, which results in a time-varying induction zone. If applied to a floating wind turbine, this time-varying thrust force will, besides changing the wake, change the motion of the platform. In light of the expected movement, this work investigates if applying the Pulse on a floating wind turbine yields similar results to that of the Pulse applied to fixed-bottom turbines. This is done by considering first the magnitude of motions of the floating wind turbine due to the application of a time-varying thrust force and secondly the effect of these motions on the wake mixing. A frequency response experiment shows that the movement of the floating turbine is heavily frequency-dependent, as is the thrust force. Time domain simulations, using a free wake vortex method with uniform inflow, show that the expected gain in average wind speed at a distance of five rotor diameters downstream is more sensitive to the excitation frequency compared to a bottom-fixed turbine with the same Pulse applied. This is due to the fact that at certain frequencies platform motion decreases the thrust force variation and thus reduces the onset of wake mixing.

This chapter is based on *The dynamic coupling between the pulse wake mixing strategy and floating wind turbines, D. van den Berg, D. De Tavernier, J.W. van Wingerden - Wind Energy Science, 2023.*

2.1 Introduction

The drive for the European Union (EU) to become carbon-neutral and energy self-sufficient has increased the demand for renewable energy production. These goals were (re)formulated in the REPowerEU Plan [61]. Offshore wind energy is often regarded as one of the key technologies to provide this green renewable energy [62]. As of 2021, offshore wind farms provided 28 GW (13.5%) of the 236 GW of installed wind capacity in Europe. These offshore wind farms are all located in shallow (less than 50 m) waters [63, 64]. However, to achieve the 480 GW of installed wind capacity (on- and offshore combined) target by 2030 [61], offshore wind needs to find access to the deeper waters of the European Union, and the United Kingdom, where 80% of the total wind energy resources can be found [48]. Floating wind turbines (FWTs) will play a key role in enabling access to these energy resources. As the technology matures, floating turbines will likely be clustered into large wind farms, similar to the bottom-fixed wind farms in shallower waters.

It is well-known that wind turbines within a wind farm interact with the wakes of surrounding turbines. This results in an extensive reduction of the power production of the individual turbines, which may be in the order of 10 to 25% [65, 66]. Since wake interaction is a major source of energy loss, a significant amount of research has been performed on understanding wake effects. In steady design and operational conditions, considerable advances have been made since the first engineering method presented by [67]. However, particularly in unsteady inflow or operational conditions that are inevitable for floating turbines, wake losses and mitigation techniques remain elusive.

With this work, we will study to what extent the wake losses of floating wind turbines can be minimised using dynamic induction control techniques. In particular, we will look at the Pulse wake mixing technique. More specifically, we will consider if floating wind turbines can leverage their extra degrees of freedom while using this wake mixing strategy.

2.1.1 Background

For bottom-fixed turbines, various strategies have been proposed in the literature in order to reduce wake losses. These strategies include wind farm layout optimization, steady-state control solutions and active wake control strategies [28].

Since the introduction of (engineering) wake models, the placement of wind turbines within a wind farm has received major attention, typically for the goal of wind farm layout optimization. The work by [68] and [69] show that optimizing the layout of the wind farm for a given type of turbine, plot size and historic wind information is possible. More recently, [37] achieved an increase in power production in the order of 2% simulating two real-world wind farms for which the turbines have been redistributed using genetic optimization algorithms. These approaches assume the turbine to be static, where the only degree of freedom is the placement of the turbine with respect to each other. As input to the optimization, historical wind data is used to maximise the potential power gain for the prevailing wind. Because the optimization is static, this potential gain is limited for wind directions that occur less often.

A different approach considers using an optimal steady-state control solution using the available degrees of freedom of a bottom-fixed turbine. The two methods that have gained traction in literature are wake re-direction and induction control. Using the yawing availability of the turbine, the rotor can be statically misaligned with the mean wind direction to divert the wake away from downstream turbines. This increases the power output of downwind turbines at the cost of power loss on the upwind turbine for an overall net gain [23, 30, 32]. A downside of this method is that, as the number of wind turbines in a farm increases, a diverted wake for one pair of turbines could overlap with a different turbine. Furthermore, the yawed turbine will experience increased loading which reduces the turbine's lifetime [70]. Yaw misalignment is an example of *steady-state* optimal control. The use of engineering wake models, such as FLORIS [35, 71], allows for calculating an optimal yaw angle based on measurements within a wind farm. Once the turbine is positioned in the new desired configuration, it is kept steady until the wind conditions change. Recent advances in these engineering wake models have introduced dynamic behaviour [36]. This allows for optimizing wind farm control under time-varying conditions.

Steady-state induction control (also called de-rating control) is another approach used to increase farm output. It uses the induction factor of the turbine as a control input. Similar to wake redirection, the performance of the first turbine is sacrificed for the benefit of downwind turbines. Induction control has shown great potential in different simulation and optimization environments [38, 39, 41]. However, wind tunnel experiments and full-scale experiments have shown that the gain of induction control is negligible [40, 42], contrary to what is found using wake redirection [33, 42]. The work described in [41] is currently being tested in a real-world wind farm to evaluate the effectiveness of their proposed induction control solution and could potentially yield a different conclusion to [42] and [40].

As an alternative to the steady-state optimal control techniques, new forms of active, time-varying, control have gained interest within the scientific community and were first introduced by [45]. As a result of this research, two notable active control techniques have emerged: the Pulse (formally Dynamic Induction Control or DIC) [43, 72] and the Helix (formally Dynamic Individual Pitch Control or DIPC) [44]. Both methods rely on disturbing the wake using dynamic blade pitching such that the natural mixing process starts at an earlier distance downstream. For the Pulse wake mixing approach, the blade pitch angle of all rotor blades is varied collectively in a sinusoidal manner. For the Helix strategy, on the other hand, the blade pitch angle of the blades is controlled individually and varies sinusoidally with a phase offset between the blades. Both methods have shown in simulations to increase the power of a two-turbine wind farm by up to 5% for the Pulse and up to 7.5% for the Helix under turbulent inflow conditions [44].

The proposed techniques to mitigate wake interaction between turbines can also be applied to floating wind turbines. In fact, where bottom-fixed turbines are limited to one degree of freedom (yawing), a floating turbine has the ability to move in all six degrees of freedom. In general, these motions add significant complexity to the design of floating wind turbines, but for wake control purposes, they can potentially be leveraged. Moving turbines could be used for the purpose of repositioning the wind farm, and thus for active layout optimisation. This idea is used by [57] and [58] to actively optimise a wind farm based on wind conditions. In [58] several wind farms of differing sizes, placed in a grid layout with a 7-rotor diameter ('7D') spacing between turbines, are optimised. In their research, they showed that the overall farm efficiency could be increased by 5-10% by actively optimizing the layout, where the actual percentage of gain depends heavily on wind farm size and wind direction.

Alternatively, for certain types of floater designs, the orientation of the turbine can be changed by changing the ballast. This is done by [60], where wake deflection is realised by pitching the platform instead of yawing the turbine. Here, the wake deflects either upwards or downwards, where re-directing the wake downwards showed to increase the overall power production of a two-turbine wind farm [60].

When wake mixing techniques such as the Pulse and Helix are used, the thrust force will vary over time. The research presented in [73] and [58] showed that the thrust of the turbine can be used to alter the state of the floating turbine, and the platform to translate and/or rotate. For the Helix wake mixing technique, this is explored in [74]. In their work, the yaw moment originating from the Helix is found to primarily excite the yaw degree of freedom of a floating turbine. By enabling the platform motion in yaw during Helix operation, the wind speed downstream increased by up to 10%, compared to a bottom-fixed turbine with the same Helix operation. Furthermore, it was found that the floating turbine, using the Helix, showed a similar performance as a bottom-fixed turbine, using the Helix with double the pitching amplitude. This gain is thought to originate from the fact that not only the wake is mixed but also dynamically deflected. Further research is required to confirm this statement. For the Pulse wake mixing technique, it is not yet clear if a similar positive coupling between the wake mixing technique and floater dynamics exists.

2.1.2 Research objective

The main contributions of this paper are twofold: (i) a frequency analysis of the motions of the floating turbine and its coupling to the Pulse dynamics, and (ii) time domain simulations to investigate the effect of the motions on wake mixing with the system represented by its full non-linear dynamics. These simulations are executed in *QBlade* [75], a simulation suite capable of fully simulating hydro-, aero-elastics and wake dynamics. The wake is modelled using a free-wake vortex model.

The remainder of this paper is organised as follows: Section 2.2 introduces the simulation tool and settings used in this research. Section 2.3 gives a short summary of the Pulse wake mixing technology. It also provides insight, using frequency response functions, into the dynamics of a floating turbine when exposed to the Pulse. Section 2.4 gives time domain results for the floating NREL 5MW turbine with the Pulse at three different frequencies. Finally, Section 3.6 will present the conclusion of this work.

2.2 Simulation tools and Research Methodology

In this research, *QBlade* is used as the simulation tool [75]. *QBlade* uses a free-wake vortex method to simulate the flow field, and thus also the wake, around a turbine. The vortex method is known for its accuracy in the near wake [76, 77], as well as being computationally more efficient than comparable Large Eddy Simulation (LES) methods [78]. However, free-wake vortex methods are prone to numerical instability, especially in the far-wake region. Nevertheless, the vortex method can be used to analyze the wake further downstream, see for example [79, 80]. *QBlade* is used as it is able to simulate both the hydrodynamics, as well as the near- to mid-wake. All the simulations will be run with uniform and steady inflow. This provides a best-case scenario for the wake mixing technique. When unsteady inflow is considered natural mixing already occurs in the wake which reduces the effectiveness of the wake mixing techniques. However, wake mixing can still be beneficial even when turbulence is considered [44].

Throughout this research, without loss of generality, the NREL 5MW turbine [81] mounted on an OC3 spar-buoy [82] is used. Section 2.4 will touch upon how the results presented in this work would or would not differ for different turbines and different floaters. The OC3 floater with NREL 5MW turbine has been extensively verified against OpenFast calculations and experimental data within the Floatech project [83].

2.2.1 Numerical set-up

In this section, the settings used in *QBlade* will be motivated. As for any aerodynamic simulation, the chosen settings are a trade-off between computational time and accuracy. In a free-wake vortex method, this trade-off is primarily dictated by the number of vortex elements in the wake, as computational time grows exponentially with the number of wake elements. The settings that influence computational time and accuracy can be divided into two groups. The first directly regulates the number of elements in the wake and is categorised under wake modelling in *QBlade*. In the second group are settings that influence vortex modelling. These settings generally have a larger impact on the accuracy of the wake and less on computational efficiency. Finally, the blade and time step discretization will also influence the number of vortex elements released into the wake and therefore will also have an impact on computational time and accuracy. Figure 3.7 shows an image of *QBlade* with the fully panelised near wake visible.

Table 2.1: Numerical simulation settings that regulate the wake discretization. These settings are used for all simulations presented in this paper.

Wake Modeling	**Setting**
Wake Relaxation	1 (No relaxation)
Max. Wake Elements	200000 [-]
Max. Wake Distance	100 Rotor Diameters
Wake Reduction Factor	0.001 [-]
Near Wake Length	0.5 Revolutions
Wake Zone 1/2/3 Length	6/12/6 Revolutions

The wake modelling settings are summarised in Table 2.1. These settings all directly influence the length of the wake and as such also the number of wake elements. The wake is cut-off when either the maximum number of wake elements or the maximum wake distance is reached. Wake relaxation, when enabled, blends the starting vortex and influences the length of the wake. When enabled, the resulting wake is too short for the analysis in this work, hence, for this reason, it is disabled. The wake reduction factor dictates when wake elements are removed based on their current vorticity strength compared to newly released vortices. The final length of the wake is a trade-off mainly between these settings. Throughout the simulations carried out in this work, the wake reduction was the most stringent setting when it comes to the number of wake elements as they were removed before reaching either the maximum number of wake elements or the maximum wake distance.

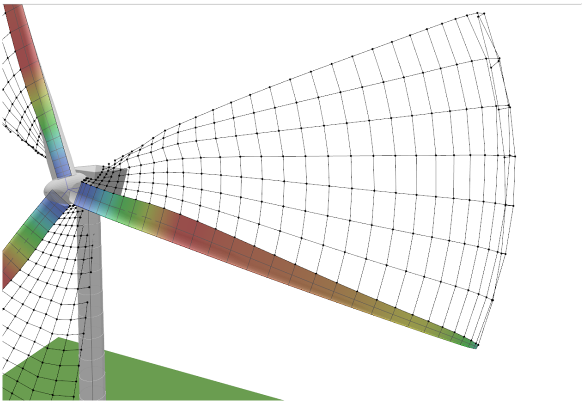

Figure 2.1: A close-up of the discretised blades and near-wake in QBlade. The image is taken at the start of the simulation at which only the near wake is visible. The colour on the blade represents the loading over the blade, with red indicating high load and green/blue lower loading. The vortex elements are represented by the black lines.

Table 2.2: Numerical simulation settings related to the aerodynamic modelling and vortex definition. These settings are used for all simulations presented in this work.

Vortex Modelling Settings	**Setting**
Initial Core Radius	0.05% Chord
Vortex Viscosity	800 [-]
Vortex Strain	Disabled
Trailing Vortices	Enabled
Shed Vortices	Enabled

The full wake is subdivided into four distinct areas. Of this, the near wake is a finely resolved wake close to the turbine which mainly influences the performance of the turbine. Typically, the near wake does not need to be resolved much further than half a rotor diameter for accurate results [78]. After the near wake, the wake transitions to wake zone 1. Wake zone 1, and consecutively wake zones 2 and 3, are regions in which the wake is increasingly sparsely resolved. When the wake transitions to a different zone, vortex filaments are merged to reduce the number of elements, which increases computational efficiency. The wake zones are defined in terms of revolutions of the turbine, which, based on the average velocity in the wake, can be translated to a distance. Based on an in-depth grid study, the values in Table 2.1 were found to give a good trade-off between wake accuracy and computational time. Appendix 2.A provides more detail on the effect of different wake zones on the velocity in the wake.

Settings that influence the vortex modelling are summarised in Table 2.2. The size of the core radius influences the stability of the wake, the larger the core radius the higher the stability. However, having a too-large core size can also limit the wake mixing dynamics. Vortex viscosity is set to 1100, which was found to work well for modelling large rotors [84, 85]. Finally, having both trailing and shed vortices increases the accuracy of the wake.

Table 2.3 summarises key settings for the blade modelling. For each simulation, the time step is set to 0.05 [s]. With an inflow speed of 9 [m/s], the azimuthal step of the turbine is $\Delta\psi = 3.3^{\circ}$ at rated speed. This azimuthal step was found to be a good compromise between accuracy and computation time [78]. Finally, the blade is discretised in 18 panels, which are sinusoidally distributed over the blade. Appendix 2.A shows, through a convergence study, that this yields accurate results and prevents a large increase in computational time. The simulation is run with the Beddoesh-Leishman unsteady aerodynamic model with the corresponding coefficients based on the research presented in [86]. These values were validated using data from the MEXICO campaign in [87].

Table 2.3: Numerical simulation settings related to the turbine modelling. These settings are used for all simulations presented in this work.

Turbine Settings	**Setting**
Dynamic Stall Model	Beddoesh-Leishman
Pressure Lag Constant	1.7 [-]
Viscous Lag Constant	3.0 [-]
Time Step	0.05 [s]
Azimuthal Step	$\Delta\psi = 3.3^{\circ}$ [deg]
Inflow Velocity	9 [m/s]
Discretization Panels #	18 [-]
Discretization Method	Sinusoidal

2.3 The Pulse and Platform Dynamics

This section will summarise the driving principle behind the Pulse wake mixing mechanism. It also provides an analysis of the motions of a floating turbine initiated by the Pulse. This analysis is done based on frequency response functions [88]. The frequency responses provide insight into how the hydrodynamics of the floating turbine is coupled to the dynamics of the Pulse.

2.3.1 The Pulse Wake Mixing Strategy

The principle of the Pulse is derived from the work of [45] and [43] in which a global optimization for an entire wind farm provided an optimal thrust coefficient C_t' input for the wind turbines with the aim of power maximization. From the optimised wind field, temporal variations in shed vorticity were identified which disrupted the wake. This behaviour in the wake can be mimicked by adding a time-varying offset to the Betz-optimal coefficient, $C_t' = 2$, which can be expressed as Equation 2.1:

$$C_t'(t) = 2 + A\sin\left(2\pi St\frac{V_\infty}{D}t\right), \tag{2.1}$$

$$\text{with: } St = \frac{f_e D}{V_\infty}, \tag{2.2}$$

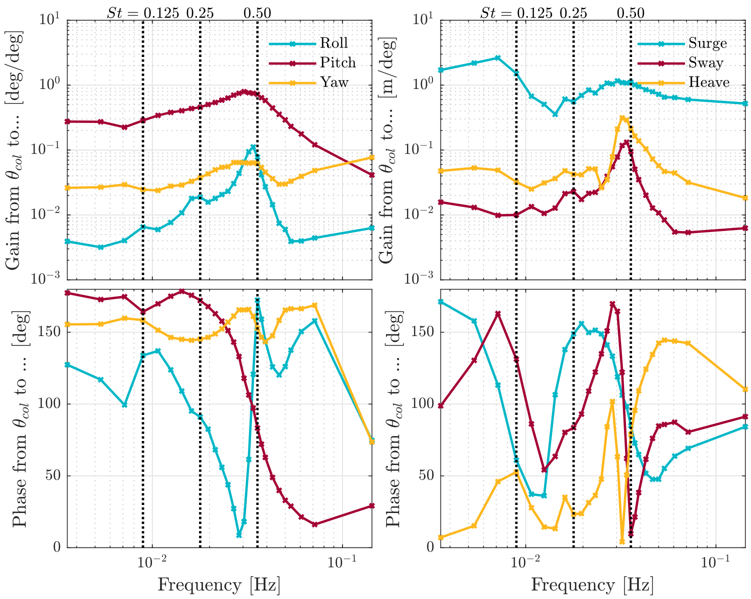

Figure 2.2: Frequency response functions for NREL 5 MW turbine on the OC3 spar-buoy platform. These frequency responses show all translational and rotational motions the turbine will undergo. The vertical dotted lines indicate where blade pitching frequencies at 3 different Strouhal numbers would align with this data. For example, pitching at a frequency of $St = 0.50$ for the NREL 5 MW turbine also means that the system is excited close to the eigenfrequency of the platform pitch motion. In the y-axes label θ_{col} refers to the collective pitch angle of the blades.

where A is the amplitude [-], D the rotor diameter in [m], V_∞ the inflow velocity in [m/s] and St is the Strouhal number [-], in which f_e is the pitching frequency in Hz. Finally, t is the time in [s]. With this time-varying thrust coefficient, the overall thrust force on the rotor will vary in a sinusoidal manner. This method only works for free stream turbines and not necessarily waked turbines. If a similar type of actuation is beneficial for waked turbines requires further research. In this paper, we adopt the strategy proposed in [89]. The time-varying thrust force as described in Equation 2.1 can be realised by pitching the turbine blades with a similar sinusoidal signal.

2.3.2 Floater Dynamics

To capture the behaviour of the OC3 platform [82], several frequency response simulations are performed. The Pulse is applied at different frequencies after which the floating turbine reaches steady-state behaviour. Using the steady-state signals, the gain and phase between input and outputs can be mapped.

Platform Motions

Figure 2.2 shows the frequency responses for each of the degrees of freedom of a floating turbine. The turbine response shows that the type of motion that the floating turbine undergoes is dependent on the excitation frequency, with different movements becoming

2

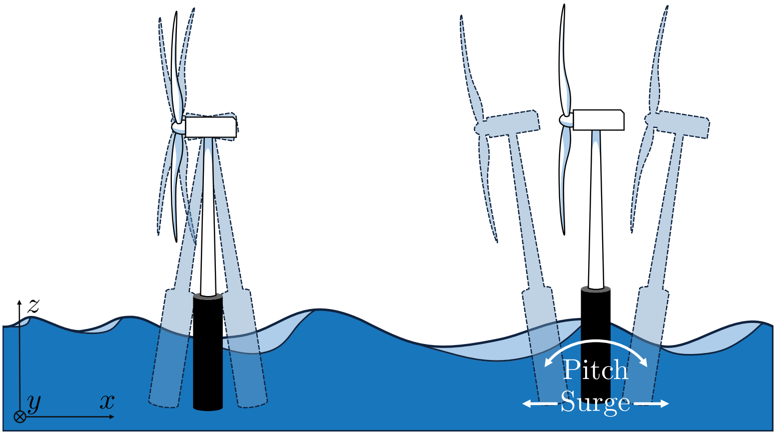

Figure 2.3: Two examples of floating turbines undergoing both surge and pitch motion resulting in different displacements of the nacelle.

dominant at different frequencies. For example, while the surge motion is dominant at lower frequencies, the floating turbine undergoes a combination of pitching and surging motions at higher frequencies. All other motions typically appear with at least an order of magnitude lower amplitude than the surge or platform pitching motion. Therefore, they will be neglected in further analysis.

Effect on Nacelle Displacement

The motion of the nacelle is mainly dependent on the magnitude of and coupling between surge motion and platform pitch, which is a result of floater design [90]. While generally it is expected that a surge and pitch motion results in a nacelle displacement, it is possible that the surge and pitch motion counteract each other, causing the nacelle to remain almost stationary. An example of this is given in Figure 2.3: it depicts two floating turbines which are both pitching and surging whilst having different nacelle displacements. As will be shown in the frequency analysis, this is dependent on the phase and gain difference between the two motions. The movement of the nacelle is of interest as it will cause the turbine to experience a time-varying inflow and thus a time-varying thrust loading. It is expected that this may interfere with the working principle of the Pulse. Therefore, the movement of the nacelle is also included in the frequency analysis. The frequency response diagrams for platform pitch, surge and nacelle motion are shown in Figure 2.4.

At low frequencies, that is until 0.01 [Hz], the motion of the nacelle is nearly one-to-one coupled to the surge motion, as the platform pitch angles are negligible. This can also be seen in the phase data, where the phase of the surge motion and nacelle motion are locked. Between 0.01 and 0.02 [Hz], the nacelle motion is the smallest for the frequency range considered. Within this frequency range the platform surge and pitch motion are almost 180 degrees out of phase. This, combined with the lower surge motion, results in the floating turbine undergoing pitching and surging motion, without any significant nacelle displacement. This behaviour is depicted in the left situation of Figure 2.3. At its lowest point, the absolute gain from blade pitch angle to nacelle displacement is only 0.4 [m/deg],

2

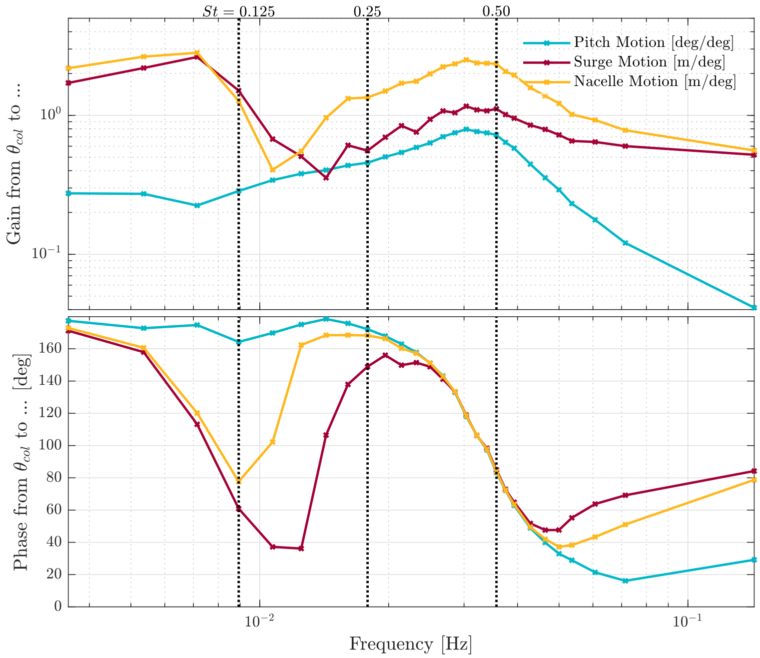

Figure 2.4: Frequency response functions for platform pitch, surge and nacelle motion for NREL 5 MW turbine on the OC3 spar-buoy platform. In the y-axes label θ_{col} refers to the collective pitch angle of the blades.

meaning for every degree of blade pitch angle the nacelle only moves by 40 centimetres. As frequency increases, the phase difference between surge and platform pitch diminishes and both motions enhance the nacelle motion, graphically depicted in the right situation in Figure 2.3. This is most prominent at $St = 0.5$, where the nacelle motion achieves its second-to-maximum gain (the first being at a lower frequency).

Effect on Turbine Thrust

Up till this point, only the displacement of the floating turbine at different frequencies has been considered. For a bottom-fixed turbine the frequency, and blade pitching amplitude, at which the Pulse is applied, significantly impact the wake mixing behind the turbine. Typically, the frequency of $St = 0.25$ is taken as ideal when considering two aligned turbines spaced 5 rotor diameters apart [43]. It could be, however, that this is no longer the case for floating turbines, as the effect of the motion of the floating turbine has to be taken into account. It could well be that actuating at different frequencies on a floating turbine, yields different (local) optima.

One turbine parameter that provides insight into the expected wake mixing is the thrust force. By varying the thrust force, the wake is disturbed through the resulting time-varying wind field. As the turbine moves, it will experience a different relative wind speed, influencing the thrust force of the turbine. It could be that the extra dynamics could

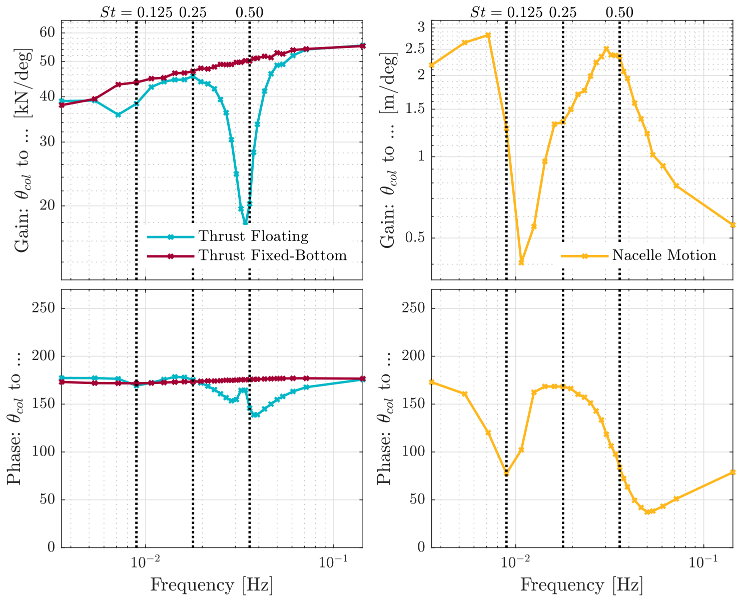

Figure 2.5: Frequency response functions for thrust force variation and nacelle motion, for NREL 5MW turbine on the OC3 spar-buoy platform. The resonance frequencies in nacelle motion coincide with the anti-resonance frequencies in thrust force variation. In the y-axes label θ_{col} refers to the collective pitch angle of the blades.

lead to locally higher, or lower, peaks in the thrust force variation. Figure 2.5 shows the frequency response of the thrust force as well as the nacelle motion.

Within Figure 2.5 two antiresonances can be identified in the floating thrust force. One is located at 0.008 [Hz] and a more prominent antiresonance is between 0.03 and 0.04 [Hz]. At both frequencies there is also a peak in the motion of the nacelle, indicating that there is indeed a coupling between platform and Pulse dynamics. This coupling, however, seems to have a negative impact, as in, as the motion of the nacelle increases the variation in thrust force decreases. The difference in the size of the antiresonance can be explained by considering the frequency at which the motion is at its maximum. The second peak occurs at ≈ 5 times the frequency of the first peak, which means the nacelle is moving with a higher velocity.

At $St = 0.25$ the opposite behaviour to the antiresonance frequencies can be seen. Here, the nacelle motion has an antiresonance and the thrust has a peak. At higher frequencies (> 0.06 [Hz]) the gain in thrust reaches its highest gain. However, it is also at this frequency that the Pulse becomes less effective as the blades are pitching too quickly to excite the wake roll-up dynamics. The frequency area of interest is therefore between $St = 0.125$ and $St = 0.5$. Also included in Figure 2.5 is the gain from blade pitch angle to turbine thrust for a bottom fixed NREL 5MW turbine. At all frequencies, the gain for the bottom-fixed turbine is equal to or greater than that of the floating turbine. At frequencies where the nacelle is not moving, or moving at low velocity, the gain for thrust approaches that of the bottom-fixed turbine. At the resonance peaks of nacelle motion, there is a large difference in thrust force when compared to a bottom-fixed turbine.

The frequency analysis, as presented in this section, is a form of linear system analysis to describe how a system responds to an input signal with one distinct frequency. It fails to capture any non-linear dynamics in the system when the input signal is not a single sinusoid or the amplitude is time-varying. The full, potentially non-linear, behaviour of a floating wind turbine is captured within the time domain simulations. Based on the frequency analysis it is clear that the nacelle motion has an effect on the time-varying thrust force. The full impact on the onset of wake mixing of the wake due to the nacelle motion and the physical displacement of the rotor plane is analyzed in the following section. Based on the thrust analysis it is expected that the movement will affect the degree of wake mixing.

2.4 Time Domain Results

This section investigates if the floating turbine movement for different Pulse frequencies has any noticeable impact on wake mixing. This is done by performing time domain simulations at three different Strouhal numbers: $St = 0.125$, $St = 0.25$ and $St = 0.5$ for both a bottom-fixed and floating turbine. The first and last frequencies correspond to a frequency where the floating turbine shows significant displacement. All floating turbine simulations are compared to a bottom-fixed turbine with the Pulse at the same frequency. First, the time domain results for nacelle displacement and corresponding thrust force will be shown and discussed. Then, for each simulation, the average wind in the wake will be evaluated.

In total 8 different simulations are performed from which it is possible to evaluate downstream wind speeds at different locations. For these simulations, the settings as described in Section 2.2 are used. In each of the simulations, the turbine is floating unless stated otherwise. The eight simulations are:

1. Constant blade pitch angle (bottom-fixed baseline).
2. Constant blade pitch angle (floating baseline).
3. Pulse with 4° pitching amplitude at $St = 0.125$, bottom-fixed.
4. Pulse with 4° pitching amplitude at $St = 0.125$, floating.
5. Pulse with 4° pitching amplitude at $St = 0.250$, bottom-fixed.
6. Pulse with 4° pitching amplitude at $St = 0.250$, floating.
7. Pulse with 4° pitching amplitude at $St = 0.500$, bottom-fixed.
8. Pulse with 4° pitching amplitude at $St = 0.500$, floating.

2.4.1 Turbine Performance in Time Domain Simulations

Figure 2.6 shows the nacelle displacement as well as the resulting thrust for the three different frequencies considered. Alongside the data for the nacelle displacement, a simulation with a constant blade pitch angle is depicted for reference. This shows the steady-state

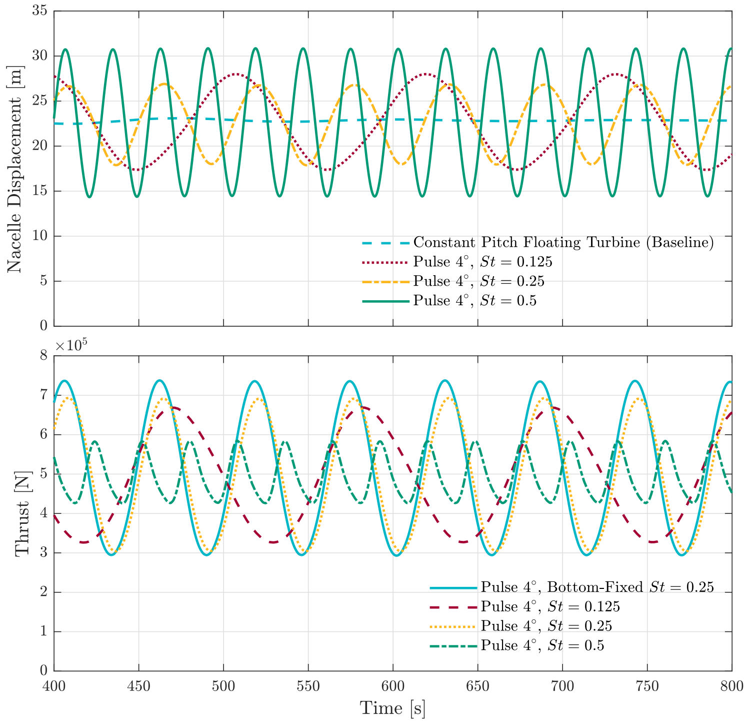

Figure 2.6: Time domain results for platform motion at three different Strouhal numbers. Each frequency has noticeable nacelle displacement which leads to differing behaviour in the thrust force. Note that the cases to which the floating simulations are compared differ between the top and bottom graphs. The top graph shows nacelle displacement with respect to its steady-state un-actuated position, the bottom graph compares thrust force variation to the best-case bottom-fixed simulation.

position around which the floating turbine is oscillating. For the thrust force data, a reference case with a bottom-fixed turbine excited with the Pulse at $St = 0.25$ is also included. At $St = 0.5$ the nacelle undergoes the largest displacement, with a total movement of 15 metres. As this occurs at the highest actuation frequency, it results in the highest velocity perceived by the nacelle. This combination of large amplitude and high frequency is of greater interest, as it equates to a larger fluctuation in relative wind speed.

The effect of this becomes apparent when looking at the thrust force of the turbine. For $St = 0.5$ the variation in thrust is significantly diminished compared to the bottom-fixed case. This observation is reinforced by looking at the $St = 0.125$ case. For that case, the total nacelle displacement is not significantly less than for $St = 0.5$, but due to the lower frequency, the variation in velocity experienced by the turbine will be substantially slower. This is reflected in the variance of the thrust force, which is larger compared to the $St = 0.5$ case. As this time-varying thrust force is the driving mechanism behind the Pulse, it is expected that the lower peak-to-peak amplitude results in less wake mixing and thus lower downstream wind speeds.

In conclusion, the lower peak-to-peak amplitude in the thrust force due to the platform motion can be compared to applying the Pulse to a bottom-fixed turbine, but with a smaller amplitude. This is likely reducing the overall effectiveness of the wake-mixing strategy, as investigated in the next section.

2.4.2 Average Wind Speed Downstream

Thus far, the focus has primarily been on turbine performance and its, potential, relation to wake mixing dynamics. The time domain data confirms that the fluctuation of the thrust force varies significantly for different operating frequencies. Up to this point, it is hypothesised that this will affect the degree of wake mixing behind the turbine. This section analyzes the wind speed in the wake, which is directly related to wake recovery due to wake mixing.

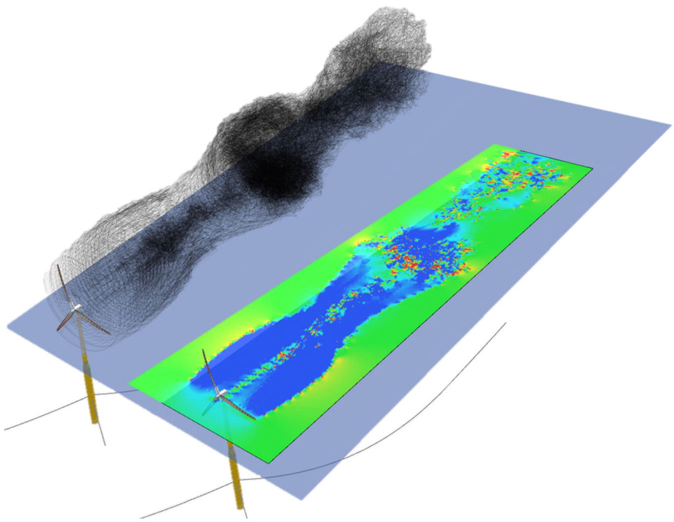

Figure 2.7: A screenshot from QBlade during one of the floating simulations. The left floating turbine shows the wake as represented by the free vortex implementation. Each black line in the wake represents a vortex element. The contraction and expansion of the wake as a result of the time-varying thrust force are clearly visible in the wake. A 2D velocity plane of the same wake is shown on the right-hand side. The bright green colour signifies areas of higher wind speed and blue areas denote areas of low wind speed. Each point in the velocity field is calculated with respect to each of the vortex elements. If a point in the velocity grid is very close to a vortex element it can lead to higher than free stream wind speeds in wake due to the nature of calculating the induced velocity. Such a point is represented by the small red points in the velocity profile.

For each simulation the wind speed is calculated at $0.5D$ distance spacing, starting $0.5D$ in front of the turbine up to $7D$ behind the turbine for a total of 16 velocity measurements. At each $0.5D$ a YZ-plane measuring 360 by 360 metres and centred at turbine level is exported for every 0.5 seconds. This plane is sectioned in squares of 3 by 3 metres yielding a grid of 120 by 120 individual velocity measurements. These dimensions were chosen such that wake expansion is fully captured over the entire domain. For each velocity plane, the average velocity experienced by a second NREL 5 MW turbine downstream, is computed for each time step for 10 minutes of data (1200 data points per simulation). An example of the wake and its 2-dimensional velocity profile at hub height can be seen in Figure 2.7.

Figure 2.8 shows a comparison between cases with the same Pulse frequency and their respective baselines. Between the floating and bottom-fixed baseline there is, when averaged, no difference in downstream wind speed even though there is a slight difference in operating conditions. For the $St = 0.125$ and $St = 0.25$ cases, there is little difference between bottom-fixed and floating cases. At distances of $4D$ and higher, the floating $St = 0.125$ case does show lower wind speeds compared to its bottom-fixed counterpart. However, the most notable difference in downstream wind speed can be seen at $St = 0.5$. Over the entire distance of the considered domain, the wind speed remains lower compared to the bottom-fixed case. As seen in the previous section, it is also the frequency at which the smallest peak-to-peak amplitude in thrust force is seen in the time data.

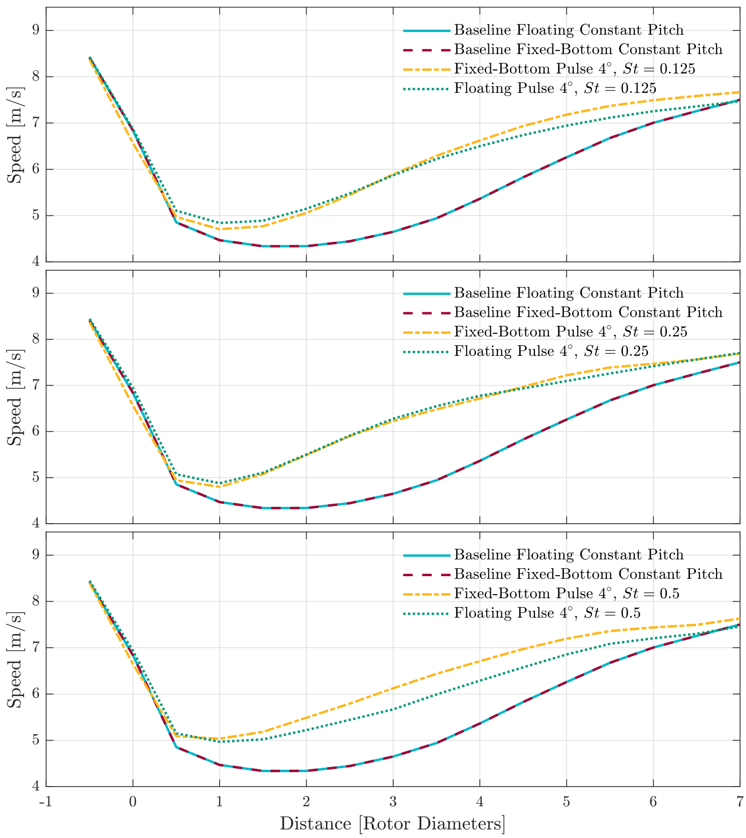

Figure 2.8: Average wind speeds over the analyzed domain for all simulations. Each floating simulation is compared to its bottom-fixed counterpart. Also included in the graphs are both baselines. The top figure shows all the cases for which the excitation frequency is $St = 0.125$, the middle figure has all the cases for $St = 0.25$ and the bottom figure the cases with $St = 0.5$.

Figure 2.9 shows the same data but then all of the bottom-fixed and floating cases are compared with each other. For the bottom-fixed cases, there is a difference in wind speed close to the turbine. As the wake progresses downstream the wind speed converges to similar values between the cases. These findings are different with respect to the work presented in [43] in which there is a difference in energy capture for the different Strouhal numbers. This is likely a result of using a vortex representation to model the wake as it is prone to wake breakdown due to numerical instabilities in the wake. This accelerates the mixing process. For the floating cases, there remains a distinct difference in wind speed, where the $St = 0.25$ outperforms both other pulse cases over the entire domain.

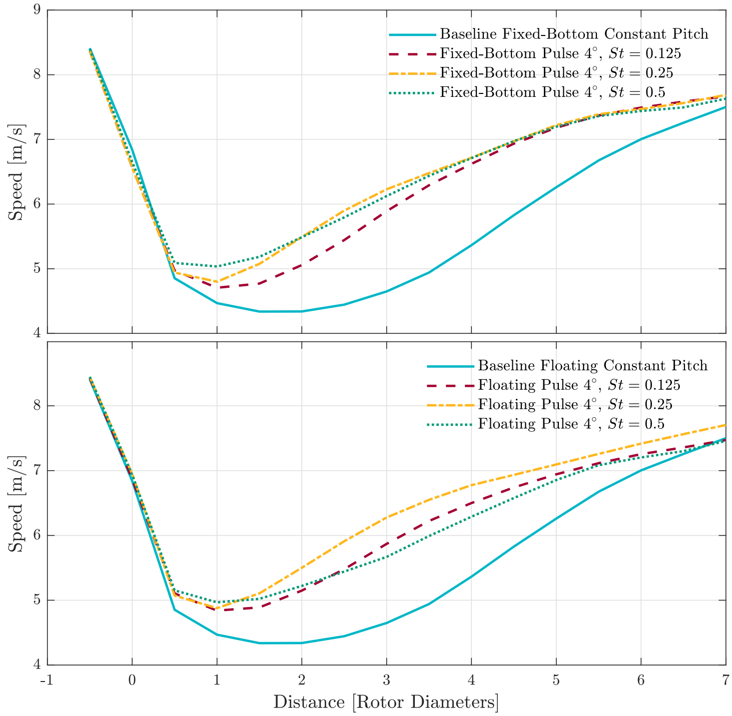

Figure 2.9: Average wind speed comparison between cases with the same mounting method. Where all bottom-fixed cases converge to the same wind speed, a difference between floating cases can be identified. The top graph compares all bottom-fixed cases, the bottom graph compares all floating cases.

2.4.3 Discussion

Based on the analysis presented in this section it is clear that the additional dynamics of a floating turbine do not necessarily lead to an increase in wake mixing. More importantly, one can conclude that when applying the Pulse whilst disregarding floater dynamics, it could lead to lower performance of the Pulse when applied to an otherwise identical bottom-fixed turbine. In Section 2.2 it was stated that this work uses the NREL 5MW turbine on the OC3 platform without loss of generality. In this section, a discussion is presented that will elaborate on this statement.

Recent work presented in [91] confirms the findings in this section. In that work, an adjoint optimization is performed to find the ideal Pulse signal for a 2-turbine floating wind farm, in which only the first turbine is actuated. The optimal excitation signal has a frequency which matches the frequency at which the nacelle is moving the least. The floating turbine in [91] is modelled as a second-order mass-spring-damper system. Surge motion is represented by a translational mass-spring-damper and platform pitch by a rotational mass-spring-damper system.

In general, the movement of a floating structure/vessel can be modelled as a mass-spring-damper system in which the stiffness and damping properties depend on the hydrodynamic properties and the mooring solution of the floater [92]. Depending on these values a floating turbine will exhibit eigenfrequencies in pitch and surge, which could result in a similar coupling to nacelle motion as for the OC3 used in this work. As the moment arm from turbine thrust to the centre of gravity of the system is unchanged, the coupling between Pulse dynamics and platform dynamics will remain the same: a change in thrust force will be counteracted by the resulting movement of the platform.

The extent to which this will influence the wake mixing technique depends on the floater type and mooring solution. For example, tension leg platforms will show different dynamics to that of a semisubmersible or single spar platform [92]. The degree to which this coupling exists depends on their respective stiffness. Since floating wind is still a (fast) emerging technology, a desire to use wake mixing techniques in a floating wind farm could influence floater choice and/or design.

Turbine size could also affect the overall effectiveness of the Pulse wake mixing technique on a floating wind turbine. The Strouhal number is, among other parameters, dependent on the turbine diameter. The larger a turbine is the lower the excitation frequency will be to actuate at a desired Strouhal number. The dynamics of the floating turbine are mainly a result of the hydrodynamic properties of the floater and less so the size of the turbine. The ideal mixing frequency of $St = 0.25$ could therefore align with the anti-resonance in nacelle motion, leaving the wake mixing technique largely unaffected by the limited platform movement. An opposite scenario is also possible. In such a scenario a different, potentially less effective, excitation frequency should be chosen to get a desirable amount of wake mixing.

It is expected that for different floating turbines the findings in this work would remain largely the same: Given the coupling between floater dynamics and the turbine thrust extra care should be taken when choosing an excitation frequency for the Pulse wake mixing technique.

Finally, it should be mentioned that with dynamic blade pitching techniques such as the Pulse the loading of the turbine will be impacted. Differences in loading might impact the effectiveness of the wake mixing technique. How the potential gains of wake mixing are influenced by the loading of the turbine is a different area of research, see for example [93] and [94].

2.5 Conclusion

For bottom-fixed turbines, the effectiveness of the Pulse wake mixing strategy depends on both the application frequency as well as the amplitude of the sinusoidal signal. This work shows that the same holds for floating wind turbines. However, the turbine motion induced by the Pulse at different frequencies, predominately in the surge and pitching direction, will further influence its effectiveness and make it more sensitive to the excitation frequency. The dynamic coupling between thrust and the resulting nacelle displacement is such that at certain frequencies the large nacelle displacement results in lower downstream wind speeds, a direct result of a reduction in wake mixing.

This nacelle displacement causes the turbine to experience a varying relative wind speed which negatively impacts the thrust force of the turbine. When the floating turbine is moving due to the Pulse, the movement is such that it lowers the peak-to-peak amplitude of the thrust force. Time domain simulations for three different frequencies show that this lowering of the peak-to-peak amplitude of the thrust force correlates to lower wind speeds downstream in the wake. This implies that the degree to which wake mixing occurs is lowered due to the movement of the floating turbine at certain frequencies.

The work presented in this paper shows that the coupling between wake mixing dynamics and floating turbine dynamics will present a new challenge in finding the right operating frequency, should the Pulse be deployed in a floating wind farm. With this specific floater turbine combination, movement is undesired from a wake mixing perspective. However, new floater designs will also introduce different floating dynamics which might produce different results, or floaters could potentially be designed such that they are guaranteed to enhance wake mixing through their design.

2.A Convergence Study

This appendix covers the in-depth convergence study that was done to set the simulation settings used in this research. This convergence study focused on the effect that blade discretization has on turbine performance. Two parameters are analyzed, the turbine thrust and blade tip deflection. The first variable is key to being accurately resolved for the purpose of this research. The second variable is a direct result of the accuracy at which the aerodynamic force is resolved on the blade. Blade discretization also influences the number of vortex elements released into the wake (see Figure 3.7), which directly impacts computational time.

The results of the convergence study are shown in Figure 2.10. A blade discretization with 30 panels is chosen as the baseline, as it is likely this gives the most accurate representation of the turbine. As will be shown in the results, going higher than 30 yields diminishing marginal gains in terms of accuracy at the cost of computational time. All other data are presented as percentual differences with respect to it. The turbine thrust converges already at 10 panels. The blade tip deflection, however, converges at 15 panels or higher.

Furthermore, as the number of panels increases, so does the computational time. Ultimately the choice of the number of blade panels is a trade-off between the desired accuracy and computational time. *QBlade* is provided with a model of the NREL5MW turbine in which the blade is discretised into 18 panels. A data point for 18 panels is also included in the convergence plot.

The effect of having different wake zones on the wake is also investigated. This is done by looking at the wind speed in the wake. Whenever the wake transitions from one zone to another, the number of vortex elements is reduced by interpolating among vortex elements and replacing them with a representative, new, vortex elements. Within *QBlade* the length of a wake zone is defined in the number of turbine revolutions. The total number of revolutions for all wake zones summed is kept at 10 for this investigation. A further half revolution is reserved for the near wake, which is a fully panelised wake and is visible in Figure 3.7. The influence of the different distributions of wake zones is analysed by looking at the velocity in the wake at a distance of 400 metres downstream. The results are presented in Figure 2.11. From the results in Figure 2.11, it is clear that there is no difference between cases 1 to 3. This is likely due to the fact that the wake only transitions after the chosen distance of 8 wake zones. This is confirmed by looking at case 4, where the length of zone 2 is expanded. In that case, the velocity field fully falls in zone 2. This results in a slight increase in wind speed and a larger variance which implies that the wake is less stable. Transitioning to wake zone 3 further increases the downstream wind speed and corresponding variance. The biggest takeaway is that allowing the wake to transition to zone 2 impacts the stability of the wake slightly and results in a small increase in wind speed. However, keeping the velocity field of interest in zone 2 seems to provide a good trade-off between accuracy and computational time. Therefore, the wake zones chosen for this research, as presented in Table 2.2, are chosen such that the wind field fully falls into zone 2 whilst also allowing zone 1 enough time to fully develop.

2

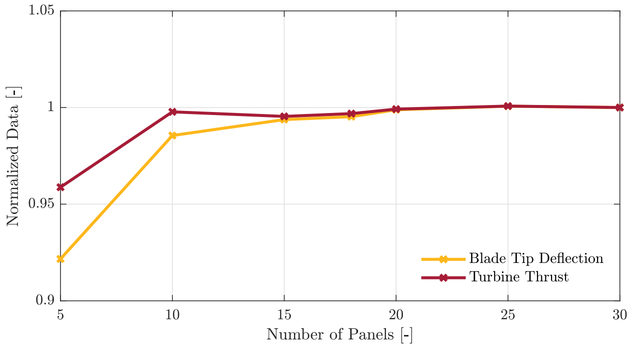

Figure 2.10: Selected results for the convergence results. The plot shows convergence for both an integral parameter (thrust) and an instantaneous parameter (blade tip deflection).

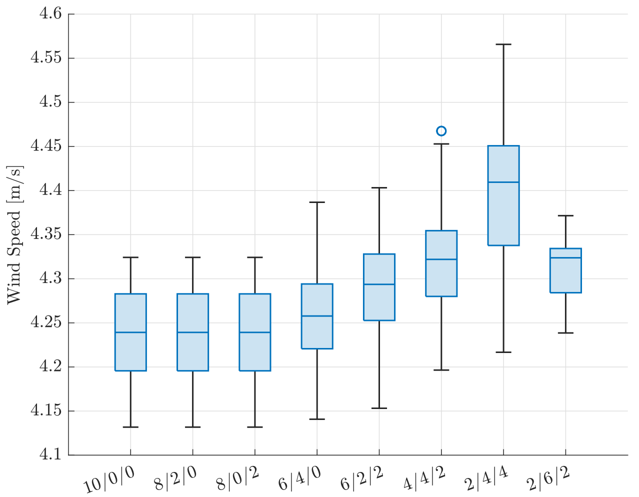

Figure 2.11: Average wind speeds downstream for different wake zones. The numbers on x-axis indicates the unit length of measure for Wake Zone 1/2/3 respectively. The 25^{th}, 50^{th} and 75^{th} percentile are shown as a box. The bars indicate the distance to the, non-outlier, minima and maxima in the data set. Any circles indicate data outliers excluded in the boxplot.

3

Investigating the Helix Wake Mixing Method for Floating Turbines

Energy production of a wind farm can be increased by reducing the wake interaction between turbines within the farm. In recent years, control solutions such as dynamic induction control and dynamic individual pitch control have shown the potential to decrease this interaction by actively triggering the wake mixing process behind the turbine.

As floating wind technology matures, these floating wind farms will run into similar wake interaction challenges as their bottom-fixed counterparts. However, when transitioning wake control solutions from bottom-fixed turbines to floating turbines they interact with the platform dynamics of these turbines. This coupling depends on the type of floater on which the turbine is mounted and results in the movement of the whole turbine. Typically this movement is undesired and extensive research has gone into the control of floating turbines with the aim of minimising platform movement.

Recent work has also shown that these movements can be leveraged to increase wind farm efficiency. This work investigates the coupling between the Helix wake mixing method and the platform dynamics of the floating turbine for the IEA 15MW turbine mounted on the VolturnUS-S floater. More specifically, it investigates if movement is triggered when the Helix is applied and how any potential movement impacts the wake-mixing dynamics.

For this floater type, the frequency range within which the Helix wake mixing method typically is applied encompasses an eigenfrequency in yaw. At this eigenfrequency, which coincidentally lies close to the ideal mixing frequency, a typical blade pitch of 4° *amplitude results in yaw motion of up to* 8°. *When the wind speed behind the actuated turbine is analysed for both a bottom-fixed turbine and a floating turbine a reduction in wake recovery is seen for the floating turbine. Moreover, the impact on wake recovery is largest at the eigenfrequency in yaw for this particular floating turbine and the ideal mixing frequency has shifted compared to the IEA 15MW bottom-fixed turbine.*

3.1 Introduction

Achieving the European Union's target of 510 GW of installed wind energy capacity by 2030 requires a significant expansion of the currently installed capacity of 255 GW [61, 95]. As a consequence of these ambitions, the power density of newly developed wind farms is rising by increasing the number of turbines within a wind farm and the size of individual turbines [96]. The larger wind farms are predominantly located offshore where wind conditions are more consistent and, on average, wind speeds are higher compared to onshore locations [21]. Furthermore, over 80% of Europe's wind energy resources can be found in waters too deep for bottom-fixed turbines [48, 97], resulting in a sharp increase in the interest in floating wind turbines over the past decade.

3

As wind turbines extract energy from the incoming wind, they create an area of turbulent, low-velocity airflow behind them, often referred to as the turbine's wake. The force that the turbine exerts on the flow also creates an area of low velocity in front of the turbine. This area is often referred to as the induction zone of the turbine, as it induces a lower velocity in the free stream. An example of the wake effect of a turbine can be seen in Figure 3.1, where the wakes of the upstream turbines in the Horns Rev wind farm are visible due to specific atmospheric conditions at the time of photographing. As these wakes travel downstream, they interact with the turbines behind the upstream turbines.

This interaction causes extensive losses in energy production for the waked turbines. Research indicates that this loss can amount to up to 25% of the energy production of an otherwise unwaked turbine [65, 66]. Since wake interaction accounts for a significant loss in a wind farm's efficiency, it has been an area of substantial research [28]. The first investigation into the wake interaction between turbines dates back to the 1980s, with work discussing wake steering, [98], and work that aims to develop a fast analytical model of the wind turbine wake in 1983 [67]. This model, often referred to as the Jensen model, introduced in [67] formed the basis of the development of many subsequent wake models each further expanding upon their capabilities, see for example [99].

With the introduction of fast analytical wake models, the first major attempt at increasing the wind farm's efficiency was using wind farm layout optimization. Early work by [68] explored an optimization trading off power production and installation costs using the Jensen wake model to model turbine interaction. In more recent work [37], an increase in a wind farm's power production by 1 to 2 per cent is realized by optimizing two existing wind farms using different wake modelling techniques. Current research focuses mainly on comparing optimization algorithms [100–102] or considers more complex onshore terrain complicating the optimization [103]. These optimizations typically assume the turbines to be static and aligned with the incoming wind direction. In this scenario, the layout is designed such that power production is maximised for the prevailing wind direction, with diminishing gains for the remaining wind directions.

These diminished gains can be recovered by using a wake steering controller. Although the concept of wake steering was first introduced in [98] in 1982, it was only discussed within a purely academic framework. In 2001 [104] and 2005 [105] it was again covered but the method significantly gained traction in both the scientific and industrial setting [26] in

This chapter is based on *D. van den Berg, D. De Tavernier, D., Marten, J. Saverin and J.W. van Wingerden. Wake Mixing Control for Floating Wind Farms - Analysis of the Implementation of the Helix Wake Mixing Strategy on the IEA 15MW Floating Wind Turbine in IEEE Control Systems, vol. 44, no. 5, pp. 81-105, Oct. 2024.*

Figure 3.1: Visualization of wind turbine wakes for the Horns Rev wind farm. Atmospheric conditions were such that water vapour condensed due to the pressure change behind the wind turbines resulting in visible wakes. Image courtesy of Vattenfall, distributed under the CC BY-ND 2.0 license.

the past two decades. With wake steering, the turbine's nacelle is yawed to divert the wake away from any downstream turbine, increasing overall farm power production [23, 24, 30–33].

As discussed in the aforementioned work, wake steering is an example of steady-state optimal control that is used to increase wind farm power production. Using engineering wake models, like FLORIS [35], lookup tables can be generated for ideal yaw angles for each turbine in a wind farm at given wind directions. Once yawed, the turbine's orientation is kept constant until the environmental conditions change. Recently, attempts have been made at incorporating control techniques such as wake steering into the layout optimization problem [106, 107]. Another recent advance in these wake models is the inclusion of dynamic behaviour of the wind field [36, 108]. This enables active control of turbines during time-varying wind conditions.

3.1.1 Dynamic Wake Mixing Techniques

Other forms of control of wind turbines involve wake mixing techniques. Wake mixing control solutions can be classified as control techniques that use existing, or potentially novel, actuators available on the wind turbine to excite aerodynamic instabilities in the wake. Contrary to wake steering control, the primary goal of wake mixing is to dissipate the wake by promoting the wake roll-up dynamics. When a wake starts to mix, it re-energises itself with the outside flow, increasing downstream wind speeds. The first wake mixing

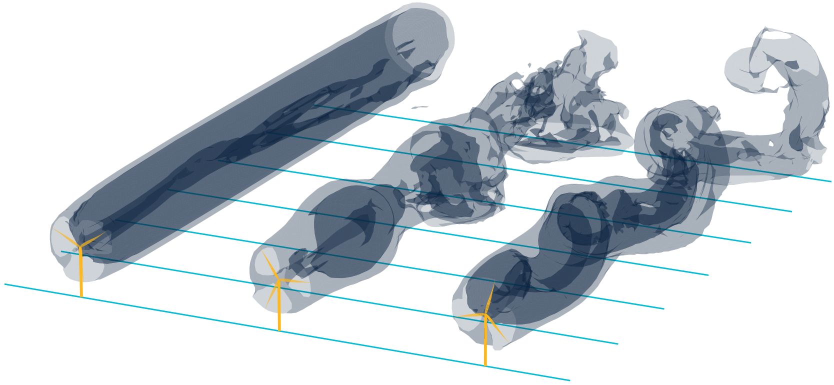

Figure 3.2: Wakes of three turbines each with different control targets. The domain is 1500 metres long with every blue line spaced by 250 metres. The turbine on the left is set to what is called 'greedy' control as it aims to extract the most amount of energy from the wake. This creates a long uniform wake of low wind speed, represented by the darker colour. The middle turbine and the rightmost turbine use the Pulse and Helix respectively. Notice how the wake for the Pulse expands and contracts over distance. This pulsating (hence 'The Pulse') effect promotes wake mixing. Both methods induce wake mixing which disrupts the wake and increases downstream wind speed. Image generously created by Marcus Becker.

technique was proposed by [45], and a similar idea was already patented in [109].

In [45], an optimal control solution was sought to increase the energy capture through the boundary layer of the wake. In that work, a conjugate-gradient optimization method was used to find an optimal coefficient of thrust for each turbine such that energy extraction of the wind farm was maximised. The adjoint optimization was run within a large eddy simulation of a wind farm of aligned turbines. The optimal control input resulted in a time-varying coefficient of thrust and led to an increase of 6.0% energy extraction of the wind farm. Analysing the wake dynamics showed that the driving factor behind this increase is that with this control method, the wind speed in the wake becomes time-varying which promotes the mixing process.

The results presented in [45] led to the development of two active blade pitching techniques that are capable of achieving similar results as described in that work. These are: Dynamic Induction Control (DIC or the Pulse) [43] and Dynamic Individual Pitch Control (DIPC or the Helix) [44, 110] with the latter also being patented [111]. Both techniques use the blade pitch angle to control the turbine's thrust to promote the onset of wake mixing behind the turbine. The Pulse method uses the collective blade pitch angle to create a time-varying thrust coefficient. The Helix method differs from the Pulse in that regard, as with the Helix method, each blade is controlled individually, creating a helical induction zone. Simulations carried out in [44] for an aligned two-turbine wind farm showed that the aggregate power of the farm can be increased by 4.6% using the Pulse and 7.5% using the Helix method. For this investigation, the turbines are spaced at a distance of five rotor diameters apart. An example of the wakes of turbines actuated with the Pulse and Helix wake mixing methods is shown in Figure 3.2. Included in the figure is the wake of an unactuated turbine which often serves as a baseline comparison.

For novel techniques like the Pulse and the Helix another area of research concerns the loading of the actuated turbine. The increase of downstream wind speed from wake mixing methods comes at the cost of increased loading of the upstream turbine [93, 94]. This needs to be taken into account when deciding to use these techniques on both bottom-fixed and floating turbines. Furthermore, when looking at the farm level the turbines directly behind the actuated turbine will also see an increase in loading, due to the increased wind speed they experience. For example, in [93] an increase of 8% in blade loads is reported for the second turbine when the Helix is activated on the upstream turbine.

3.1.2 The Transition To Floating Wind

Within this work, we explore how dynamic wake mixing control interacts with floating wind turbines and if it can significantly reduce this wake interaction between turbines. In particular, we will consider if the extra six degrees of freedom of a floating turbine can be leveraged to mitigate the wake interaction. These six degrees of freedom consist of three translational ones: surge, sway and heave, and three rotational ones: roll, platform pitch and yaw, which are defined in Figure 3.3. These extra degrees of freedom typically complicate the design of these kinds of turbines and controllers. However, from a control perspective, it also offers extra opportunities for mitigating the wake interaction between turbines. One such example is the ability to actively relocate the turbines within a floating wind farm to minimize wake overlap [57–59]. This topic is also covered in the contribution in this edition of Control Systems Magazine titled “Floating Offshore Wind Farm Control via Turbine Repositioning” by Niu et al. By altering the yaw angle and magnitude of the thrust vector, [58] increased the efficiency of an idealized wind farm by 5 to 10% by relocating the floating turbines. The exact gain depends on the wind direction for which the farm is being repositioned.

Alternatively, some of the mechanical properties of the floater can also be adapted during operation. For specific floaters, water can be pumped into the columns altering the roll or platform pitch angle of the platform. Pitching the platform of a floating turbine has a similar effect on the wake as when the nacelle of a turbine is intentionally misaligned in yaw with the incoming flow. In both cases, the misalignment creates a force component perpendicular to the incoming flow that deflects the wake behind the turbine. The concept of pitching the floating platform is explored in [60], where a 5% increase of the cluster is realized when the floater of the upstream turbine is pitched forward by 20 degrees. At this platform pitch angle, the turbine deflects the wake towards the sea allowing higher energy flow to enter from above the wake and reach the downstream turbine.

When the aforementioned wake mixing techniques are applied to a floating turbine, the time-varying thrust will excite the six degrees of freedom. If and how this movement influences the effectiveness of the wake mixing technique depends on the coupling between the wake control method and floating turbine dynamics. For the Pulse and the Helix, this is explored in [74, 91, 112]. Furthermore, using the motions of the turbine for the benefit of wake mixing is patented in [113].

For the Pulse, the coupling was found to *reduce* the effectiveness of this particular wake mixing method. The work presented in [74] used prescribed motions to mimic the motions of a floating wind turbine. This approach, however, does not capture any further coupling between the platform motions and the mechanisms behind the Helix wake mixing technique.

This highlights one of the research gaps when transitioning controllers from bottom-fixed to floating turbines. Controllers optimized for bottom-fixed turbines might underperform when coupled to a floating turbine, or new optimal operating conditions need to be derived to account for the platform dynamics of the turbine.

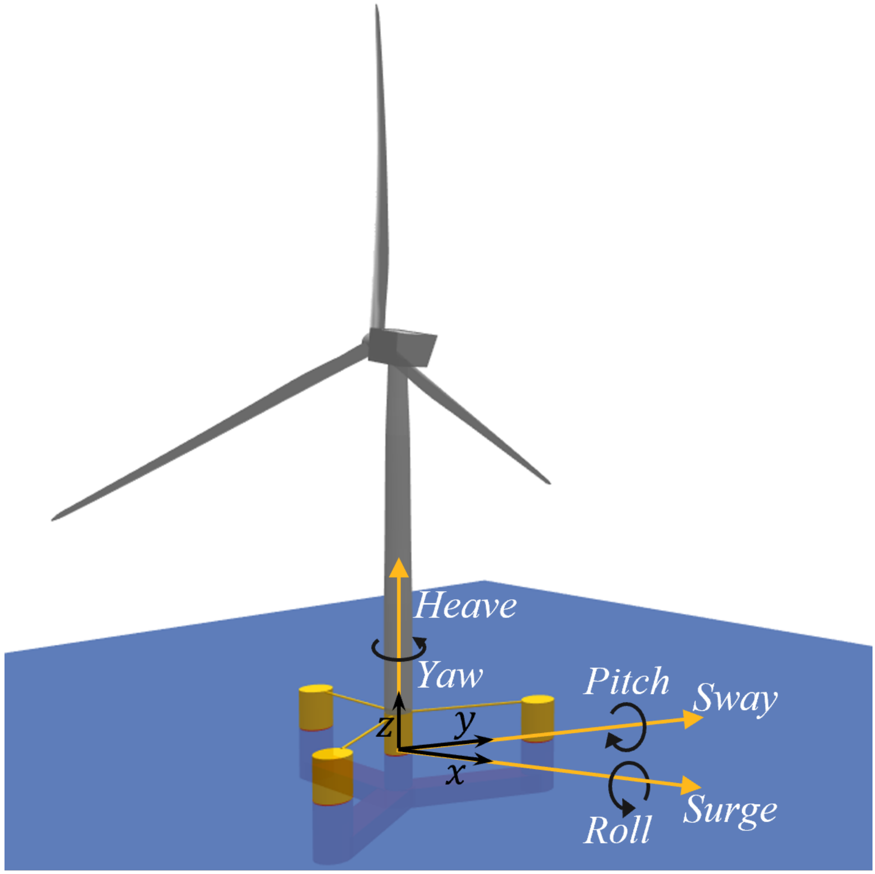

Figure 3.3: Axes system showing the six degrees of freedom for a floating turbine.

3.1.3 Research Objectives

This work presents a comprehensive overview of the Helix wake mixing method and the coupling between aerodynamics and the structural- and hydrodynamics of a floating wind turbine. First, a frequency domain analysis of the coupling between Helix and platform motions is presented and second, time domain simulations are executed to investigate the system using its full nonlinear representation. For these simulations, QBlade is used [114]. QBlade is a simulation suite capable of simulating hydro-, aero-elastics and wake dynamics.

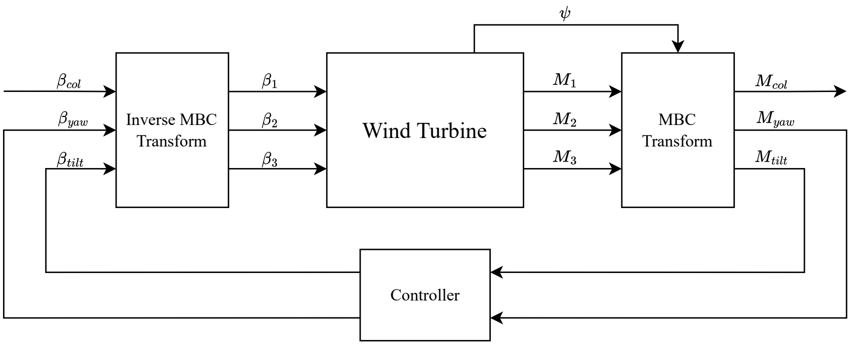

Figure 3.4: General closed-loop control scheme for the IPC control method. Individual blade pitch angles are given by β_i with $i \in [1,2,3]$ and the out-of-blade root bending moments by M_i. The main objective of IPC is to minimise the fixed-frame tilt, M_{tilt}, and yaw, M_{yaw}, moments, which can be obtained from the blade individual moments using the MBC transform.

3.2 The Development of the Helix Method

This section will introduce the Helix wake mixing method. First, the Helix method's principle, derived from individual pitch control (IPC) for load mitigation and dynamic induction control, will be introduced. Second, an interpretation will be given of the Helix's effect on the wind turbine's thrust vector and finally, how it induces wake mixing and its effect on the downstream wake. The appendix "Background on Wake Mixing" provides a short aerodynamic background to the mixing process.

3.2.1 Individual Pitch Control

The Helix method was first proposed in [110] and further explored, e.g., in [44]. The main characteristic of the Helix is that it leverages the blade pitch degree of freedom of a wind turbine to manipulate the location of the point of origin of the resulting thrust vector. As a result of this dynamic thrust vector, the force exerted on the incoming flow will also be time-varying which, when excited at the right frequency, can lead to wake mixing increasing the power production of the downstream turbine. The inputs required to create the Helix are based on the same signals that are used for load mitigation using IPC. It is, therefore, useful to consider the development of IPC and its, mainly mathematical, similarities to the Helix method.

IPC was developed with the goal of load mitigation [115, 116] and continues to be a topic of active research, see for example [94, 117]. Typically, the dynamics and thus loads of a wind turbine are described in the rotating frame. The objective of an IPC controller is to minimise the fixed frame loads to extend the lifetime of the turbine. The loads on the blades that are described in the rotating frame, can be translated into loads on the fixed turbine using the multi-blade-coordinate transformation (MBC) [118].

The scheme of Figure 3.4 shows the general form of an IPC loop using the MBC. The blade root moments M_i, with $i \in [1,2,3]$, are transformed into the fixed-frame moments using the MBC transformation. Mathematically the MBC transformation can be expressed

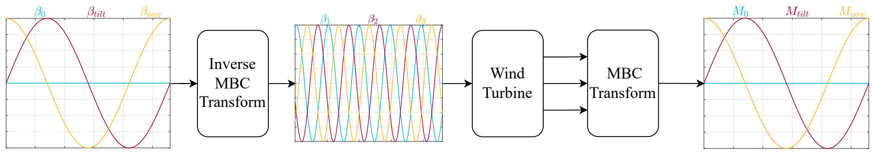

Figure 3.5: General open-loop control scheme for the Helix wake mixing method. Contrary to IPC, the individual blade pitch angles are derived using the inverse MBC transform from the fixed-frame input signals. When applied to the turbine, the resulting fixed-frame moments are similar to the input fixed frame blade pitch angles.

3

as

$$\begin{bmatrix} M_{col}(t) \\ M_{tilt}(t) \\ M_{yaw}(t) \end{bmatrix} = \frac{2}{3}\begin{bmatrix} 0.5 & 0.5 & 0.5 \\ \cos(\psi_1(t)) & \cos(\psi_2(t)) & \cos(\psi_3(t)) \\ \sin(\psi_1(t)) & \sin(\psi_2(t)) & \sin(\psi_3(t)) \end{bmatrix}\begin{bmatrix} M_{y,1}(t) \\ M_{y,2}(t) \\ M_{y,3}(t) \end{bmatrix}, \tag{3.1}$$

in which M_{col}, M_{tilt} and M_{yaw} are the fixed-frame moments and ψ_i the azimuth angles of the individual blades with $i \in [1,2,3]$. The subscript col in M_{col} refers to the *collective* moment, i.e., the moment on the entire rotor rather than the tilt or yaw axis. The transformation from individual blade pitch angles to fixed frame blade pitch angles is synonymous to (5.3). The controller will output fixed-frame blade pitch angles which can be transformed back to individual blade pitch angles using

$$\begin{bmatrix} \beta_1(t) \\ \beta_2(t) \\ \beta_3(t) \end{bmatrix} = \begin{bmatrix} 1 & \cos(\psi_1(t)) & \sin(\psi_1(t)) \\ 1 & \cos(\psi_2(t)) & \sin(\psi_2(t)) \\ 1 & \cos(\psi_3(t)) & \sin(\psi_3(t)) \end{bmatrix}\begin{bmatrix} \beta_{col}(t) \\ \beta_{tilt}(t) \\ \beta_{yaw}(t) \end{bmatrix}, \tag{3.2}$$

which is known as the inverse MBC transform.

3.2.2 From IPC to the Helix

While the main goal for IPC is to minimize the time-varying tilt and yaw moments (M_{tilt} and M_{yaw}), with the Helix method, a time-varying tilt and yaw moment is applied to the turbine. This is achieved by applying, in open loop, a time-varying signal to the fixed frame tilt, β_{tilt}, and yaw, β_{yaw}, pitch angle. A schematic representation of the open loop is given in Figure 3.5.

The type of signal used as an input in the fixed-frame can be chosen freely. For this work, the inputs derived in [44] are used, which are two sinusoidal inputs on both the tilt and yaw axes

$$\beta_{tilt} = A_t \sin\left(2\pi S_t \frac{V_\infty}{D} t\right), \tag{3.3a}$$

$$\beta_{yaw} = A_y \sin\left(2\pi S_t \frac{V_\infty}{D} t \pm \frac{\pi}{2}\right), \tag{3.3b}$$

in which A_t and A_y are the blade pitch angle amplitudes [deg], V_∞ the free-stream wind speed [m/s], D the rotor diameter [m] and S_t is a dimensionless frequency characterized by the Strouhal number. The Strouhal number is defined as

$$S_t = \frac{f_e D}{V_\infty}, \tag{3.4}$$

in which f_e is the actuation frequency [Hz]. The phase difference $\pm\frac{\pi}{2}$ in (3.3b) determines if the Helix is applied in a clock-wise or counter-clockwise manner [44]. For example, the signals shown in Figure 3.5 are for a counter-clockwise Helix (which equals to a phase lead of $\pi/2$ in (3.3b)). The work in [44] shows that both clock- and counter-clockwise versions of the Helix are able to increase downstream wind speeds, but the counter-clockwise version proved to be more effective. The reasons for this are a current topic of research. As such, the counter-clockwise Helix will be used throughout this work.

Varying the tilt and yaw moment causes the origin of the thrust vector of the turbine to change its location with respect to the centre of the turbine. This is schematically depicted in Figure 3.6, which shows the front view of a wind turbine. Each blade is colour coded to match the individual pitch angle signals shown in Figure 3.5.

At any given time, each of the blades will have a different pitch angle except at certain time instants when at most two blades have the same pitch angle. The differing blade pitch angles result in different aerodynamic forces acting on each blade. As a result, the overall turbine thrust vector is no longer centred in the rotor plane but rather at an offset to the centre. In Figure 3.6, this offset is represented by the green arrows, which also, *schematically,* represents the path of the resulting thrust vector during one period of the Helix. This period is in order of 10 times longer than the rotational period of the turbine, i.e., when the Helix has completed one period the turbine has rotated approximately 10 times. In reality, the offset is significantly smaller, typically in the order of a few meters. A major difference to the Pulse wake mixing technique is that with the Helix, the magnitude of the thrust force remains unchanged and only the origin of the thrust force changes over time considering ideal conditions.

The effect of this moving thrust on the wake velocity profile can be seen in the wake of the rightmost turbine in Figure 3.2. The darker shaded area behind the turbine indicates an area of lower wind speed than the free stream, which is transparent. As the thrust vector is moving over the rotor plane, the incoming wind is most slowed down at its location. Directly opposite to the thrust vector the local induction, i.e., force opposing the incoming flow, is the lowest resulting in the highest local wind speed. This creates a rotating area of lower and higher wind speeds that, as it moves downstream from the turbine, create a characteristic helical shape of wind speed in the wake. The Helix method obtains its name from this shape.

The area of low wind speed in Figure 3.2 starts to dissipate after travelling roughly 4 rotor diameters of distance downstream as the wake mixes with the outside flow increasing downstream wind speed. The effectiveness of the Helix is dependent, among other factors, on the amplitude of the blade pitch angles and its application frequency. Current research indicates that the most gain in wind speed for the Helix is achieved between $S_t = 0.30$ and $S_t = 0.40$ for a two-turbine wind farm with turbines spaced at $5D$ [119, 120]. The exact aerodynamic principle behind this is still a topic of research, see, for example, [121–124]. It should be noted that the relative gain is distance-dependent. As the wake travels further downstream, more natural mixing occurs and the overall contribution of the Helix is lower.

3

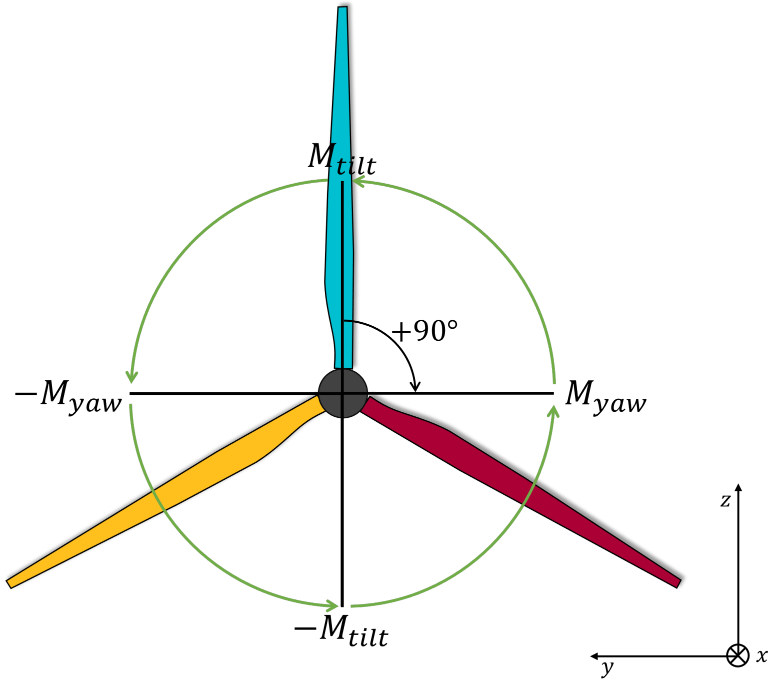

Figure 3.6: Front view of the rotor plane of a wind turbine. As each blade is pitched the thrust vector will move, off-centre, clock or counter-clockwise over the rotor plane. This dynamic induction zone promotes the onset of wake mixing.

Closer to the turbine the natural mixing process has not started yet and the wind speed in the wake is still low.

Typically, research into wake mixing methods focuses on increasing the energy of a turbine located at a distance of five rotor diameters. On average the spacing in current offshore wind farms is ten rotor diameters [125, 126]. Furthermore, if significant gains in power production can be achieved for distances closer to the upstream turbines, it is also feasible to pack more turbines within the same wind farm, further increasing its power production.

For bottom-fixed turbines, the Helix has shown significant potential to mitigate the turbine-to-turbine interaction. The time-varying moments which are applied to the turbine using the Helix method will interact with a floating structure. When a tilt moment is applied, the turbine will likely change its floater pitch angle, changing the inflow angle. When a yaw moment is applied, the floating turbine will yaw, resulting in yaw misalignment of the turbine with respect to the flow. These movements will affect the flow behind the turbine. Furthermore, the misalignment of the turbine with respect to the incoming flow creates a tangential force component at the location of the rotor thrust vector. Either or both of these effects can potentially influence the wind speed downstream, be it by affecting the wake mixing technique directly or by interacting with the aerodynamic mixing process.

3.3 Coupling Between the Helix Method and the IEA 15MW Floating Turbine Motions

This section provides an in-depth analysis of the movements of the IEA 15MW turbine [127] mounted on the VolturnUS-S floater [128] when using the Helix method. To gain a better understanding of the coupling frequency response functions are analyzed. These responses are obtained from input-output data acquired from identification experiments [88]. The identified response functions provide insight into how the platform dynamics of the floater and the dynamics of the Helix couple. The frequency response data give insight into the dynamics of a single turbine and how it interacts with the Helix method, but not the impact on the wake mixing process. The influence of the resulting motion on the wake is discussed in the next section.

3.3.1 Simulation Tools and Research Methodology

All investigations presented in this research are conducted using QBlade [114]. QBlade is capable of simulating coupled aerodynamics, structural dynamics and hydrodynamics. To model the turbine and wake aerodynamics, a free wake vortex method is used. The vortex method was originally developed for modelling the wake of helicopter rotors [76, 77]. Its benefits over comparable computational fluid dynamic methods primarily come from being computationally more efficient without major loss of accuracy [78].

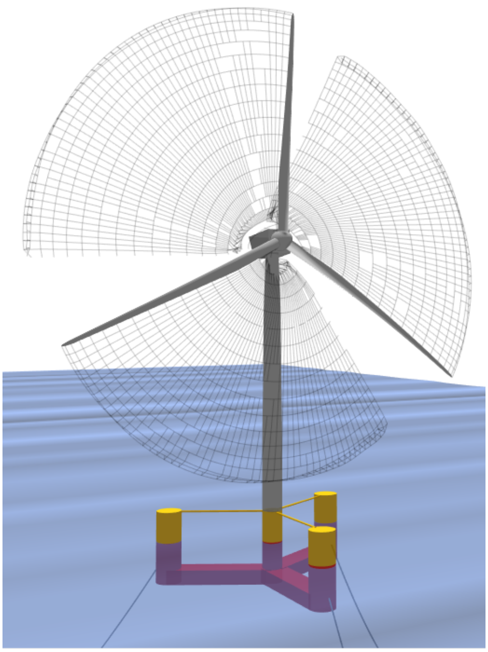

Figure 3.7: A close-up of the IEA 15MW turbine on the VolturnUS-S floater in QBlade. The image is taken at the start of the simulation at which only the near wake is visible represented by the black lines which are vortex elements released in the wake.

The free vortex method as used in QBlade can be viewed as a low-cost alternative method of simulating the wind turbine wake. The majority of the research investigating the wakes of individual wind turbines or wind farms uses some form of large-eddy simulations to investigate near and far wake behaviour whilst being reasonably efficient. However, for LES simulations the whole domain needs to be discretized with finite-volume elements. In general, reducing the size of these volume elements increases the accuracy of the resolved wake at the cost of growth in computational costs.

The free vortex method models the wake and flow field using a Lagrangian approach. These methods have previously successfully been used to model wind turbine wakes [79, 80, 129–131]. In [79] the predicted wake breakdown location is analyzed using the same free vortex wake code as used in this work. It is compared to an identical simulation carried out in LES and other literature data. It was observed that the transition position aligns well with the predictions of LES modelling. Beyond the point of transition, however, the LLFVW model does not accurately capture the effect of turbulent diffusion. Furthermore, the same work also describes how the actuation of flaps located near the tip of the blade can accelerate the tip-vortex pairing, a process that instigates wake breakdown. Finally, it also proposes a solution to improve upon the accuracy of the current implementation of the free vortex wake method.

An important distinction between [79] and this work is that the frequency at which the control is implemented is an order of magnitude lower for the Helix method compared to the flap control used in [79]. As this work focuses on the behaviour of the wake near the upstream turbine and only up to five D downstream, the free wake vortex method can be used. To understand the wake behaviour a quantitatively accurate method such as LES is required to validate these approaches and explore more accurately the impact of turbulent statistics in the post-transition region.

The IEA 15MW, [127], on the VolturnUS-S, [128], floater, as modelled in QBlade, can be seen in Figure 3.7, including part of the wake represented by the free vortex elements. For every simulation conducted in this work, the inflow wind speed is uniformly distributed and set at 9 m/s. This represents an ideal case scenario for the wake mixing strategy. At this wind speed, the turbines are operating in below-rated conditions and extract all available energy from the flow. In above-rated conditions, there is typically enough energy in the flow behind the turbine that any waked downstream turbines can also operate near or at rated power [24, 132]. A further reason for choosing a fixed wind speed is that the excitation frequency, defined by the Strouhal number, (3.4), is wind speed dependent. Considering multiple wind speeds would complicate the analysis and increase the number of simulations.

Finally, the flow is considered to be laminar. When turbulent inflow is used, natural mixing occurs in the wake. This reduces the relative effectiveness of the wake mixing technique. However, wake mixing can still be beneficial even when turbulence is considered. The work in [123] and [124] use synthetic turbulence in their simulation, i.e., turbulence is superposed onto a mean inflow. For both works the turbulence intensity (TI) is around 5%. Similarly, work on the Helix in [44] and [122] includes turbulence developed in an atmospheric boundary layer. In [44] the TI is set to 5% over the whole domain whereas [122] uses a TI that varies between 3% at the top of the turbine and 5.8% at the bottom. What these four investigations have in common is that the turbulence level is relatively low. It is expected that this control strategy will be applied in conditions with a TI level in this range as it is most effective for those conditions. Omitting turbulence from the simulation enhances the effect of the Helix method on the wake allowing for easier comparison of the wake behaviour between that of a bottom-fixed turbine and a floating turbine.

For the simulations of the floating turbine, a wave field is included in the simulation. The presence of a wind field above a still body of water will generate waves [133], so-called wind-swept waves. The exact nature of the waves is site-dependent and is determined through site-specific assessments. When site-specific information is not available during the design phase of the turbine, the IEC 61400-3-1:2019 standard can be used [134]. The table with wind speeds and associated wave parameters can be found in [128], see Table 12 in that work. The size and frequency content of these waves is parameterized using a JONSWAP wave spectrum [135]. For the interested reader, a detailed description of QBlade can be found in the appendix "Aero-servo-hydro-elastic models in QBlade". The specific settings used in this work can be found in the Chapter 2.

3.3.2 Frequency-Domain Analysis

To capture the dynamics of the IEA 15MW floating turbine, the system is excited using a chirp signal. This signal is chosen such that it excites the system over $1 \cdot 10^{-3}$ to 1 Hz frequency range. The input is logarithmically distributed over the full duration of the experiment such that more of the data collected is generated at lower frequencies. The full experiment produces 28800 seconds (8 hours) of data. In previous work, it was identified that for semi-submersible platforms, like the VolturnUS-S platform, the yaw motion is dominant [74]. For that reason, the chirp is applied to the fixed frame β_{yaw} input.

Figure 3.8 shows the frequency response for all six degrees of freedom of the floating turbine as a function of blade pitch angle. The data is presented as the ratio between the input and output spectra. Beyond 0.1 Hz the system becomes insensitive to any input which is the reason the data is displayed up to 0.1 Hz even though the system is excited to 1 Hz. Included in Figure 3.8 are vertical lines at three frequencies typically considered for wake mixing. The corresponding Strouhal number for the IEA 15MW turbine is annotated above the dashed lines. Between $S_t = 0.10$ and $S_t = 0.50$, the wake mixing process is most effective. Higher Strouhal numbers result in less effective wake mixing as the blade pitching is no longer triggering the wake instabilities.

In terms of absolute gain, two of the six degrees of freedom are excited almost equally. These are the sway and yaw motions, both with a peak gain of 2.5 albeit at different frequencies. However, given the scale of the turbine, the absolute displacement of the sway motion can be considered negligible. For example, if the Helix were applied with a four degree blade pitch amplitude on both fixed frame coordinates, the turbine would displace at most 10 metres which is considered small compared to the rotor diameter. On the contrary, the same input results in ± 10 degrees of yaw misalignment, which can be considered a sizeable yaw misalignment angle. Aside from these two motions, the remaining 4 degrees of freedom are excited an order of magnitude smaller or are excited at frequencies outside the range of interest for wake mixing.

The presence of waves will also cause the platform to undergo a degree of motion. However, wave excitation often occurs in a frequency range an order of magnitude higher than that of the Helix. When designing a floating vessel Response Amplitude Operators, or

RAOs, are constructed to represent the response of the vessel to wave inputs at different frequencies [92]. For the VolturnUS-S reference platform, the RAOs can be found in [128]. The platform motions for a wavefield with a similar wave height as used in this work are small such that their impact on the wake is negligible. Especially in yaw, the Helix-induced yaw motion will be significantly larger than that of the wave forces.

From the frequency response data, it is possible to evaluate if the yawing motion affects the Helix method. This can be measured by evaluating the transfers from the fixed frame blade pitch angles to the fixed frame tilt and yaw moments. These transfer functions provide insight into the full coupling between the aero- and platform dynamics. The relations between blade pitch input and fixed frame tilt and yaw moments are shown in Figure 3.9, where the data for M_{tilt} and M_{yaw} is normalized with respect to the maximum value of M_{yaw}. In the same figure the response of the yaw motion to β_{yaw} is also included.

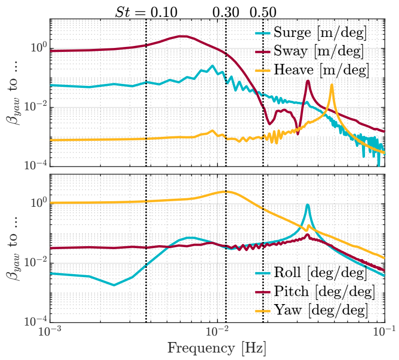

Figure 3.8: Frequency responses for the IEA 15MW turbine on the VolturnUS-S semi-submersible platform for all 6 degrees of freedom. The vertical dotted lines represent the frequencies for 3 different Strouhal numbers. At different actuation frequencies, the platform will undergo differing types of motion.

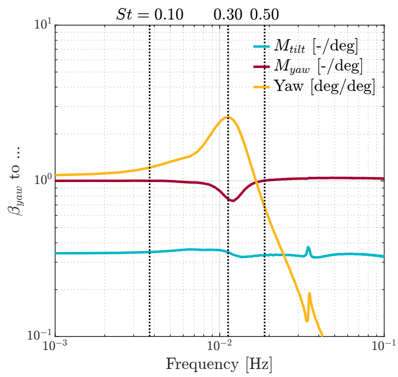

Figure 3.9: Frequency responses showing the gain in yaw motion and the gain in M_{tilt} and M_{yaw}. The M_{tilt} and M_{yaw} responses are normalized with respect to the maximum value of M_{yaw}. The vertical dotted lines represent the frequencies for 3 different Strouhal numbers.

Even though the experiment only uses the β_{yaw} input, there is still a response on the M_{tilt} axis. Hence, a coupling exists between the fixed-frame yaw and tilt axis with this implementation of the MBC transform. This can be solved by including an azimuth offset in the transformation [117]. When the yaw motion is small (gain ≈ 1 or lower), the gain for the yaw moment remains constant. However, at the eigenfrequency of the yaw motion, there is a small antiresonance in the yaw moment. Coincidentally, the frequency range where the yaw motion is most prominent is also the frequency range where the Helix is most effective.

The investigation presented in this section indicates that there exists a two-way coupling between the dynamics of the Helix and the platform dynamics of the floating turbine. The yaw movement of the floating turbine reduces the yaw moment of the Helix. The impact that this has on the wake mixing behind the turbine will be investigated in the following section.

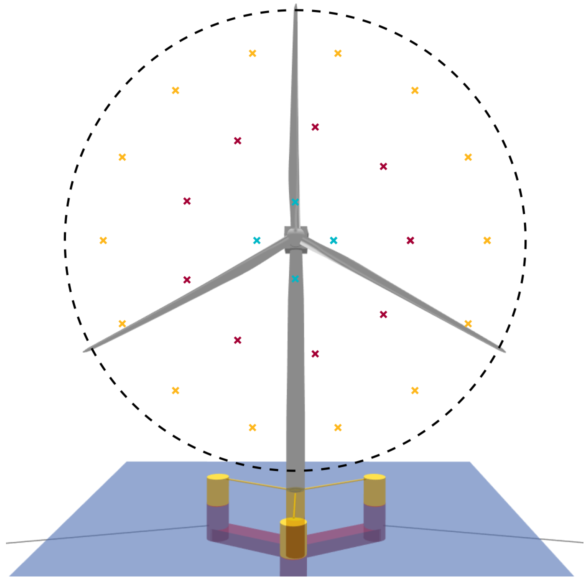

Figure 3.10: Front view of the IEA 15MW turbine mounted on the VolturnUS-S platform with the points at which the wind speed is measured. The rotor swept area is indicated by the dashed circle.

3.4 Time-Domain Analysis of Wake Recovery

This section will analyse the dynamics of the wake mixing process and whether the yaw movement has any impact on it. This is done by comparing the wind speed downstream of the turbine for different Strouhal numbers. Wake recovery can be evaluated by comparing the wind speed at different distances downstream to a baseline case. Furthermore, all simulations will be run for two different amplitudes for the blade pitch angles, to assess the impact of different blade pitch angles.

For comparison, the same simulations will be executed for a bottom-fixed version of the IEA 15MW turbine. By comparing the simulations for a floating turbine to those of a bottom-fixed turbine, the impact of the motion can be better analyzed. First, the simulation cases and the metrics that are being analysed will be introduced. Second, the results of the simulations are presented.

3.4.1 Time-Domain Simulation Scenarios

All simulations carried out in this work were done using the software-in-the-loop interface of QBlade [136]. The settings, as described in Chapter 2, were used for all simulations. The total simulation time for each simulation was 1600 seconds, of which the first 400 seconds were omitted to remove transients from the simulation initialisation. The remaining 1200 seconds were used for the data analysis.

For the baseline case, both the bottom-fixed and floating turbines have their blade pitch angle set to 0 degrees. Maximum power extraction is achieved by employing a $k\omega^2$ controller that controls the generator torque such that the turbine operates at the optimal

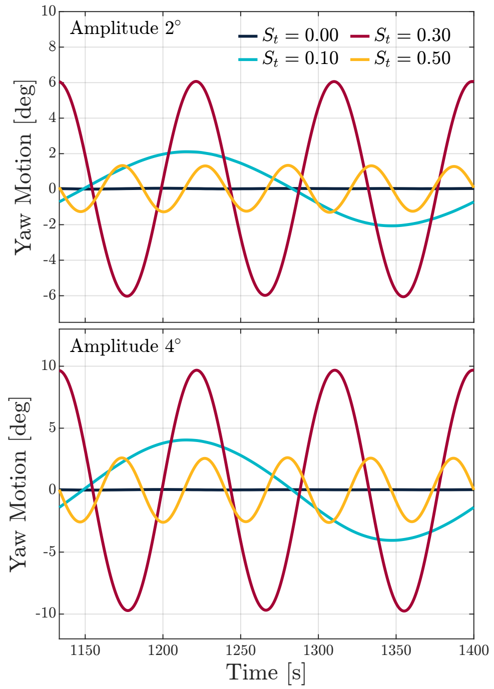

Figure 3.11: Yaw motion for the 2-degree (top figure) and 4-degree (bottom figure) Helix input amplitudes. The selected data are the results for the baseline cases and 3 different Strouhal numbers. The yaw motion at $S_t = 0.30$ exhibits the largest amplitude. The amplitude in yaw motion for the 2-degree input is slightly larger than the gain found in the frequency response functions.

tip-speed ratio [137]. For each simulation, the wind speed is retrieved at the following distances

$$D = \begin{bmatrix} -1.0 & 0.0 & 1.0 & 2.0 & 2.5 & 3.0 & 3.5 & 4.0 & 4.5 & 5.0 & 6.0 \end{bmatrix}. \tag{3.5}$$

As the floating turbine has a steady-state surge offset, an offset of ≈ 16 m is applied to (3.5). The average wind speed is retrieved at the points shown in Figure 3.10. This number of points was found to be a good trade-off between computational expense and accuracy. The average wind speed as measured at these locations provides insight into the potential power production for a second downstream turbine.

The Helix is applied with a blade pitching amplitude of 2 and 4 degrees. At these amplitudes the wake mixing process will be triggered by the Helix method and at the same time it provides insight into a, potential, non-linear relation between yaw motion and the Helix method. It could be that at smaller platform yaw angles it provides a benefit which is diminished at larger yaw angles. To investigate the impact of the motion, the application frequencies used in this work cover the full range in which wake mixing is effective. The following Strouhal numbers were chosen

$$S_t = \Big[0.00\ 0.10\ 0.15\ 0.20\ 0.25\ 0.30 \ldots \\ \ldots 0.35\ 0.40\ 0.45\ 0.50\ 0.60\ 0.70 \Big], \tag{3.6}$$

in which $S_t = 0.00$ represents the baseline case. Research indicates that an optimum frequency exists for wake mixing, which is dependent on the distance to the next downstream turbine. For dynamic induction control, this is $S_t = 0.25$ for a two-turbine wind farm spaced at 5 rotor diameters [43]. By evaluating the wind speed over distance, (4.3), and Strouhal number, (3.6), this ideal frequency can be found for the Helix. Furthermore, comparing the data from bottom-fixed and floating turbines can provide insight on whether the optimum changes are due to the extra dynamics of a floating turbine.

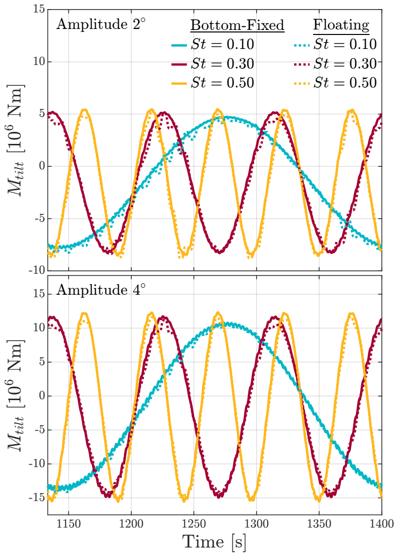

Figure 3.12: Tilt moment for the 2-degree (top figure) and 4-degree (bottom figure) blade pitch amplitudes for the same 3 Strouhal numbers considered in Figure 3.11. The solid lines represent the data from the bottom-fixed IEA 15MW turbine and the dotted lines that of its floating counterpart. The high frequency variations in tilt moment are due to the waves hitting the floating turbine.

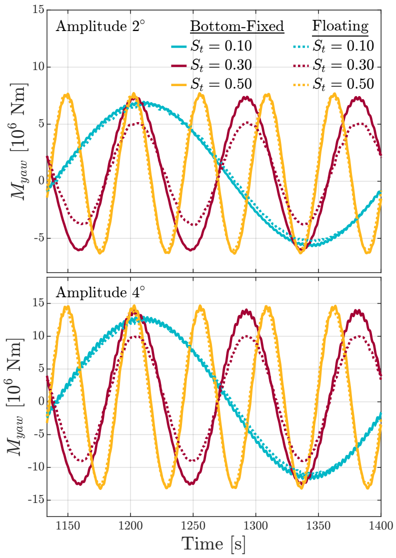

Figure 3.13: Yaw moment for the 2-degree (top figure) and 4-degree (bottom figure) blade pitch amplitudes for the 3 different Strouhal numbers considered in Figure 3.11. The solid lines represent the data from the bottom-fixed IEA 15MW turbine and the dotted lines that of its floating counterpart. For both $S_t = 0.10$ and $S_t = 0.5$, there is essentially no difference between bottom-fixed and floating cases. At the eigenfrequency in yaw motion, there is a notable decrease in the yaw moment.

3.4.2 Time-Domain Simulation Results

The results will be presented in three different subsections. First, the yaw motion and yaw- and tilt moment for both blade pitch amplitudes will be shown. For these data sets,

3

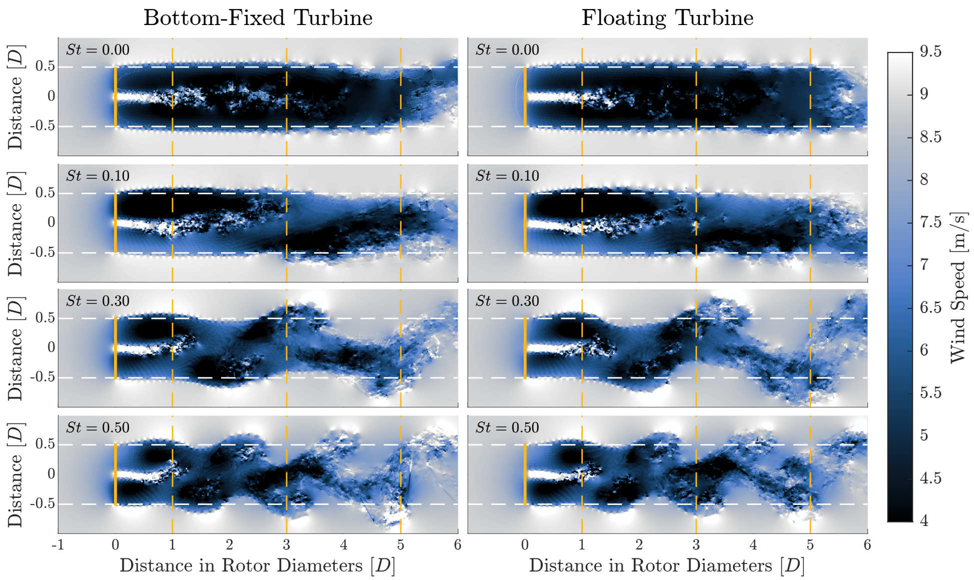

Figure 3.14: Instantaneous velocity slices at hub height for 4 different actuation frequencies. From top to bottom, the following frequencies are shown: $S_t = 0.00$, $S_t = 0.10$, $S_t = 0.30$ and $S_t = 0.50$. The left column shows results for the bottom-fixed turbine and the right column the floating turbine. The solid yellow line indicates the position of the turbine. Notice how the wake at $S_t = 0.30$ has deflected more at $3D$ and $5D$ for the floating turbine. Colour map courtesy of [138].

three different Strouhal numbers are chosen. These Strouhal numbers represent the system behaviour before, at, and after the eigenfrequency. Furthermore, the time-domain data at these three frequencies can be used to verify the results found using the frequency response functions. Secondly, the average wind speed downstream is evaluated. By looking at the wind speed downstream and comparing it to the baseline case the accelerated wake recovery can be quantified. Finally, the average aggregated power production of the two turbine wind farms is compared. Higher actuation frequencies and larger amplitudes lead to a loss in the power production of the actuated turbine. Furthermore, if an optimum exists for wake recovery, i.e., a Strouhal number and distance where the relative gain in wind speed is largest, this combination of Strouhal and distance does not necessarily result in the highest gain of power production.

Turbine Time-Domain Response

The yaw motion for the three different Strouhal numbers and both blade pitch amplitudes are shown in Figure 3.11. The time range shown is equal to one period for $S_t = 0.10$. Included in Figure 3.11 is the yaw motion for the baseline case. The incoming waves do not perturb the turbine such that they create any significant yaw motion. This is for two reasons. First, the wave field used is aligned with the incoming flow and does not excite the yaw degree of freedom. Second, the wave field used represents a calm sea for this wind condition and therefore wave forces are relatively small.

The amplitude in yaw motion for the two-degree input peaks at six-degrees. This is

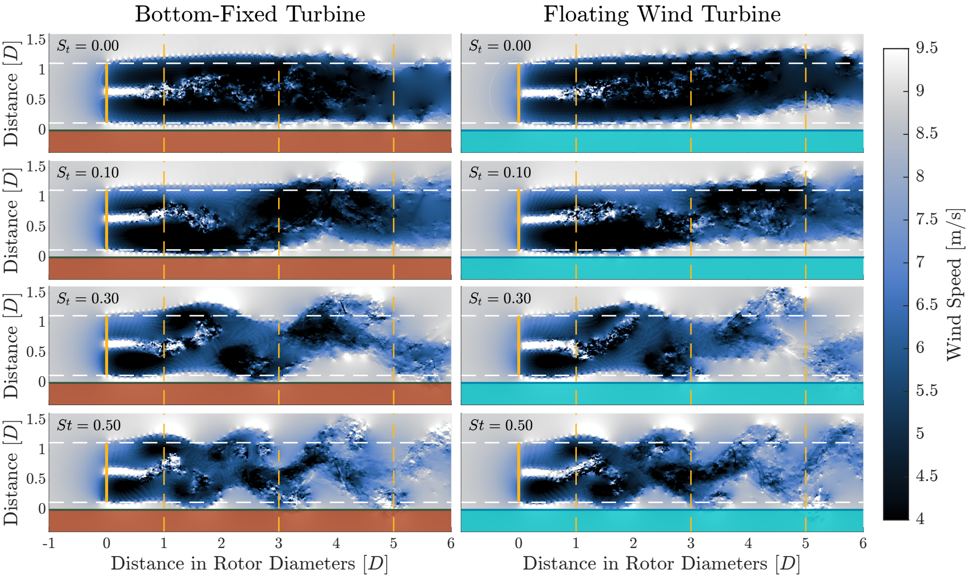

Figure 3.15: Instantaneous velocity slices taken from a side view for 4 different actuation frequencies. From top to bottom, the following frequencies are shown: $S_t = 0.00$, $S_t = 0.10$, $S_t = 0.30$ and $S_t = 0.50$. The left column shows results for the bottom-fixed turbine and the right column the floating turbine. The solid yellow line indicates the position of the turbine. The ground and sea are marked by the coloured rectangles. Notice how even without actuation the wake deflects upwards for the floating turbine, a result of the whole floating structure having a floater pitch offset. Colour map courtesy of [138].

higher than the expected amplitude based on the gain found in the frequency response experiment. For the four-degree input, the amplitude of the yaw motion matches the gain, as the identification input is four degrees. The greater-than-expected motion at two degrees can be explained by the fact that both the stiffness and damping of a floating vessel are dependent on the amplitude and velocity of the motion [92]. At the lower blade pitch amplitude, the platform has a lower yaw velocity and thus the interaction between the floater movement and the water is different compared to the four-degree case. This nonlinear behaviour of the stiffness and damping can be one of the reasons why there is a difference in expected versus actual yaw amplitude.

The tilt and yaw moments for the bottom-fixed and floating turbines are shown in Figures 3.12 and 3.13. For the tilt moment, see Figure 3.12, there are only small differences in peak-to-peak amplitude when comparing the floating and bottom-fixed turbines. This can potentially be put down to the nacelle moving forward and backwards due to wave-induced motion or the applied tilt moment. The larger yaw movement does have an impact on the yaw moment that is generated by the Helix.

Figure 3.13 shows the comparison of the yaw moment for the bottom-fixed and floating turbine. When actuated at $S_t = 0.30$ there is a significant reduction in yaw moment which confirms the frequency analysis. The reduction in yaw moment can be explained by the fact that as the turbine is undergoing yaw motion part of the turbine is moving away from the incoming flow, reducing the effective wind speed. If the fixed frame thrust force, which

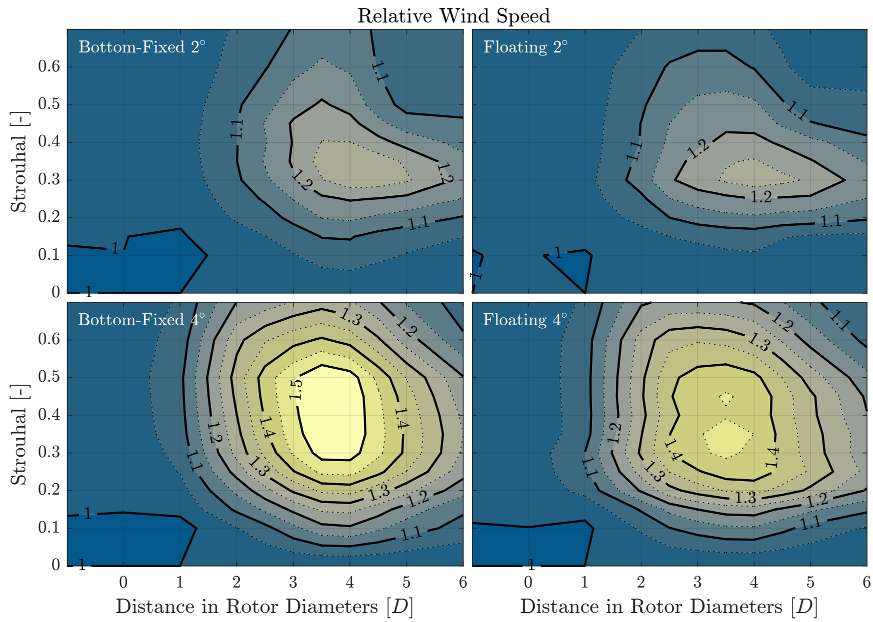

Figure 3.16: Contour plots that show the relative gain in the time-averaged downstream wind speed for both hypothetical bottom-fixed and floating turbines for both blade pitch amplitudes. The wind speed is measured directly behind the upstream turbine. For all actuated cases, wake recovery is accelerated with respect to the baseline case. Furthermore, there exists an area where the gain is highest, indicating that the relative wake recovery is highest at that Strouhal and distance. Colour map courtesy of [138].

is a function of effective wind speed, is located in the half moving away from the flow the thrust will be reduced. This translates to a reduction in applied yaw moment. A change in phase coupling between blade pitch input and yaw motion could therefore also lead to different behaviour.

There exists no such reduction in tilt moment for the Helix method. A reduction of tilt moment would be expected if the platform undergoes either surge, platform pitch motion or a superposition of both. The fore-aft motion influences the relative velocity the turbine experiences which affects the thrust of the turbine. However, the eigenfrequency in surge and platform pitch are located at 0.007 and 0.036 Hz respectively [128], the latter being outside the Strouhal range of interest. Both eigenfrequencies can be seen appearing in Figure 3.8.

For the effect on the Helix, these time domain results can be interpreted as follows: where for a bottom-fixed turbine the thrust vector would move in a circular pattern over the rotor plane, it now resembles more of an oval path. As the wake mixing performance is related to the variation in the strength of the released vorticity, this reduction in yaw moment would, all other things being equal, lead to a reduction in wake mixing. However, this assumes that the extra yaw misalignment has no positive impact on this process, which is evaluated in the next section.

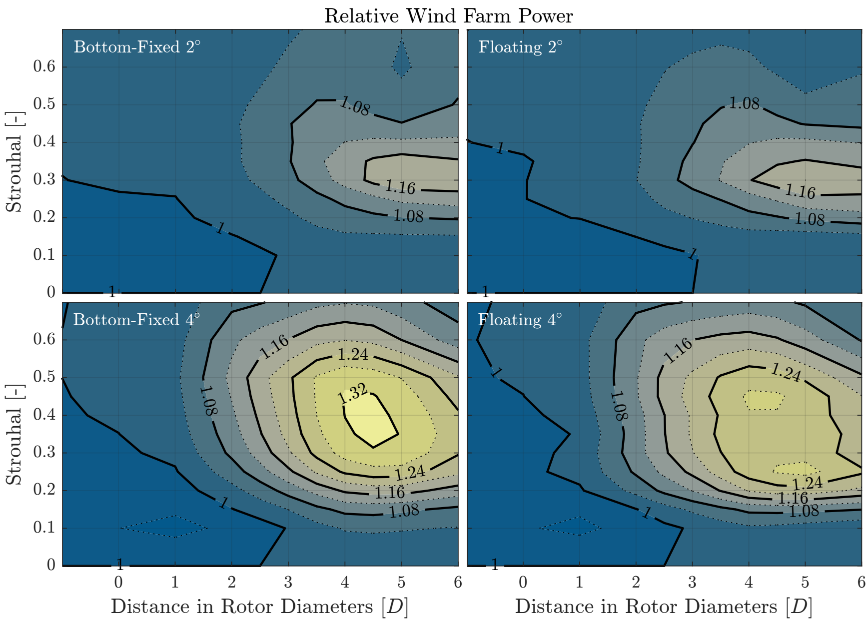

Figure 3.17: These contour plots show the relative gain in power production for both bottom-fixed and floating wind farms for both blade pitch blade amplitudes. As the wake recovers to higher windspeeds, more power can be produced by the wind farm. The areas of the highest relative gain have moved further downstream with respect to the wind speed results. For the four-degree results with the floating turbine, two areas of equal gain appear. Colour map courtesy of [138].

Average Wind Speed Results

An instantaneous snapshot of the wakes from both a top and side view are shown in Figures 3.14 and 3.15. The left column shows the wake of the bottom-fixed turbine, while the right column shows the wake of the floating turbine. For all actuated cases, the blade pitch amplitude is four degrees. Areas of darker colour indicate areas of low wind speed, and the higher the wind speed the lighter the colour. For the baseline cases ($S_t = 0.00$), wake recovery only starts around $5D$. When the Helix is enabled, the wake shows patches of lower and higher wind speed. The patches of lower speed are part of the helical structure in the wake that is specific for the Helix method, see Figure 3.2. At higher frequencies, more of these patches appear as the thrust vector rotates with a higher velocity over the rotor plane, creating more helices. When comparing the wake for the bottom-fixed and floating turbines at $S_t = 0.30$ it can be seen that the wake for the floating turbine shows more lateral movement. Especially at $3D$ and $5D$, the wake has moved further sideways compared to the bottom-fixed turbine. In the side view an upward deflection of the wake can be recognised. This deflection is a result of the platform pitch angle which results from the thrust force on the floating structure.

The wake mixing performance can be evaluated using the time-averaged downstream wind speed. The fact that the wake deflects under dynamic yaw motion is apparent from the snapshot depicted in Figure 3.14. Figure 3.16 shows the average gain in wind speed with respect to the baseline for both blade pitch amplitudes and turbines. The left column shows the results for the bottom-fixed turbines and the right column presents the results for the floating turbine. For the two-degree blade pitch amplitude cases, there is a distinct area where the gain in wind speed is highest. The largest increase, relative to the baseline, is achieved around $S_t = 0.3$ to $S_t = 0.4$ for bottom-fixed, and around $S_t = 0.3$ to $S_t = 0.35$ for the floating turbine. The relative gain in windspeed is the same between both turbines, only the frequency range in which this gain can be achieved is smaller for the floating turbine. This data suggests that an optimal Strouhal number exists for wake mixing and that this remains the case for the floating turbine albeit for a smaller frequency range.

When the blade pitch amplitude is doubled, this area with the highest gain increases in size and moves further upstream. This can be explained by the larger amplitude in the blade pitch angle, which increases the difference in magnitude of the shed vortices, accelerating the wake mixing process. Contrary to the two-degree case, there is now a difference in relative gain between both turbines. Likewise, the area of the highest gain is smaller for the floating case. The downstream distance at which this gain is highest remains similar between both turbines.

Wind speed is a measure of wake mixing, but recall that the goal is to maximize the power production of a wind farm. A large, relative, gain in wind speed might not equal a similar increase in power. The main cause for this is that the wind speed in the baseline case also increases as the wake recovers due to the natural mixing process. The relative contribution of the Helix might be lower further downstream due to this, but the overall power of the wind farm could still be higher. How the results differ between wind speed and power production will be discussed in the next subsection.

Average Wind Farm Power Results

The power production of the wind farm is calculated by adding a second, hypothetical, IEA 15MW turbine directly in line with the first turbine. The power production of this hypothetical turbine is calculated under the assumption that it is operating at a fixed power coefficient, using greedy control. With this assumption, the power can directly be calculated using the wind speed information from the previous section.

The power production of the upstream turbine is included in the analysis to calculate the power of the two-turbine farm. Actuating the Helix will result in a small loss in power for the upstream turbine which is dependent on blade pitching amplitude as well as its actuation frequency [122]. Likewise, yaw misalignment also causes a loss in power production. Because of these two effects, it is important to include the first turbine in the power calculation.

Figure 3.17 shows the average gain in wind farm power production with respect to the baseline case. The layout of the graph is the same as that of the wind data in Figure 3.16. Recall that this gain is still relative to the baseline case, i.e., the highest gain doesn't necessarily equate to the largest possible power production within the presented data set.

Looking at the data, the shape of the surfaces has changed significantly with respect to the wind speed data. In particular, the Strouhal range within which the highest gain can be achieved has narrowed to an area around $S_t = 0.3$ for the 2-degree case. Furthermore, the downstream distance at which it occurs is also 1 rotor diameter further downstream, which is due to the wake continually recovering to higher wind speeds as it travels downstream.

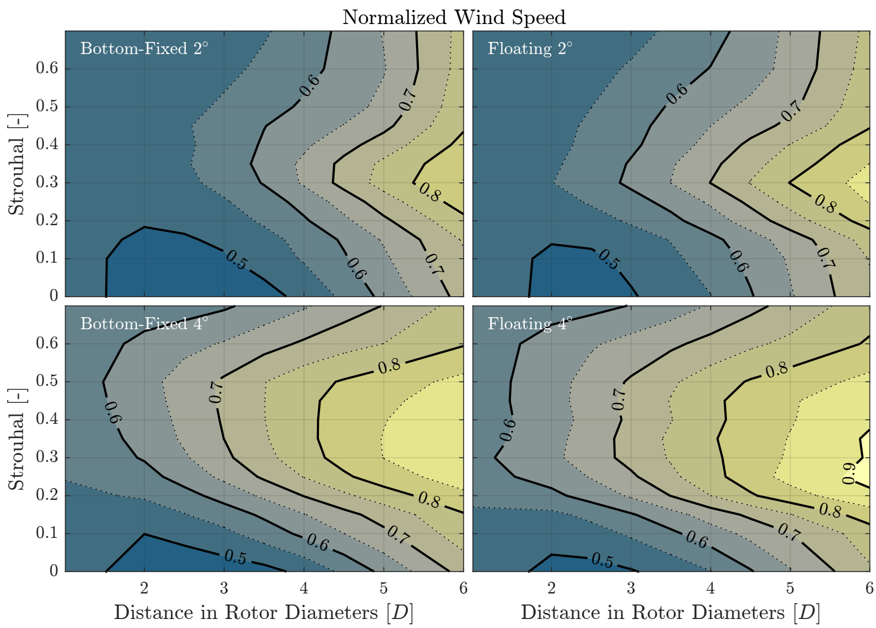

Figure 3.18: Absolute wind farm velocity normalized with $V_\infty = 9$ m/s. Between $S_t = 0.3$ and $S_t = 0.35$, the gain in wind speed is the highest for both types of turbines. Increasing the blade pitch amplitude increases the frequency range at which higher wind speeds can be achieved. Colour map courtesy of [138].

Similar to the wind speed results, the range in which the maximum is achieved for the floating turbine is smaller compared to the bottom-fixed case.

The 4-degree results show that the largest increase in power production relative to the baseline case is between 4D and 5D. The affected frequency range is still the same. For the floating turbine, this conclusion no longer holds for this input. While previously, there was one optimal frequency and distance, there are now two distinct areas for the floating turbine. These optima lie outside the range where this floating turbine has the largest yaw motion, indicating that the extra yaw motion cannot compensate for the loss in wake mixing.

Up to this point, all the results that have been presented are with respect to the baseline. Comparing the results to a baseline case shows how much can be gained from the Helix wake mixing technique for both bottom-fixed and floating turbines. Figure 3.18 shows the wind speed normalized with the inflow velocity. A gain of 1 would mean that the wake has fully recovered to the 9 m/s wind speed. The ideal mixing frequency can be identified to be around $S_t = 0.3$, which is in line with the results from the relative comparisons. The natural increase in wind speed for the baseline is also visible in the data.

When comparing the baseline case, represented by $S_t = 0.0$ for both floating and bottom-fixed, the downstream distances at which the contour lines meet the x-axis are closer to $D = 0$ for the floating turbine than the bottom-fixed turbine. This implies that the floating baseline case has, on average, a higher wake recovery compared to the bottom-fixed turbine. Even without blade pitch actuation, the floating turbine is undergoing motions due to the waves hitting the floater that causes some degree of wake mixing. As such, when looking at absolute data, the floating turbine actually reaches a higher downstream velocity than the bottom-fixed case even though the relative gain is lower. In general, the absolute wind speeds echo the results of the relative wind speed results. The highest wind speeds are centred around $S_t = 0.30$, with the area extending down to $S_t = 0.20$ and up to $S_t = 0.40$. When the blade pitch angle is increased to four degrees, the frequency and distance range increase in size.

3.5 Future Challenges

The overarching conclusion that can be drawn from the results presented in the previous two sections is that the interaction between the wake mixing controller and the floating turbine introduces additional challenges and opportunities. These stem primarily from the additional six degrees of freedom that must be taken into account when designing a control system. Furthermore, the coupling between the controller and the floating turbine is dependent on the design of the floating turbine, see for example the sidebar "**??**". This work shows that the effectiveness of the Helix is impacted when coupled with the yawing degree of freedom of the floating turbine.

However, this work focused on only one type of turbine mounted on one floater design. In reality, over 50 types of different floater designs are being considered in industry and academia alike [52]. All of these floaters have different dynamics depending on the type of floater, water depth in which it will be deployed, sea conditions, type of turbine and many more parameters. The results discussed in this work could therefore be limited to this floater, or this type of floater. This remains one of the main challenges that need to be considered when designing control solutions for a floating turbine.

For example, in [112] a similar investigation to the one presented in this work was executed for the Pulse wake mixing technique. In that work, the floating turbine considered was the NREL 5MW [139] mounted on the OC3 platform [82] which is a single spar-type floater. For more details see Chapter 2. Its dominant motion was found to be the surge and platform pitch motion which, when combined, resulted in a fore-aft motion of the nacelle. Similar to this work, at the eigenfrequencies of that motion, the effectiveness of the wake mixing technique was reduced. Conducting the same experiments in that work on the floater used in this work would result in significantly different results because the surge and platform pitch motion of this floater is much smaller compared to the OC3. Likewise, conducting the experiments in this work on the OC3 and the anti-resonance in M_{yaw} might not exist, as the OC3 has no eigenfrequency in yaw motion.

This contrast is just one specific example of two different floating turbines with differing dynamics that both couple in a way that reduces the wake mixing technique. If the floater and turbine are designed independently of each other, these kinds of couplings have to be identified before deciding on the type of wake mixing control that can be deployed. This can be solved by considering the control co-design of the floater, turbine, and its controls. This way dual optima such as in Figure 3.17 can be identified in the design stage, and the control dynamics can be optimized towards operating in that window.

3.6 Conclusion

Tackling the climate change challenge requires a significant increase in renewable energy capacity. This growth can be realized by increasing the efficiency of a wind farm by reducing the wake interaction between turbines. Control solutions designed for bottom-fixed turbines will have to be adapted to the floating turbines within those farms to accommodate the floating turbine dynamics. In this work, this transition is analyzed for the Helix method.

The effectiveness of the Helix wake mixing method depends on the application frequency and the blade pitch amplitude. For bottom-fixed turbines, this work shows that an ideal mixing frequency exists, between $S_t = 0.30$ and $S_t = 0.40$, which leads to the highest increase in wind speed downstream. A similar result was found for a floating turbine.

However, when the Helix is applied to a floating turbine, it will undergo a yaw motion. The magnitude of this motion is a function of the design of the floater and the actuation frequency of the Helix. For the turbine and floater used in this work a frequency identification experiment showed an eigenfrequency exists in yaw at $S_t = 0.30$. This yawing motion couples with the Helix method, and when yawing at the eigenfrequency it leads to a reduction in yaw moment, captured as an anti-resonance in the identification data. This reduction in yaw moment leads to a reduction in the effectiveness of the Helix, as the difference in magnitude for the shed vortices is also lowered.

How this yaw motion and reduction in yaw moment impacts the overall effectiveness of the Helix is investigated using time-domain simulations. By evaluating the evolution of the downstream wind speed, a measure of the degree of wake mixing can be identified. At the four-degree blade pitch amplitude used in this work, the relative gain is lower for the floating turbine compared to the bottom-fixed turbine. This is partly due to the higher baseline wind speed for the floating turbine, to which the results are compared, for the floating turbine and partly due to the yaw motion. The effect of the yaw motion can be better seen when looking at the relative power production of the two-turbine wind farm. It is interesting to see that rather than having one optimum, there are two for the floating turbine. These optima are centred around the yawing eigenfrequency, indicating that this coupling restricts the Helix.

The additional dynamics provide new challenges and opportunities in finding the right operating frequency for a wind farm operator desiring to use the Helix in a floating wind farm. Furthermore, future floater designs might introduce different dynamics to which wake mixing strategies couple, producing different results and requiring a new analysis. The latter can potentially be circumvented by incorporating wake mixing control into the design phase of the floating turbine. This way it might be possible to design controls that enhance wake mixing through the co-design of their (hydro-)mechanical properties and controller.

3.A Background on Wake Mixing

The underlying concept of both active and passive wake mixing strategies is to augment the flow field in the wake of the wind turbine in order to increase the rate of entrainment of high energy external flow into the wake induction zone. This increases turbulent diffusion and causes the wake to recover more rapidly. The near wake of a wind turbine can be characterised by coherent structures formed through the generation of lift and drag at the blade sections. The application of an excitation to these structures leads to their breakdown and decay, a highly nonlinear fluid dynamic process. This excitation may occur through one of two actions: Through augmentation of the circulation of coherent structures or through the displacement of these structures. Circulation augmentation may occur through either passive means, such as the addition of blade devices which modify the wake sheet [140], or through active means such as through blade pitch [44]. Circulation displacement may also occur through either passive means such as the extension of a blade tip [141], or through active means such as through the modification of rotor rotational speed [142]. A number of studies have demonstrated that wake excitation is practically achievable, however, considering the integral effect of the excitation on component fatigue, the determination of the most practical and financially feasible means of excitation is an ongoing topic of investigation.

Analytical and Numerical Results

The first analytical investigation into the stability of a helical vortex system was carried out in the seminal work by Widnall [143]. Here it was found that three fundamental modes of instability exist: The short-wavelength, the medium-wavelength (mutual-inductance) and the long-wavelength instability. These results were extended to the multiple helix case by Gupta & Loewy [144]. This work and further numerical analyses demonstrated that the mutual inductance instability appears to demonstrate the highest unstable growth rate due to an initial perturbation [144–146]. The influence of applying a volume force at a range of frequencies was investigated in the work of Sarmast et al. [147]. Here similar results were found, indicating the strong instability of the mutual inductance mode, and an empirical formula for the transition position of the wake was derived. The impact of the motion of a floating wind turbine on the wake stability was numerically investigated in [148] where it was shown that the motion of the platform at certain frequencies can contribute to the instability modes described above. A numerical analysis of the helical wake excitation described in this work was carried out by [123], where it was found that both wake deflection and increased entrainment contribute to the accelerated wake breakdown and that approximately 10% more energy can be extracted from downstream turbines through the application of the helix excitation method, see Figure 3.19.

Experimental Investigations

The mutual inductance instability was first observed in the smoke visualisation carried out by Alfredsson & Dahlberg [149]. The nature of the pairing instabilities and the transfer of kinetic energy over the shear layer were investigated through experiments of a small-scale rotor in an open-jet test section in Lignarolo et al. where it was identified that the vortex leapfrogging mechanism is the triggering event that accelerates wake recovery [150]. Both long and short-wavelength instabilities were experimentally generated in the work of

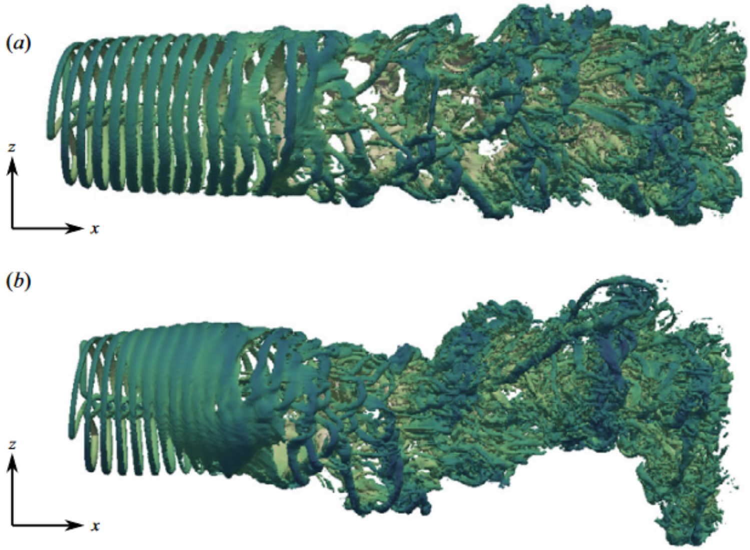

Figure 3.19: Vorticity isocontour of a wind turbine wake in standard control operation (above) and with helix wake excitation (below), from [123].

Leweke et al. [151]. The influence of displacement perturbations of the vortex structure was investigated by Quaranta et al. where it was demonstrated that the local pairing of vortices is the driving factor behind the instability of a helical wake system and that the leapfrogging results from global vortex pairing modes [142].

3.B Aero-servo-hydro-elastic models in QBlade

QBlade is a comprehensive software that enables the design and simulation of dynamics for both bottom-fixed and floating wind turbine systems [114]. When simulating floating wind energy systems, it is crucial to account for the intricate interplay between various aspects such as aerodynamics, hydrodynamics, control mechanisms, and the effects of elastic, inertial and gravitational loads. These interactions often result in highly nonlinear behaviours, which can be counter-intuitive and differ significantly from the responses observed in land-based, bottom-fixed wind turbines. To gain a deep understanding of these inherent couplings, it is imperative to explicitly resolve the nonlinear dynamics in the time domain, as simplified linearized models often fall short. QBlade is designed as a medium-fidelity simulation code that can predict coupled system dynamics in real-time or faster. This requirement has profound implications when it comes to choosing suitable numerical models capable of accurately resolving the relevant system dynamics, see Figure 3.20.

Aerodynamics

As in most numerical approaches, the modelling of aerodynamics can be broken down into two main aspects: the modelling of aerodynamic forces on the turbine blades and the modelling of rotor wake aerodynamics. Due to computational constraints, fully resolved three-dimensional computational fluid dynamics (CFD) simulations of the blades are not feasible for long-duration time-domain analyses. Therefore, the commonly adopted blade element approach [152] involves representing blade loads using precomputed lift, drag, and moment coefficient polars. These polars capture the aerodynamic characteristics of a two-dimensional airfoil section across various angles of attack. The polar data can be obtained through wind tunnel experiments or numerical simulations. By spatially integrating the two-dimensional polar data along the blade span, the rotor blade, which usually consists of multiple airfoil sections, can be effectively represented.

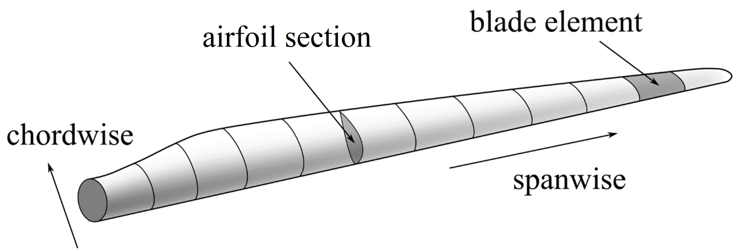

Figure 3.20: Two-dimensional airfoil sections and the discretization of a rotor blade into two-dimensional elements.

When aerodynamic forces act on the rotor, kinetic energy is extracted from the flow, leading to a reduction in flow velocity as it traverses the rotor disc. This localized region of reduced flow velocity is referred to as the rotor wake. The mechanism behind this energy extraction involves the formation of a helical vortex system trailing behind the rotor. The rotational motion of the vortex induces circular movement in neighbouring fluid particles. The combined effect of this vortex system is a decrease in flow velocity downstream of the wind turbine rotor. QBlade incorporates explicit modelling of this vortex system using Lagrangian vortex filaments, whose convective velocity is updated and integrated at every time step [129]. An example of such a wake can be seen in Figure 3.21 These filaments, which are shed from the rotor blades based on their aerodynamic loading, exert an influence on all other vortex filaments and on the rotor itself. By considering the collective impact of all wake vortex filaments at any given point in space, the induced velocities in the wake region can be accurately evaluated. It is worth noting that the rotor wake also significantly affects the velocities at the position of the rotor blades themselves, as well as the evolution of the wake itself: a phenomenon known as wake roll-up.

Structural Dynamics and Control

QBlade utilizes the versatile open-source library Project-Chrono [153] as a middleware for modelling and solving the structural dynamics of wind turbines. The approach for modelling structural dynamics involves representing the elastic and slender components of wind turbine parts (such as the tower and blades) using beam elements. These beam elements are interconnected in a multi-body formulation to represent the entire structure of the wind turbine. Each beam element is assigned properties such as mass, stiffness, and damping, which capture its complex composite structure and may vary along the length of each element.

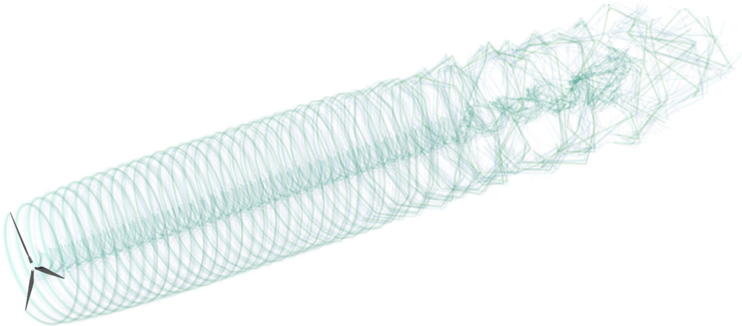

Figure 3.21: Helical rotor wake structure discretized with Lagrangian vortex filaments. The onset of wake breakdown is visible far downstream.

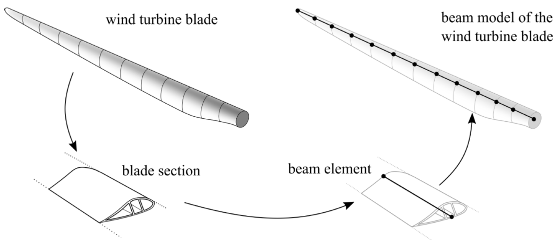

Figure 3.22: Reduction of a complete composite blade structure into blade sections and beam elements.

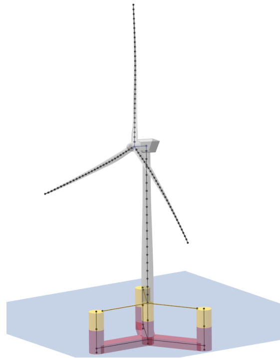

Figure 3.23: Representation of a floating wind turbine with beam elements connected in a multi-body formulation.

By using beam elements, the complete structure of a wind turbine can be represented with a manageable number of degrees of freedom, typically in the order of thousands. This is in contrast to a full Finite Element Analysis (FEA) approach, which would require millions of degrees of freedom. Despite the reduced complexity, the beam element representation still provides accurate results when resolving the coupled response of the structural system. Additionally, the flexible beam element formulation can be combined with lumped masses and rigid bodies that may represent non-deformable parts of the system, such as the floating substructure of the turbine, which is typically not susceptible to significant elastic deformations. A combination of such a set-up is shown in Figure 3.23.

Within the multi-body system of the wind turbine, various components are connected through actuators. For example, the blade elements are linked to the blade hub using rotational actuators, representing the pitch drive mechanism. Another example is the generator, which applies an opposing torque onto the main shaft connected to the rotor hub. These actuators receive signals from controller libraries which contain the complete control logic of a wind turbine, including algorithms for supervisory control tasks such as emergency shutdown events that are triggered by specific thresholds. The controller libraries operate alongside the structural simulation, receiving inputs and sending control signals to the actuators of the structural model, a schematic representation of this interface is seen in Figure 3.24. The signals could be related to blade pitch (as utilized in this study), rotor yaw, emergency brake activation or other actuators distributed over the wind turbine system.

3

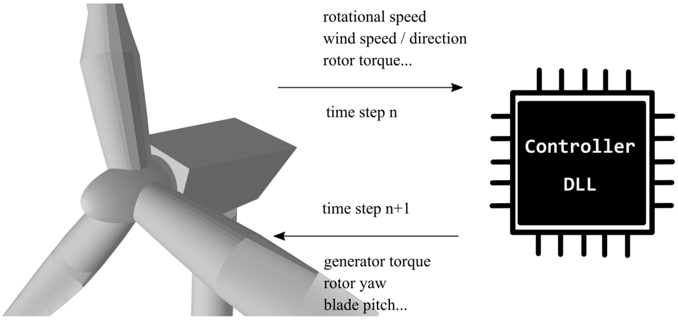

Figure 3.24: Communication between the controller and the turbine.

Hydrodynamics

QBlade incorporates two medium-fidelity methods to simulate hydrodynamic forces on offshore structures: the Morison equation combined with strip theory and a model based on linear potential flow hydrodynamics.

The empirical Morison equation [154] estimates the forces and moments on a submerged body in a wave field. The Morison equation contains three essential terms for estimating hydrodynamic forces: the inertia, hydrodynamic mass, and drag term. The hydrodynamic inertia captures the effects of fluid acceleration or deceleration around the structure.

The added mass accounts for the additional mass of fluid that contributes to the dynamic response of the body. The hydrodynamic drag term considers the quadratic drag experi-

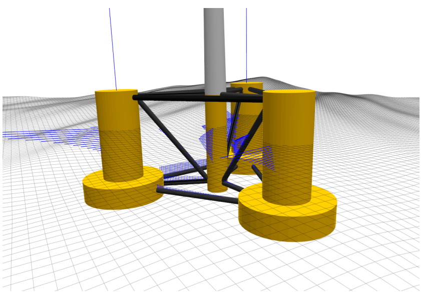

Figure 3.25: Distributed Morison drag forces, in blue, acting on the DeepCwind, [?], floater operating in a multi-directional, irregular wave field.

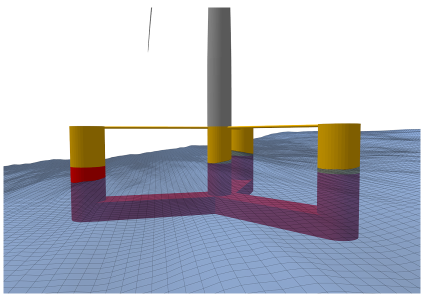

Figure 3.26: A rigid body, potential flow model of the VolturnUS-S floater operating in a multi-directional irregular wave field.

enced by the structure as it moves through the fluid. When combined with strip theory, which divides complex structures into slender strips, the Morison equation can estimate distributed hydrodynamic forces across the entire structure, see Figure 3.25. However, the Morison equation falls short in predicting hydrodynamic interactions between individual components of the same structure as each strip is solved independently. Additionally, it has limited accuracy for non-slender structures.

In contrast, the linear potential flow method [155] employed in QBlade predicts the combined hydrodynamic excitation and radiation forces on the complete structure assuming inviscid flow. This method relies on a preprocessed hydrodynamic response database obtained from potential flow solvers such as WAMIT [156], NEMOH [157], or Ansys AQWA [158]. During a simulation, this frequency-domain hydrodynamic database is converted into the time domain. One drawback is that the potential flow method typically calculates the hydrodynamic response for a single reference point, lumping together all forces and moments. As a result, it does not provide a distribution of hydrodynamic forces required to model hydro-elastic effects. However, since most floating structures are relatively rigid compared to soft and slender rotor blades, they are often modelled as rigid bodies with accurate mass and inertial properties - thereby capturing their dominant contributions to the overall system response. Figure 3.26 shows the IEA15MW turbine modelled as rigid body in an irregular wave field.

It is important to note that the potential flow theory assumes inviscid flow and therefore cannot predict quadratic hydrodynamic drag. To incorporate drag into the simulation, the potential flow method may be combined with the Morison-based strip theory. This hybrid approach provides a more comprehensive representation of the total hydrodynamic forces.

4

The Influence of Phase Offset on Wake Mixing Performance

Wake mixing techniques like the Helix have shown to be effective at reducing the wake interaction between turbines, which improves wind farm power production. When these techniques are applied to a floating turbine it will excite movement. The type and magnitude of movement are dependent on floater dynamics. This work investigates four different floating turbines. Of these four turbines, two are optimized variants of the TripleSpar and Softwind platforms with enhanced yaw motion. The other two are the unaltered versions of these platforms. When the Helix is applied to all four floating turbines, the increased yaw motion of the optimized TripleSpar results in a reduction in windspeed whereas the optimized Softwind sees an increase in windspeed with increased yaw motion. From simulations using prescribed yaw motion at different phase offsets between blade pitch and yaw motion, we can conclude that this is the driving factor for this difference.

This chapter is based on *D. van den Berg, D. De Tavernier, J. Gutknecht, A. Viré, and J.W. van Wingerden. The influence of floating turbine dynamics on the helix wake mixing method. Journal of Physics: Conference Series 2767, 032012 (2024).*

4.1 Introduction

The floating wind market is rapidly growing, with the European Union aiming to have 4 GW of installed capacity operational by 2030. This is a substantial increase from the currently operational 0.18 GW installed capacity [51]. Unlike its bottom-fixed counterpart, there is not yet a convergence on the 'optimal' design of a floating wind turbine. Currently, more than 50 different types of foundations for floating turbines are being developed in academia and industry alike [52]. Regardless of floater design one of the main challenges for floating wind is the interaction between conventional wind turbine control and the dynamics of the floating platform [55].

One area where the interaction with the floater dynamics can provide benefits is wind farm flow control. Within a wind farm, the wake interaction between turbines is a major cause of energy loss [28]. For conventional bottom-fixed wind farms, three different control techniques are actively researched that can mitigate this wake interaction, namely wake steering, axial induction control and dynamic pitch control. Over the past decade especially wake steering has been extensively researched and its potential has been proven over a large number of publications covering simulations, wind tunnel experiments and field tests [24, 42, 159].

Wake steering is also one example where the extra degrees of freedom of a floating turbine can be leveraged. In [60] wake deflection is achieved by pitching the floater backwards or forwards. Similarly to wake steering on a bottom-fixed turbine, the misalignment due to the platform pitch creates a force component that deflects the wake upwards when pitched backwards and downwards when pitched forwards. One of the main findings in [60] is that deflecting the wake downwards towards the ocean surface allows the flow in the free stream from above the turbine to enter the wake which ultimately increases the downstream wind speed.

An alternative solution to wake steering is dynamic wind farm flow control. Two notable methods that fall into this category are dynamic induction control [43] and dynamic individual pitch control (often referred to as 'the Helix' method) [44]. Both techniques use the blade pitch degree of freedom to dynamically vary the magnitude or the location of the thrust vector of the upstream turbine. The time-varying behaviour of the turbine's thrust leads to a time-varying wind speed within the wake which, when excited at the right frequency, can promote the onset of wake mixing.

When these techniques are applied to a floating turbine, the time-varying force will excite movement. The magnitude and phase of the movement with respect to the blade pitch input is heavily dependent on the type of floater on which the turbine is mounted. For example, the Helix wake mixing method applies a time-varying tilt and yaw moment to the turbine that typically is of such magnitude that the motions remain small. However, semi-submersible type floaters such as the TripleSpar [160] have an eigenfrequency in yaw motion for which the excitation frequency falls within the frequency range with which the Helix is typically applied [74, 161]. For a typical blade pitch input used for the Helix wake mixing method the resulting yaw motion can reach between 5 to 10 degrees for these type of platforms.

The influence that the yaw motion has on the Helix and the onset of wake mixing was first investigated in [74]. In that work prescribed motion was used to replicate the floating turbine motion. The prescribed yaw motion was derived from frequency responses acquired in an identification experiment for the OC4 platform [162]. An increase in downstream wind speeds was observed when the turbine was yawing. The same interaction is investigated in [161] and did not use prescribed motion but rather simulated the full coupling. In [161] it was found that actuating at the eigenfrequency, which leads to the largest yaw excursions, diminished the effectiveness of the Helix wake mixing method.

This work aims to provide an answer to the question of why actuating the Helix method at the eigenfrequency of a floating turbine can lead to reduced effectiveness of the Helix method. For this purpose, the contribution of this paper is twofold: (1) It provides an analysis of the movement that a turbine undergoes near and at the eigenfrequency using a frequency domain analysis and, (2), it investigates wake recovery behind the floating turbines using time-domain simulations.

The remainder of this paper is organized as follows. Section 2 introduces the research methodology and describes the two floating turbines used in this work. Sections 3 and 4 show and explain the frequency and time-domain results, respectively. Finally, Section 5 forms the conclusion of this work.

4.2 Methodology

In this work, QBlade [114] is used to conduct all investigations. QBlade can simulate the aero, structural and hydrodynamics of a floating turbine within a single simulation environment. The hydrodynamic solver in QBlade has extensively been verified against other simulation suites [163]. Within QBlade the wake aerodynamics are modelled using a free wake vortex method. Although such a modelling technique typically loses accuracy when wake breakdown has occurred it can be used to predict the breakdown location accurately [79]. Knowing the location of the breakdown provides insight into when the wake mixing process is triggered. QBlade has previously been used in [74, 112, 161] for a similar type of research. The settings described in [112] are also used in this work.

All simulations are carried out using the DTU 10MW [164] mounted on the TripleSpar [160] and Softwind [165] platforms are used for analysis. Both turbines are shown in Figure 4.1. The TripleSpar is a semi-submersible type of platform while the Softwind is a spar-buoy type. Two other floating turbines are also included in the simulations. These turbines are optimized versions of the TripleSpar and Softwind and have enhanced yaw motion when the Helix method is applied. The optimization was part of the FLOATECH project and the details of the optimization set-up can be read in [166].

Because the movement of the floating turbine is frequency-dependent, the Helix will be applied at different actuation frequencies. We make the actuation frequency dependent on turbine size, wind speed and desired Strouhal number. The Strouhal number is a non-dimensionalized frequency which is defined as

$$S_t = \frac{f_e D}{V_\infty}, \tag{4.1}$$

in which V_∞ is the free stream velocity in [m/s], f_e is the blade pitch frequency in [Hz] and D is the rotor diameter in [m]. The following input frequencies are used:

$$S_t = \begin{bmatrix} 0 & 0.10 & 0.15 & 0.20 & 0.25 & 0.30 & 0.35 & 0.40 & 0.45 & 0.50 & 0.60 & 0.70 \end{bmatrix}, \tag{4.2}$$

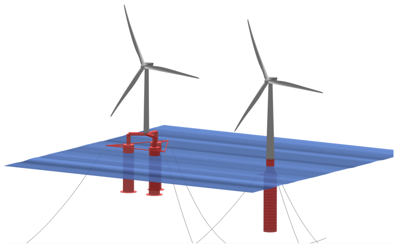

Figure 4.1: TripleSpar (left) and Softwind (right).

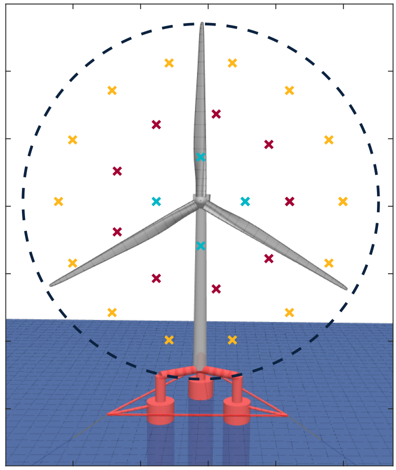

Figure 4.2: Measurement Points for analysis.

Figure 4.3: Figure 1a: A screenshot taken in QBlade showing both the TripleSpar (left) and Softwind (right) floater supporting a DTU 10MW turbine. Figure 1b: Measurement points used for analysis overlayed on the DTU 10MW turbine.

4

in which $S_t = 0$ represents a baseline case without any pitch actuation. Although it is still a topic of ongoing research, currently it is believed that the range from $S_t = 0.30$ to $S_t = 0.40$ is ideal for the Helix in terms of promoting wake recovery [119, 120]. For all simulations, the amplitude of the blade pitch angle is set to 4 degrees. The wind speed in the wake is calculated by taking 27 independent measurements at points distributed over the rotor disk of a hypothetical downstream turbine. The distribution of the points can be seen in Figure 4.2.

Wind speed measurements are taken at the following downstream distances, defined in terms of rotor diameter,

$$D = \begin{bmatrix} -1.0 & 0.0 & 1.0 & 2.0 & 2.5 & 3.0 & 3.5 & 4.0 & 4.5 & 5.0 & 6.0 \end{bmatrix}. \tag{4.3}$$

The length of the domain is limited to $6D$ because the free vortex wake method loses accuracy when wake breakdown occurs and the mixing process starts. In total 12 different actuation frequencies are evaluated for which the wind speed is measured at 11 different distances. The simulations are performed in batches using MATLAB running QBlade through a Dynamic-Link Library interface to streamline the simulation process [136].

For all simulations, the same environmental conditions is used. The inflow speed is set to 9 m/s and is considered uniform. This is an idealization of a real-world scenario as the mixing effect introduced by the Helix is more pronounced without any natural mixing coming from turbulence. Nevertheless, the Helix remains effective in turbulent conditions. The work done in [124] and [123] both used a turbulence level of 5% and found accelerated recovery when the Helix was applied. Furthermore, the wave conditions used are based on the IEC 61400-3-1:2019 standard which specifies the type of wave field to use for different wind conditions [134]. The size and frequency content of the waves are characterized using a JONSWAP wave spectrum [167].

4.3 Floating Turbine Dynamics

The Helix can be applied by setting a time-varying signal on the fixed-frame pitch signals. These signals can be transformed into individual pitch signals using the MBC transformation [118] which is defined as

$$\begin{bmatrix} \beta_{col}(t) \\ \beta_{tilt}(t) \\ \beta_{yaw}(t) \end{bmatrix} = \frac{2}{3} \begin{bmatrix} 0.5 & 0.5 & 0.5 \\ \cos(\psi_1(t)) & \cos(\psi_2(t)) & \cos(\psi_3(t)) \\ \sin(\psi_1(t)) & \sin(\psi_2(t)) & \sin(\psi_3(t)) \end{bmatrix} \begin{bmatrix} \beta_1(t) \\ \beta_2(t) \\ \beta_3(t) \end{bmatrix}, \tag{4.4}$$

in which β_{col} is the collective pitch angle and β_{tilt} and β_{yaw} are the fixed frame pitch angles. To create the Helix a sinusoidal signal is applied to the β_{tilt} an β_{yaw} with one of the signals having a 90° phase-offset to each other. The resulting time-varying individual pitch angles create time-varying out-of-plane bending moments for the individual blades. These can be transformed back into fixed-frame moments using the inverse MBC transformation, i.e.,

$$\begin{bmatrix} M_{y,1}(t) \\ M_{y,2}(t) \\ M_{y,3}(t) \end{bmatrix} = \begin{bmatrix} 1 & \cos(\psi_1(t)) & \sin(\psi_1(t)) \\ 1 & \cos(\psi_2(t)) & \sin(\psi_2(t)) \\ 1 & \cos(\psi_3(t)) & \sin(\psi_3(t)) \end{bmatrix} \begin{bmatrix} M_{col}(t) \\ M_{tilt}(t) \\ M_{yaw}(t) \end{bmatrix}. \tag{4.5}$$

In (5.3) M_i, with $i \in [1,2,3]$, are the individual out-of-plane blade root moments and M_{col}, M_{tilt} and M_{yaw} are the fixed-frame moments. The subscript col refers to the collective moment of the turbine. The time-varying fixed-frame β_{tilt} and β_{yaw} pitch angles create time-varying M_{tilt} and M_{yaw} moments. The changing moments will excite movement in a floating turbine. To capture the interaction between the Helix and both floating turbines used in this work, a frequency identification experiment is run for both the original and optimized designs. The input for identification is a chirp signal applied to the β_{yaw} channel which excites the system between $1 \cdot 10^{-3}$ and 1 Hz. Based on the measured input-output relations in each degree of freedom, transfer functions can be identified [168].

The results of the identification process are shown in Figure 4.4. The top row of plots shows the gains from blade pitch input to one of the six degrees of freedom and the bottom row shows the corresponding phase difference between the input and output signal. The left two-by-two block of plots shows the responses in translational motions, that is surge, sway and heave and the right two-by-two block the rotational motions, i.e., roll, platform pitch and yaw. The solid lines are the response functions for the unaltered floating turbines, the dash-dotted line are the response functions of the optimized floating turbines. The translational motions remain relatively small when the system is excited over the fixed-frame yaw axis. The displacement will be at most a few metres for a typical input of two to four degrees of blade pitch which, compared to the turbine size, can be considered small. This is mainly because the collective moment remains near constant and only the fixed frame yaw and tilt axis are excited.

For the rotational motions, the yaw degree of freedom is dominant for both versions of the TripleSpar platform. The difference between the unoptimized and optimized versions is a small shift in the eigenfrequency coupled with an increase in the gain. When the

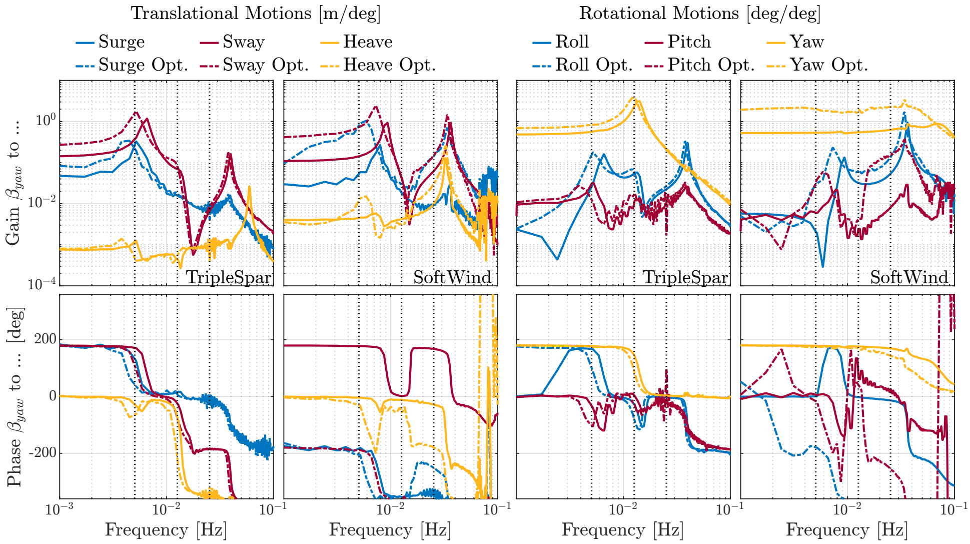

Figure 4.4: Results from the frequency identification experiments. The 2-by-2 plots on the left contain the response for the translational degrees of freedom for both the TripleSpar and Softwind platforms. The solid line is the response for the original platform design and the dash-dotted line is for the optimized version. The right 2-by-2 plots show the results for the rotational degrees of freedom. The bottom row of the plots shows the phase coupling between the input and output signal. The vertical dashed lines in each plot indicate the frequency corresponding to $S_t = 0.10$, $S_t = 0.25$ and $S_t = 0.50$ for the DTU 10MW turbine.

optimization was carried out the optimal mixing frequency was still considered to be $S_t = 0.25$, hence the shift in the location of the eigenfrequency. The unoptimized Softwind floating turbine is relatively insensitive to the input of the Helix. The optimized version, however, has a significantly increased response in yaw. The other two rotational degrees of freedom are much more subdued, except for roll which has an eigenfrequency outside the frequency range typically considered for the Helix. It is unlikely that the presence of waves will impact the motions induced by the Helix as waves excite the system at a different frequency range, typically around 0.1 Hz.

When the Helix is applied at the eigenfrequency of the optimized TripleSpar platform, both the latter and the optimized Softwind floating turbine will exhibit a comparable magnitude of yaw motion. A big difference, however, is the phase coupling between the blade pitch input and the yaw motion of the turbine. While for the Softwind platform this coupling remains relatively constant within the frequency range of the Helix, for the TripleSpar platform the phase can differ by 180 degrees as a result of the presence of the eigenfrequency. A schematic representation depicting how yaw motion can influence the Helix is given in Figure 4.5. The top row of Figure 4.5 is a front view of the rotor with the red arrows depicting the patch of the thrust vector when the Helix is applied in a counter-clockwise manner [44]. The blue dot denotes the exact location of the thrust vector at four different time instances within a single Helix period, denoted by T_p. The bottom row shows yaw motion corresponding to 90° phase offset. The blue arrow represents the thrust force.

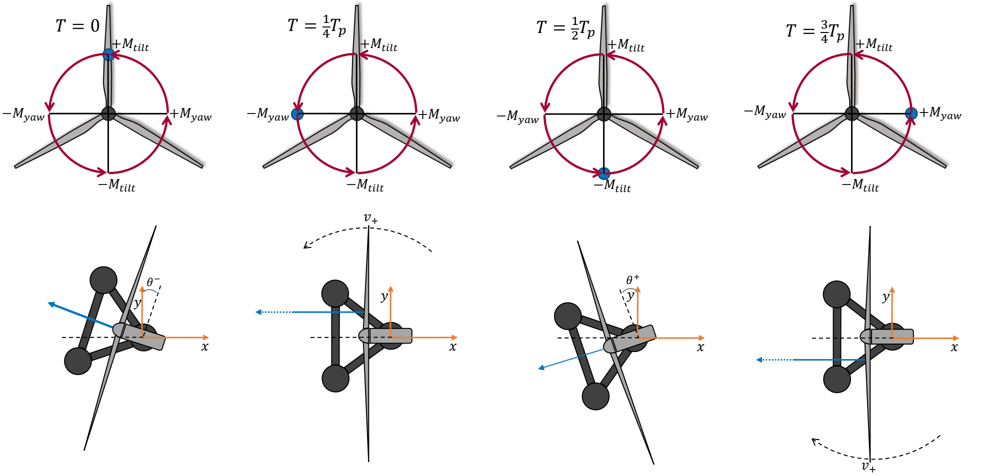

Figure 4.5: Schematic representation of the Helix and corresponding yaw motion of the floating turbine.

When the floating turbine is yawing, one-half of the turbine is moving into the flow and one-half is moving out of the flow increasing and decreasing the effective wind speed respectively. Given the phase difference in Figure 4.5, the thrust vector is located at the side which is moving into the wind. Due to the increased effective windspeed, the thrust is also increased which would increase the yaw moment. The opposite can also hold which would lead to a reduction of the yaw moment. Furthermore, something that is not taken into account in this analysis is the effect of yawing on the wake. To see how this and the change in yaw motion can impact the onset of wake mixing, time-domain simulations are required to analyze the wind speed behind the turbine.

4.4 Wind Speed Results

In this section the wind speed behind the four different floating turbines is investigated with the Helix applied at the frequencies mentioned in (4.2). Furthermore, a more synthetic simulation is also carried out. Here the Helix is applied to a bottom-fixed turbine which is yawed with prescribed motion at different phase offsets, defined with respect to the β_{yaw} input. For this simulation a single actuation frequency is chosen, close to the eigenfrequency of the TripleSpar. It will be compared to a case without yawing motion, i.e., the Helix applied to a bottom-fixed turbine and a case without the Helix which serves as a baseline.

4.4.1 Time Domain Results TripleSpar and Softwind

Figure 4.6 shows the wind speed data gathered from the simulations. The results are normalized with respect to the inflow velocity $V_\infty = 9$ m/s. The left column shows the results for baseline and optimized TripleSpar and the right column for the Softwind. The largest recovery in wind speed is found for the Strouhal range of $0.20 - 0.40$. This is in line

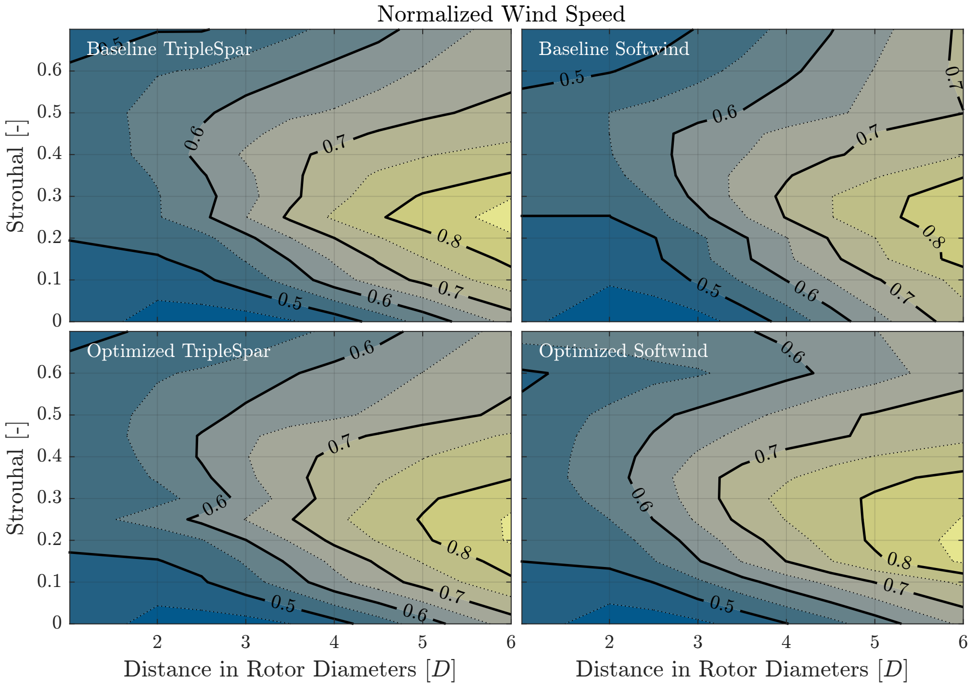

Figure 4.6: Normalized wind speed behind the four different floating turbines for different actuation frequencies.

with previous research and it remains largely unaffected by the yawing motion.

When comparing the results between the unoptimized and optimized floaters an interesting difference can be seen between the TripleSpar and Softwind turbines. For the optimized TripleSpar the wind speed is decreased with downstream distance compared to the unoptimized version. For example, for the unoptimized version, the wind speed has recovered to 80% of the inflow at 4.5D, which has moved to 5.5D for the optimized version. For the Softwind this 80% mark moves slightly forward. Furthermore, the frequency range over which this gain in wind speed can be achieved is widened.

The impact of the increased yaw motion is more noticeable when comparing the total power production of a hypothetical two-turbine wind farm. Dynamic yawing will impact the power production of the upstream turbine so it could be that a reduction in power production for the first turbine negates the gain in potential power due to increased wind speeds.

Figure 4.7 shows the relative power production for the wind farm. Based on the measured wind speed the power production for the second turbine is calculated. A relative comparison is made for the power production of a wind farm using the unoptimized floating turbine. A value larger than 1 indicates that the wind farm using the optimized turbine has increased power production. For the TripleSpar there is no major difference in power production. This is mainly because the dynamics are similar between the two floating turbines. However, at the optimization frequency of $S_t = 0.25$, there is a distinct area of reduced power production of which the frequency spans the same range in which the

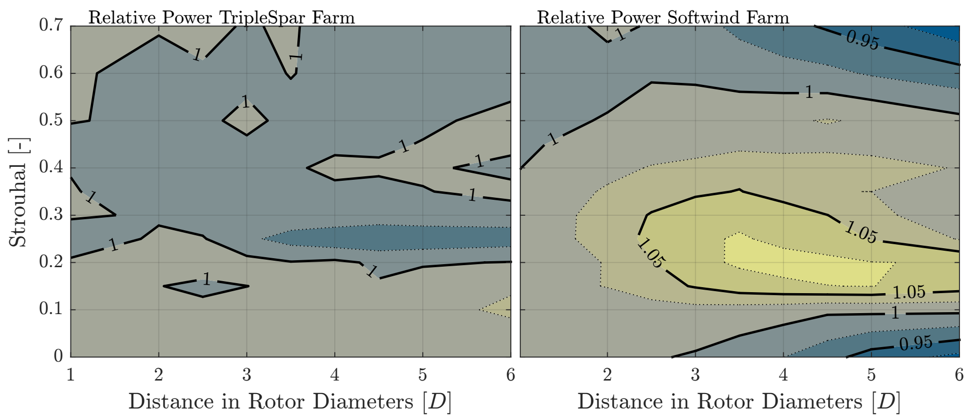

Figure 4.7: Relative power production of a hypothetical aligned two-turbine wind farm. The total power of the farm is based on the power production of the first turbine and hypothetical power based on the measured wind speed. The power production of the wind farm with the optimized turbine is divided by that of the baseline wind farm. A value of 1 or larger indicates an increase in power production.

platform will undergo yaw motion when excited by the Helix. For the Softwind turbine, there is a significant increase in power production, up to an increase of 8%. For the Softwind the increased yaw motion contributes positively to the overall wind farm power production.

4.4.2 Results for Prescribed Yaw Motion

This difference between the two floating turbines can be clarified by the results obtained using prescribed motion, shown in Figure 4.8. The yaw motion is prescribed with an amplitude of 6 degrees and the Helix with 2 degrees of blade pitch. In total four different phase offsets, varying by 90°, are analyzed and compared to the Helix without yaw motion and a baseline case without the Helix and yaw motion. At a phase offset of 180° wind speed is increased behind the turbine compared to the Helix whereas with an offset of 0°, its effectiveness is decreased. This confirms that actuating before or after the eigenfrequency has an impact on the performance of the Helix. The reason for this remains an open question. It could partially be because the thrust is affected by the movement but also because the dynamic yawing interacts with the development of the structure in the wake.

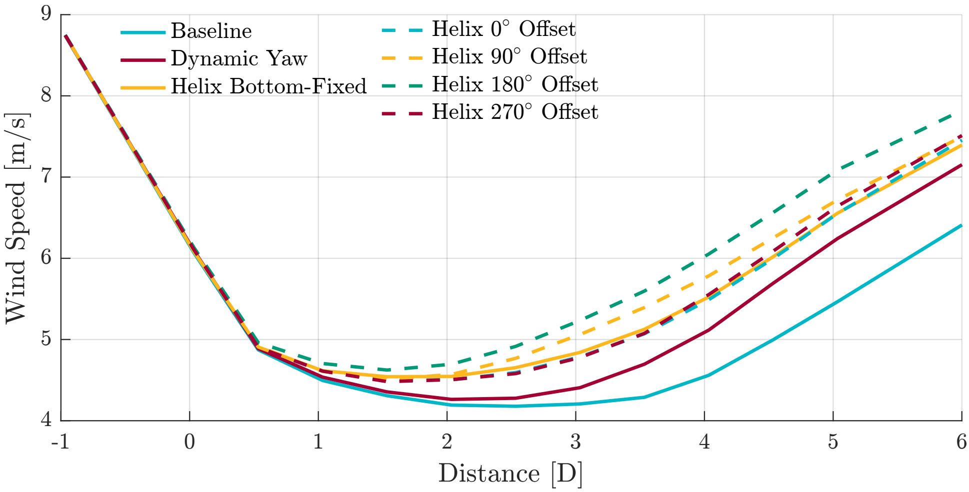

Figure 4.8: Wind speed analysis using prescribed motion on a bottom-fixed turbine with the Helix at a single frequency. This data has been obtained using the IEA 15MW [169] turbine as results for that turbine were easier to analyze. Whether the interaction between the Helix and yaw motion is diameter-dependent is still an open question.

4.5 Conclusion

This work investigates how the dynamics of a floating turbine interacts with the Helix wake mixing method. Two optimized and unoptimized floating turbines are used in this analysis, where the optimized versions of the floating turbine have enhanced yaw motion. For the TripleSpar, yaw motion is excited by applying the Helix at its eigenfrequency. A consequence of actuating near the eigenfrequency is a potential change of 180° in-phase coupling between the Helix blade pitch input and the yaw motion of the floating turbine. This will influence the moments that are applied to the turbine as well as the deflection of the wake. This is not the case for the Softwind platform. Its optimized version also has increased yaw motion, but the phase coupling remains constant. The interaction with wake mixing is quantified by measuring the wind speed behind the floating turbine. When comparing the optimized TripleSpar with its unoptimized version, a decrease is observed in the wind speed in the wake which implies that the yaw motion negates part of the wake mixing. This is also seen in the relative wind farm power, which shows a distinct area of lower power production centred around the eigenfrequency. However, the opposite is found for the Softwind platform: an increase in yaw motion goes together with an increase in wind speed and power production. Further analysis using prescribed yaw motion confirms that a 180° shift in phase coupling can be the difference between outperforming or underperforming with respect to the Helix without any yaw motion.

5

Phase-controlling the motion of floating wind turbines to reduce wake interactions

The wake interaction between wind turbines causes significant losses in wind farm efficiency that can potentially be alleviated using wake control techniques. We provide detailed experimental evidence that the coupling between the so-called Helix wake control technique and a floating turbine's yaw dynamics can be used to increase wake recovery. We use tomographic particle image velocimetry during wind tunnel experiments, enabling three-dimensional analysis of the wake dynamics and its coupling to a floating wind turbine. The measurements show that ensuring the floating turbine's yaw motion is in phase with the blade pitch dynamics of the Helix technique enables an increase of 12% in available power in the flow on top of the Helix method applied to bottom-fixed turbines. We find that the in-phase scenario results in an earlier interaction between tip and hub vortex inside the wake, which leads to the desired breakdown of the wake, thus accelerating the energy advection into the wake.

This chapter is based on *D. van den Berg, D. van der Hoek D. De Tavernier, J. Gutknecht and J.W. van Wingerden. Phase-controlling the motion of floating wind turbines to reduce wake interactions. In Review.*

5.1 Introduction

Wind energy plays a key role in efforts to decarbonise energy production. For example, the European Commission aims to increase its offshore wind production from 38 GW today to 450 GW by 2050, in order to meet 30% of Europe's electricity demand at that time [95]. Meeting this target requires a major expansion of the wind energy production capacity at offshore locations, where the majority of Europe's wind energy resources can be found [49]. However, 60% of these energy resources are located in waters too deep for conventional bottom-fixed wind turbines to be economically feasible [49]. It is therefore expected that floating wind turbines will be deployed in wind farms of similar sizes as currently seen with bottom-fixed turbines [51]. Although individual turbines are capable of operating near their theoretical peak efficiency, a wind farm can experience an efficiency drop by up to 40% [23–25].

As a wind turbine extracts energy from the incoming airflow, it leaves a zone of turbulent air with reduced wind speed behind it, referred to as the wake. To mitigate turbine-to-turbine wake interaction, methods such as wake steering [24, 33, 34, 36, 107, 170], static induction control [40, 41], and dynamic blade pitch control [45, 110]have been developed. Thus far, the development of control approaches to mitigate wake interactions has focused on bottom-fixed wind farms [28, 29]. When implementing controllers designed for bottom-fixed turbines on floating turbines, the coupling to the dynamics from the additional six degrees of freedom can significantly affect controller performance [54, 55, 171].

Recent studies [74, 112, 161] revealed that collective and individual pitch control techniques can excite the motion of a floating turbine. The magnitude of the motion is dependent on the excitation frequency of the wake mixing technique and its coupling to the floating turbine dynamics. In the case of collective pitch control, the time-varying magnitude of the thrust force creates a fore-aft motion of the turbine rotor. The coupling between the blade pitch input and this motion is found to reduce the effectiveness of the wake-mixing technique, leading to reduced wake recovery [112].

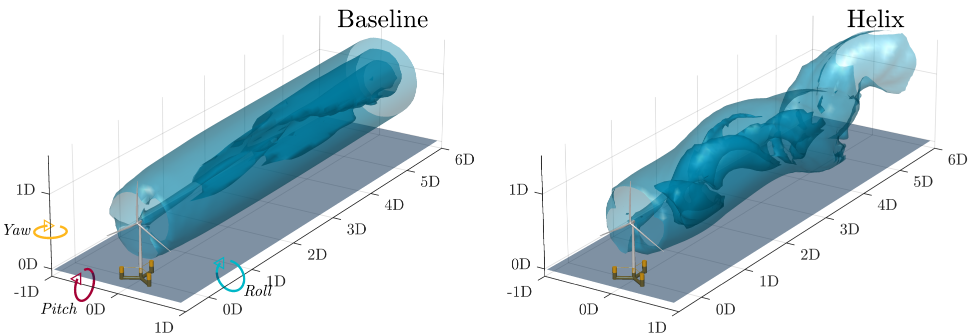

Figure 5.1: Model of the IEA 15MW turbine mounted on the VolturnUS-S floater with the upper figure showing the wake when using a baseline controller and on the lower figure the distorted wake when the Helix method is enabled.

Here, we focus on dynamic control of the *individual* blade pitch, often referred to as the Helix method [44, 111]. The Helix method imposes sinusoids on the blade pitch actuators, displacing the resulting thrust vector out of the centre of the rotor, creating a helix-shaped wake. This, in turn, results in time-varying tilt and yaw moments being applied to the turbine. Figure 5.1 shows the IEA 15MW [169] turbine mounted on the VolturnUS-S foundation [128]. The upper figure shows the wake when the turbine is using baseline control and the lower figure when using Helix control. Floating turbines mounted on a semi-submersible foundation, like the VolturnUS-S, were found to have a natural frequency in the yaw motion near the actuation frequency of the Helix method, resulting in significant yaw motion when excited near or at that frequency [74, 161, 172].

The frequency at which the Helix is applied is typically characterised by the Strouhal number

$$St = \frac{f_e D}{U_\infty}, \tag{5.1}$$

where f_e is the actuation frequency in Hz, D is the rotor diameter in m, and U_∞ is the free stream wind speed in m/s. The frequency at which the Helix is most effective is found to be consistent for different-sized turbines and lies between $St = 0.20$ and $St = 0.40$ when considering two fully aligned turbines spaced a distance of 5 rotor diameter (often referred to as '5D') apart [119, 120, 124]. The dynamics of a typical floating turbine using the Helix control method are shown in Figure 5.2 as a frequency response curve that quantifies what roll, pitch and yaw angle is achieved by applying the Helix method with a blade pitch amplitude of 1 degree. Supplement 1 provides greater detail on the identification experiments and compares the dynamics of different floating turbines. At its eigenfrequency of approximately $St = 0.30$, every degree of blade pitch results in approximately 2.5° yaw angle.

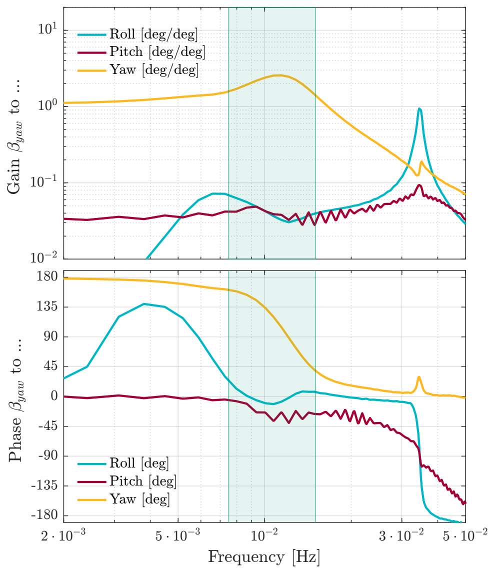

Figure 5.2: Turbine roll (blue line), pitch (red line) and yaw (yellow line) are characterised by their magnitude (top) and phase shift (bottom) with respect to blade pitch input, as a function of Helix excitation frequency. The green shaded area indicates the frequency range St = [0.20, 0.40].

This implies that a typical 4° blade pitch angle input leads to turbine yaw angles similar to those used for wake steering, albeit in a time-varying fashion. However, a small change in actuation frequency close to the eigenfrequency greatly affects the phase of the yaw motion. Using a first-of-its-kind experimental setup to study the three-dimensional wake aerodynamics, we show that carefully controlling the phase of a floating turbine's yaw provides a means to mitigate the negative wake effects on nearby turbines improving the effectiveness of the Helix wake mixing method.

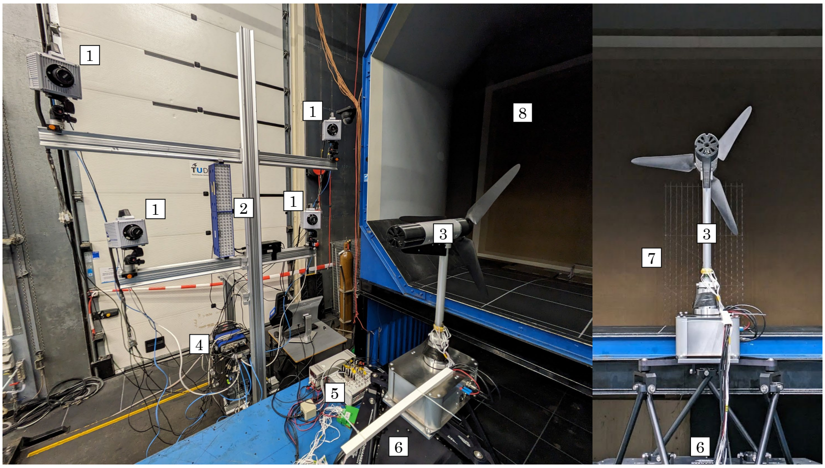

Figure 5.3: PIV setup consisting of $\boxed{1}$ four Photron FASTCAM SA1.1 high-speed cameras, $\boxed{2}$ two LaVision LED lights used to illuminate the HFSBs, $\boxed{3}$ the MoWiTO-0.6 turbine, $\boxed{4}$ a LaVision PTU-X timing unit used to synchronise the four cameras and LEDs, $\boxed{5}$ dSpace MicroLabBox used for control and data acquisition, $\boxed{6}$ the Quansar Hexapod, $\boxed{7}$ the seeding rig from which the HFSBs are released into the flow coming from, $\boxed{8}$, the Open Jet Facility.

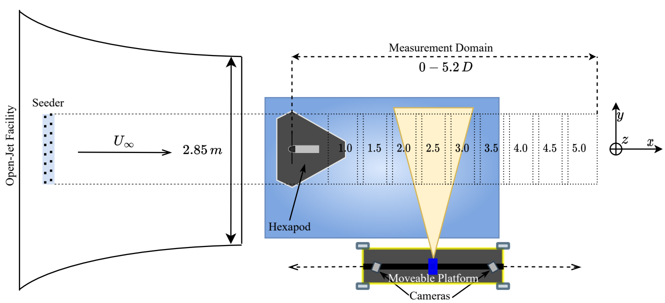

Figure 5.4: Schematic representation of the setup. The camera setup is mounted on a multi-axis linear actuator to allow movement along the x-axis.

5.2 Wind Tunnel Experiments

We provide first evidence of the impact from a changing phase offset by using wind tunnel experiments which combine a hardware-in-the-loop setup and tomographic particle image velocimetry (PIV) to represent and measure the turbine dynamics, the coupled hydrodynamics and the resulting aerodynamics. The floating turbine is modelled using a scaled turbine [173], capable of applying the Helix method, which is mounted on a hexapod. The yaw motion is imposed on the hexapod, with the imposed motion being representative of an actual floating turbine applying the Helix method. The scaled inputs are derived from the dynamics shown in Figure 5.2. The impact of the yaw motion at different phase offsets is quantified by analysing the wind speed in the wake. Tomographic PIV using neutrally buoyant helium-filled soap bubbles (HFSBs) is used to visualise the wake.

The setup is shown in Figure 5.4 and an overview of all investigated cases is presented in Table 5.1. For the cases with platform yaw motion, $\Delta\phi$ denotes the phase offset. The measurement domain spans a distance of 4 rotor diameters, from D to $5D$ behind the turbine in steps of $0.5D$. Each measurement spans 400 mm in the x-direction and 800 mm in both the y- and z-directions. Since the width of a single measurement volume is larger than $0.5D$ there exists a small overlap between every measurement which aids with post-processing. Further details on the post-processing can be found in the Methods section. Based on these measurements, the full three-dimensional wake can be reconstructed, enabling analysis of the interaction between the yaw motion of the floating turbine and the Helix wake mixing method. Using the PIV data, wake recovery as quantified by the wake velocity can be analysed. Furthermore, the same PIV data can also be used to analyse the behaviour of the wake, providing insight into the aerodynamic processes that occur behind the actuated turbine. Note that for these experiments a single actuation frequency was chosen to limit the number of individual measurements.

Table 5.1: Overview of measurement scenarios.

Case name	St	**Blade pitch Amp.**	**Yaw amplitude**	**Phase offset**
Baseline (no Helix)	0.00	0.0°	Not applicable	Not applicable
Helix Bottom-Fixed	0.27	$\pm 2.0^\circ$	Not applicable	Not applicable
Helix $\Delta\phi = 0^\circ$	0.27	$\pm 2.0^\circ$	$\pm 5.0^\circ$	0°
Helix $\Delta\phi = 90^\circ$	0.27	$\pm 2.0^\circ$	$\pm 5.0^\circ$	$+90^\circ$
Helix $\Delta\phi = 180^\circ$	0.27	$\pm 2.0^\circ$	$\pm 5.0^\circ$	$+180^\circ$
Helix $\Delta\phi = 270^\circ$	0.27	$\pm 2.0^\circ$	$\pm 5.0^\circ$	$+270^\circ$

An example of the results obtained during the measurement campaign is shown in Figure 5.5. The wind speed is shown as velocity slices in the $x-z$ (left column) and $x-y$ planes (right column). Prominent vortex structures in the wake, typically tip and hub vortices, are visualised using three-dimensional iso-surfaces of the Q-criterion [174, 175]. Comparing the baseline case with any of the Helix cases reveals distinct differences in wake dynamics. Where the baseline wake remains stable up to a distance of $4-4.5D$ from the turbine, the tip vortex structures are severely disturbed when the Helix is enabled. Furthermore, the wake is also dynamically deflected due to the Helix. Comparing the 5 Helix cases, we find that when the Helix input and yaw motion are in phase ($\Delta\phi = 0$), the

5

wake deflection is enhanced. In contrast, when they are 180° out-of-phase, the deflection is reduced. The structure of the tip vortices is also noticeably different when the platform is yawing. For the 180° out-of-phase case they are significantly deformed compared to the Helix case.

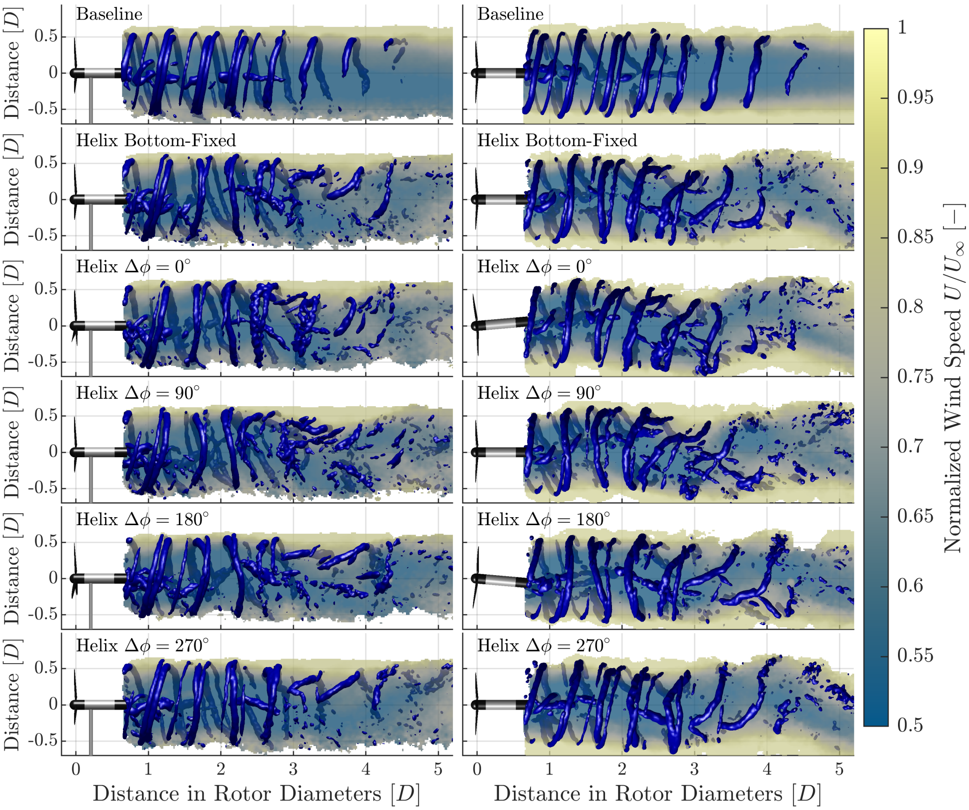

Figure 5.5: Reconstructed side view (left column: $x-z$ plane, $y=0$) and top view (right column: $x-y$ plane, $z=0$) streamwise wind speed slices and Q-criterion, represented by the blue iso-surfaces. For all cases, the data is taken halfway through a phase-averaged cycle.

The effectiveness of a wake-mixing technique can be quantified by measuring the wind speed directly behind the turbine. Figure 5.6 shows the wind speed, normalised by the inflow velocity, a hypothetical second turbine would experience when it is operating downstream of the first turbine. All cases show that the wake is recovering as it propagates downstream as indicated by the increasing wind speeds. The increased mixing induced by the Helix method leads to an increased wind speed at the end of the domain compared to the baseline case. This gain of 6.6% in wind speed can be equated to an increase of 21% in the power available in the flow a downstream turbine can potentially extract. Furthermore, when the platform is yawing in phase with the Helix input, an additional gain of 3.6% in wind speed is achieved which translates into an increased power gain of 12% in the flow. When the yaw motion is 180° out-of-phase, the gain in wind speed is reduced by

2.4%, equating to a loss of 7% in terms of kinetic energy the wake. An increase in wind

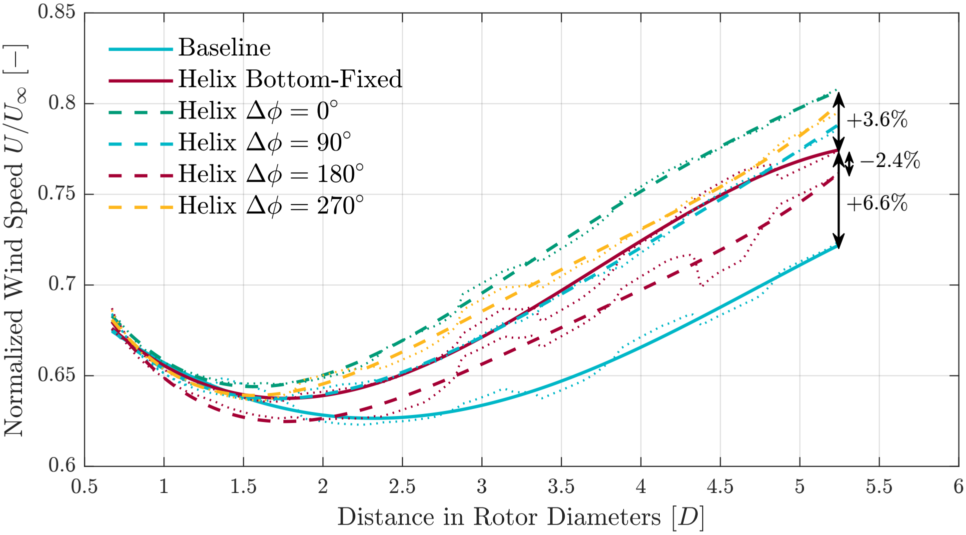

Figure 5.6: Rotor-average wind speed as perceived by a hypothetical downstream turbine in the wake. The thin dotted lines show the results as measured per individual measurement domain. The solid and dashed lines show a fourth-order polynomial fitted to the data.

speed equates to an increase in the kinetic energy of the wake. This energy is entrained from outside the wake boundary. This flux of kinetic energy is dominated by the Reynolds shear stresses [176, 177]. Figure 5.7 shows the method and results for the energy advection calculation in the radial direction over a control volume. This volume, whose boundaries are defined by the rotor surface, is schematically depicted in Figure 5.7. Since the hexapod leaves a wind shadow below the wake, the bottom part of the wake is not considered for this analysis.

The energy advection results confirm the wind speed findings, i.e., when the platform is yawing in phase with the Helix input energy advection is increased compared to the Helix case. When the yaw motion is 180° out-of-phase, the opposite holds. Furthermore, after a distance of three rotor diameters, energy advection becomes constant, and the differences between the individual Helix cases become smaller. From Figure 5.5, it can be seen that this is, on average, also the distance where the tip vortex structures start to dissolve. Hence, the gain in wind speed, due to increased energy advection happens mainly in the area where the wake still is shielded from the ambient flow by the tip vortices and the mixing process has not fully started. The cumulative results, the total energy entrained into the wake up to that point, support the finding that the in-phase case gains the most energy in the initial part of the wake.

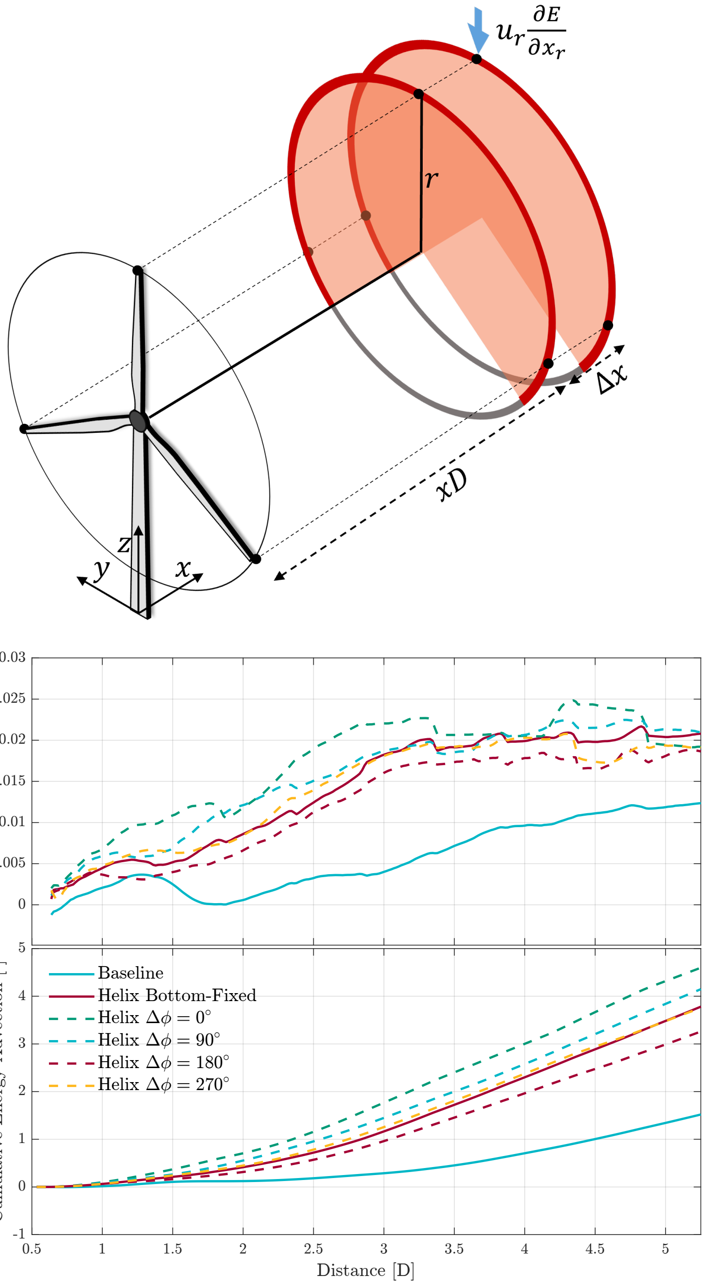

Figure 5.7: (a) Schematics of the energy advection calculation in the radial direction over a control volume. We consider a ring (bright red) of radius r located a distance of xD from the turbine, over which the energy advection is calculated per downstream distance Δx. (b) Local (top) and cumulative (bottom) results of the energy advection analysis using the phase averaged data.

Studying the behaviour of the hub and tip vortices provides insight into the differences between the Helix method and the cases where the platform is yawing in and 180° out of phase. Figure 5.8 shows the tip vortices, visualised using iso-surfaces of the Q-criterion, and the location of the hub vortex indicated by red circles. The latter is traced using a Gaussian convolution method [178, 179]. The left column shows the Helix at 4 different time instances T within one cycle T_p of the Helix excitation. The hub vortex starts to diverge from the centre at a distance of $2D$, interacting with the tip vortices at $3D$. Compared to the in-phase case (middle column) this behaviour is amplified when the turbine is yawing. The wake displacement is increased without altering the tip vortex structure until it starts to interact with the hub vortex. When the yawing is out-of-phase, the tip vortices are significantly more deformed and the curvature introduced by the Helix is reduced.

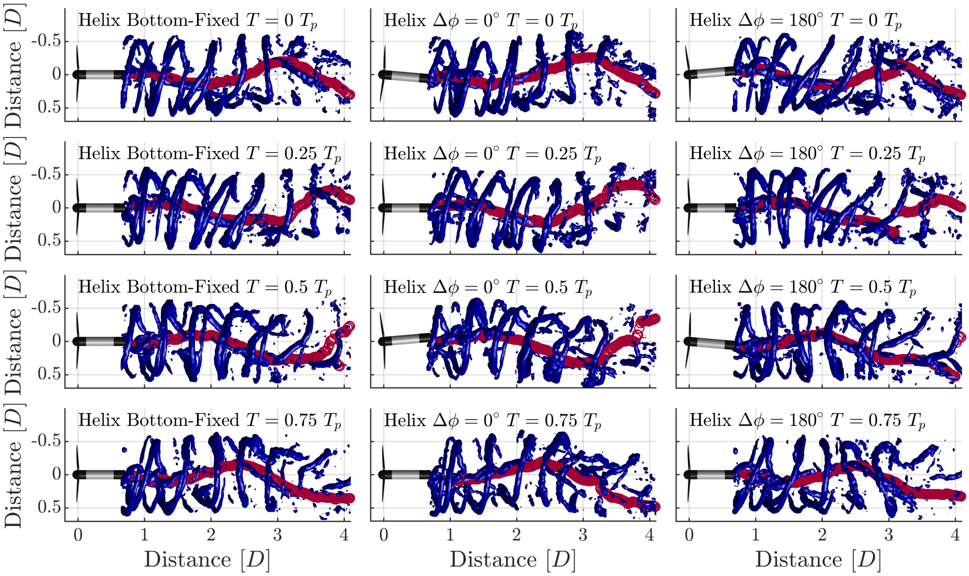

Figure 5.8: Instantaneous tip vortices and hub vortex location for the Helix case (left column), Helix case with in-phase yaw motion (middle column) and Helix case with 180° out-of-phase yaw motion (right column).

Figure 5.9 shows the average radial distance for the tip and hub vortices with respect to the nacelle. As this value is calculated for exactly one cycle of the Helix and then averaged, the displacement of the wake as a whole is filtered out of the measurement. As such, the differences in the radial distance as shown in Figure 5.9 stem from a difference in the interaction between the Helix method and the dynamic yaw motion. Especially for the Helix case with in-phase yaw motion, the tip and hub vortex approach each other the fastest, followed by the Helix method and then the 180° out-of-phase yaw case. Moreover, when the hub and tip vortex are at the same radial distance they interact and collapse, a phenomenon also referred to as (near) wake breakdown. This accelerated encroachment of the tip and hub vortex can be an explanation of the enhanced (reduced) energy advection shown in Figure 5.7 when the platform is yawing in phase (180° out-of-phase) with the Helix method.

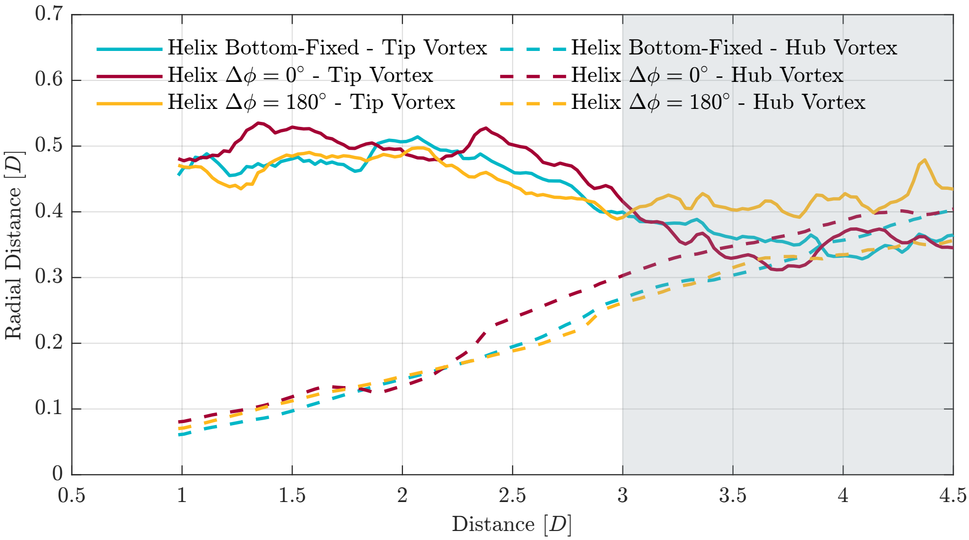

Figure 5.9: Streamwise evolution of the averaged radial position for both tip and hub vortices with respect to the center of the wake. The grey shaded area indicates the area in which wake breakdown is observed in the PIV data.

5.3 Conclusion

This work demonstrates how the dynamics of a floating turbine interact with that of the Helix wake mixing method. The presence of a natural frequency in the yaw motion for certain types of foundations can lead to different phase couplings between control input and floating turbine dynamics. By experimentally analysing the 3D wakes and aerodynamics of a floating turbine model, we find that actuating the Helix at a frequency such that the yaw motion is in-phase results in a significantly better wake recovery than when the turbine yaws 180° out of phase. Analysing the energy advection into the wake indicates that for the in-phase case, significantly more energy is transferred into the wake between a distance of 1 to 3 rotor diameters downstream. A significant reduction is found for the 180° out-of-phase case.

Using the volumetric PIV measurements allows us to visualise the location of the tip and hub vortices, revealing that the dynamic interaction between the two is influenced by the platform yaw motion. The earlier interaction between the tip and hub vortex leads to an earlier breakdown of the wake, accelerating the energy advection into the wake. When yawing at 180° out of phase, this interaction is both reduced and delayed, explaining the reduced effectiveness of the wake mixing method.

This work shows that the dynamics of a floating turbine can be effectively used to enhance the performance of wake mixing controllers. These outcomes can be used to design floating turbines that optimise both control and turbine design, a process called control co-design. This will significantly contribute to the development and deployment of advanced ‘smart’ floating wind farms.

5.4 Methods

The methods section is a special section within Nature (Energy) publications in which there is room to elaborate on the methods used to produce the results in the main work. These sections come after the conclusion, hence in this thesis, are also placed after the conclusion.

Helix wake mixing method. The Helix wake mixing method is an individual pitch control method derived from a control scheme designed for load reduction often referred to as IPC [115, 116]. This control method aims to minimise the turbine loads to increase the turbine's lifetime. The loads on the blades are dependent on the rotational position of the rotor, hence, blade loads are measured within a rotating frame of reference. Using a coordinate transformation these can be translated into loads defined in the fixed-frame making. For wind turbines, the multi-blade-coordinate transformation (MBC) [118] is used to translate bending moments on the individual blades to yaw and tilting moments acting upon the turbine. The Helix wake mixing method is applied in an open loop control scheme by setting sinusoidal input signals to the fixed-frame blade pitch angles. Using the MBC transformation these are transformed into a time-varying individual blade pitch signal that gets applied to the turbine:

$$\begin{bmatrix} \beta_{col}(t) \\ \beta_{tilt}(t) \\ \beta_{yaw}(t) \end{bmatrix} = \frac{2}{3} \begin{bmatrix} 0.5 & 0.5 & 0.5 \\ \cos(\psi_1(t)) & \cos(\psi_2(t)) & \cos(\psi_3(t)) \\ \sin(\psi_1(t)) & \sin(\psi_2(t)) & \sin(\psi_3(t)) \end{bmatrix} \begin{bmatrix} \beta_1(t) \\ \beta_2(t) \\ \beta_3(t) \end{bmatrix}, \tag{5.2}$$

where ψ_i is the azimuth angle of the blade, and β_{col}, β_{tilt} and β_{yaw} are the fixed-frame pitch angles with the subscript col referring to the mean pitch angle of all three blades. These inputs are transformed into the individual blade pitch angles β_i, with $i \in [1, 2, 3]$ using a rotation matrix dependent on the azimuth angle of the turbine. The time-varying pitch angles create time-varying out-of-plane bending moments $M_{y,i}$ which can be transformed back into fixed frame moments using the inverse MBC transformation:

$$\begin{bmatrix} M_{y,1}(t) \\ M_{y,2}(t) \\ M_{y,3}(t) \end{bmatrix} = \begin{bmatrix} 1 & \cos(\psi_1(t)) & \sin(\psi_1(t)) \\ 1 & \cos(\psi_2(t)) & \sin(\psi_2(t)) \\ 1 & \cos(\psi_3(t)) & \sin(\psi_3(t)) \end{bmatrix} \begin{bmatrix} M_{col}(t) \\ M_{tilt}(t) \\ M_{yaw}(t) \end{bmatrix}, \tag{5.3}$$

where M_{col}, M_{tilt} and M_{yaw} are the fixed-frame moments with the subscript col referring to the collective moment of the turbine. With the Helix method M_{tilt} and M_{yaw} are varied in a sinusoidal manner, with one signal being phase-shifted by 90° to the other. An interpretation of this input is that it moves the thrust vector off-centre and in a circular motion of the rotor plane leading to the helical shape in the wake.

Experimental setup. The experiments were carried out at the Open Jet Facility of the Delft University of Technology. This is an open jet, closed-circuit wind tunnel with a width and height of 2.85 m. All experiments were run at a constant wind tunnel velocity of $U_\infty = 5$ m/s. The turbulence intensity inside the jet was within the range of 0.5−2%, which was primarily due to the presence of the PIV seeding rake that ejects the helium soap bubbles into the flow [119].

A modified version of the MoWiTO-0.6 turbine [119, 173] with a rotor diameter of $D = 0.58$ m was used. The turbine was mounted on top of a Quanser hexapod [180], allowing motion in six degrees of freedom. Both turbine and hexapod were connected to a dSpace MicroLabBox, enabling real-time control and data transferral between the turbine and hexapod at a sampling rate of $f = 2$ kHz. Once the hexapod was calibrated and zeroed, each of the six degrees of freedom could be controlled and synchronised to the blade pitch input of the wind turbine.

Figure 5.4 shows the experimental setup. The wake behind the turbine was visualised by neutrally buoyant helium-filled soap bubbles (HFSBs) [181] which were ejected into the flow by a seeding rake with dimensions of 2 m by 1 m. The HFSBs were illuminated from the side using two LaVision LEDs, enabling them to be used as tracers for flow reconstruction. Four Photron FASTCAM SA1.1 high-speed cameras were used to record the wake at 500 frames per second at a resolution of 1024×1024 pixels. A multi-axis linear actuator moved the PIV setup downstream of the turbine to measure multiple sections of the wake.

For the experiments, a zero-degree pitch angle was defined as the position of the blades when they are set perpendicular to the incoming flow. The maximum power coefficient (C_p) was found to be $C_p = 0.20$, which was achieved at a pitch angle of $\theta = 9^\circ$. For every experiment, this is also the mean pitch angle around which the Helix method was implemented. The turbine was controlled using a PI controller on the generator torque to control rotor speed. With $U_\infty = 5$, we adjusted the rotor speed f_r such that the optimal tip-speed-ratio $\lambda = \omega_r D/2U_\infty = 5$ was achieved, with ω_r is the rotor speed in rad/s. This yielded $f_r \approx 13.7$ revolutions per second.

Post processing. Each PIV measurement consisted of 10 seconds of raw camera footage. The flow tracers were reconstructed using the Shake-The-Box algorithm [182] with LaVision's DAVIS 10 software. On average, each frame consisted of 10,000 reconstructed particles within the measurement volume. After the particle reconstruction, a dataset for all time steps of three-dimensional particle positions and velocities is obtained. For the wake analysis, the particles were spatially averaged to a Cartesian grid over smaller sub-volumes with a Gaussian weighing function.

We used two cell volumes: $40 \times 40 \times 40$ mm^3 to analyse tip vortex behaviour, and $60 \times 60 \times 60$ mm^3 to calculate more general wake properties such as wind speed and energy advection. A 75% overlap between volumes was chosen to have smooth transitions between subsequent volumes, resulting in a grid spacing of 10 mm and 15 mm, respectively.

Time-averaged velocity fields were acquired by binning the particles from all time steps following the previously described averaging process. To obtain time-varying flow fields, the particles from each time step can be binned separately. However, insufficient particles in parts of the volume can result in gaps in the flow fields. By averaging the particles for specific phases based on turbine measurements, such as the rotor azimuth position ψ, the number of particles used in the binning process increases, and the measurement uncertainty is reduced.

In the case of baseline operation, the phase averaging procedure was relatively straightforward. The rotor azimuth position was divided into 12 bins of 30°, and particles were collected into these bins based on the measurement of ψ. Here, we assume that the wake dynamics are sufficiently represented by 12 discrete phase bins. Subsequent averaging for each of these phase bins resulted in consecutive flow fields that show the wake over a single rotor rotation. The Helix method complicates the phase-averaging procedure as the time-varying pitch actuation introduces additional dynamics to the wake that cannot be adequately captured in a single turbine rotation. Since the Helix actuation can be represented by a thrust force vector moving around the rotor plane, we introduced the Helix azimuth ψ_h as an additional phase variable for the binning process [119]. More specifically, the actuation frequency of $St = 0.27$ was selected such that each Helix (and yaw) cycle coincides with 6 rotor rotations, i.e., $f_e/f_r = 6$. Hence, the wake dynamics of the Helix cases are represented by $6 \times 12 = 72$ phase-averaged flow fields, of which a selection is presented in Figures 5.5 and 5.8.

6

Conclusions and Recommendations

Conclusion

When wind turbine controllers developed for bottom-fixed turbines are implemented on floating turbines the performance of the controller can significantly change. This is because the controllers interact with the extra degrees of freedom of a floating turbine. The research in this thesis explores how wake mixing controllers interact with a floating turbine. The primary research question in this thesis was:

> *Can the extra dynamics of a floating turbine be used to enhance dynamic wake mixing techniques and if so can a floating turbine be optimised such that it promotes wake mixing?*

The short answer to this question is: *yes*, it is possible to use floating turbine dynamics to enhance the wake mixing performance, especially for the Helix method. Formulating this answer required a multi-pronged approach. First, this dissertation focuses on characterising the interaction between two dynamic wake mixing techniques, dynamic induction control (or the Pulse method) and dynamic individual pitch control (or the Helix method) and different types of floating turbines which immediately highlights that answering the main research question is quite an intricate problem. The foundations on which floating wind turbines are mounted can have different design targets, resulting in different dynamics.

Chapter 2 investigates the coupling between the Pulse method and a spar-type floating turbine and finds that it excites a coupled platform pitch and surge motion. The same platform, without modifications, has a weak coupling to the Helix method whereas a semi-submersible type floater as investigated in Chapters 3, 4 and 5 displays strong coupling to the Helix method. Both the resulting fore-aft motion for the Pulse method as well as the yaw motion for the Helix was found to be of such magnitude that they have an impact on the effectiveness of the wake mixing techniques, which is also the main finding for the second contribution of this thesis.

The fore-aft motion that is excited by the Pulse method results in time-varying inflow conditions for the floating turbine. The time-varying inflow conditions lead to a time-varying thrust, similar to that applied by the Pulse method. However, as shown in Chapter 2, the Pulse method couples in such a way with the motion that the time-varying thrust from the motion counteracts with the Pulse method, reducing its effectiveness. Using a frequency domain analysis it was shown that at the eigenfrequencies in fore-aft motion, the frequency behaviour of the thrust force variation is that off a notch filter, i.e., reduced peak-to-peak amplitude for the thrust variation.

The Helix method was found to excite an eigenfrequency in yaw motion for semi-submersible type foundations, leading to dynamic yaw misalignments of up to $\pm 10^{\circ}$ depending on the blade pitch angle. Chapter 3 presents a similar investigation to that of Chapter 2 where the coupling is investigated using a frequency analysis. Simulations performed in QBlade are used to examine the effect of this yaw motion on the effectiveness of the Helix method. In Chapter 3, a gain in wind farm power was found when the platform was yawing, however, this gain was found not exactly at the eigenfrequency but at a frequency just before or just after the peak of the eigenfrequency.

Chapter 4 further explores this finding by comparing two different floater types, both altered in such a way that the yaw motion is enhanced. Even though the yaw magnitude of both floating turbines was similar a difference in performance could be found between them. One turbine saw a reduction in wind farm power by up to 2.5% whereas the other achieved a wind farm power uplift of nearly 8%. The main difference between both turbines was the phase coupling between the Helix input and yaw motion. An investigation using computational fluid dynamics simulations with prescribed yaw motion showed that the phase difference influences wind speed recovery. The final contribution of this thesis explores this difference using wind tunnel experiments which are covered in Chapter 5 of this thesis.

The main results of those tests confirm those of Chapter 4: phase offset plays a crucial role in the effectiveness of the Helix wake mixing method. Using a tomographic PIV setup the wake behaviour could be captured and analysed. It was found that when yawing in phase with the Helix method the wake entrains more kinetic energy, leading to enhanced wake recovery. When yawing out of phase the opposite was found. Energy entrainment was reduced compared to the Helix method and the effectiveness of the Helix method was reduced.

Returning to the main research question in this thesis, the work presented shows that the movement of a floating turbine can be excited using a wake mixing method. Furthermore, this movement has an impact on the wake mixing method. If this impact has a positive contribution is dependent on the phase coupling of the wake mixing method to the motion that is excited.

Recommendations

This thesis carries out an in-depth investigation into wake mixing controllers and their interaction with floating turbines. The research predominantly focuses on the types of movement and the interaction with the wake mixing dynamics. However, although the general findings in this work are promising, further improvements could be made to strengthen the work or shed light on topics that have not been investigated in this thesis. For that reason, we make some recommendations directly related to the work presented in the thesis.

Validation of Simulation Suite

All simulation-based results in this thesis come from a single software suite (QBlade). Although the dynamics were verified using OpenFast (not presented in this thesis), there is still a reliance on all the modelling assumptions made within QBlade, and to extend other simulation suites. Ideally, the dynamics of a floating turbine are experimentally verified, either by using a scaled model or full-scale testing. Especially for dynamics such as the eigenfrequency behaviour can be significantly different if all the non-linear dynamics are represented.

Another aspect that requires validation is the wake dynamics. QBlade relies on a free-vortex wake model to model the wake dynamics. Free-vortex models were originally developed to accurately model complex rotor dynamics and as such are capable of accurately representing wake dynamics close to the rotor. However, the accuracy of the free-vortex model diminishes as the wake starts to travel downstream and enters the region where wake mixing effects typically start to dominate the wake behaviour. This loss in accuracy can skew results. Carrying out similar investigations using either established CFD tools or wind tunnel experiments allows for validation of the findings obtained using a free-vortex implementation for the wake.

Investigating the Structural Implications

The loading and lifetime of a floating turbine is an aspect that can be considered equally or even more important when it comes to floating turbine design. It is something that is also disregarded in this thesis but requires attention. A critical aspect of wake mixing that needs to be tackled is the extra loading that the turbine is subjected to when the blades are being pitched. The potential monetary gains from the increase in power production could be significantly diminished if more maintenance is required on the turbine side. Although for the Helix the benefits seem favourable even when taking loading into account [93, 94], it remains very much an open research question.

This work adds a new dimension to the discussions on turbine loading by also dynamically moving the whole floating turbine. Although it can be argued that less actuation from the turbine might be required to achieve a similar level of wake mixing it is not yet understood what the movement means for the turbine's lifetime. For a floating turbine, the connection of the electricity cable is a critical point, and increased movement from the turbine will only put more stress on that part. Furthermore, the mooring lines will also be subjected to significant displacements and thus increased wear and tear.

The main reason for this is that it is difficult to model and predict how certain components will degrade in the challenging conditions turbines are subjected to. Although the majority of edge cases are analysed using pre-determined load cases it remains a statistical analysis based on assumptions and models. To better understand the loading impact coming from both the wake mixing method as well as the floating turbine motion large or full-scale testing is required. Only when these methods are tested for longer periods, and enough data have been gathered, it is possible to properly analyse this trade-off.

A Broader Perspective

The last sentence of the previous section has many interesting implications. When looking at the broader challenge faced with the development of floating wind turbines there is a movement towards co-optimising the control systems and floating turbine design. Rather than designing control systems for an existing system more optimal designs can be obtained when doing control co-design. The work presented in this thesis can be used as an example of how such an approach can lead to overall better-optimised floating wind turbines and subsequent wind farms. The work in this thesis predominantly uses floating wind turbines that have not been altered or when they have been altered it has been a one-sided optimisation. In none of the chapters, both the controller and platform have been optimised in conjunction. Here, however, lies more potential, hence we also make some recommendations for future work. As each chapter has its separate conclusion and recommendations specific to that work the recommendations discussed here can be considered more general.

Co-Design of Floating Wind Turbines

It is clear that with the right phase coupling the effectiveness of the Helix method can be increased. This work investigates 4 different phase offsets, spaced 90 degrees apart. However, further investigations over all different phase offsets are required to find the ideal phase offset. It could well be that between, e.g., 0 and 90 degrees a further gain could be found. This extra coupling to the hydrodynamics through the phase offset also introduces an extra dimension to finding the optimal frequency for the Helix method as the floating turbine dynamics interact with the gain in wind speed due to the Helix method.

This added dimension is a function of the behaviour of a floating turbine, most notably near and at its eigenfrequency. The frequency analysis indicates that this behaviour can be well approximated using a second-order mass-spring-damper system. The ability to parameterise the dynamics of a floating turbine into a linear transfer function enables it to be incorporated into (potentially linear) optimisation problems. In Chapter 5 we show that in phase yaw behaviour of a floating turbine enhances the wake mixing strategy. For these experiments, the yaw amplitude has been kept the same enabling direct comparison between different measurements. However, the yaw amplitude and phase offset are linked, and ensuring in phase yaw behaviour will lead to reduced yaw magnitude given the dynamics near the eigenfrequency. Using an optimisation including the floating turbine yaw stiffness and damping this yaw behaviour can potentially be tuned to have a higher magnitude and the right phase behaviour within the ideal frequency range of the Helix.

Further Investigations of Wake Dynamics

The Helix method is not yet fully understood from the perspective of fluid dynamics. Why exactly it instigates wake maxing is a topic of active research. Wind tunnel experiments as those presented in Chapter 5 can aid in trying to understand which aerodynamic effects are dominant when the Helix method is enabled. More challenging is trying to fully understand and explain the interaction between dynamic yaw and the Helix method, which essentially is happening on a floating wind turbine when yawing under a Helix input. Although we can analyse the behaviour of the wake and quantify differences in behaviour using the PIV data a true explanation of why those differences matter remains elusive. Performing similar experiments within a simulation environment might provide the necessary details required to understand and explain the wake behaviour. Such simulations could also provide valuable insight into the effect of the nacelle-to-blade length ratio. For scaled turbines such as those used in this thesis, this ratio differs significantly from that of a full-sized wind turbine which can influence wind tunnel measurements [183]. Since the interaction between aerodynamic effects from the nacelle and blades seems to be the driving factor behind the Helix method it is important to take this into account when generalising the results.

A further argument to be made for finding such an explanation is one based, again, on controls co-design. Wake mixing methods trigger an instability in the wake structure causing a breakdown and consequent re-energisation. This process is Strouhal (or frequency) dependent, implying there are fundamental dynamics within the wake that can be triggered when excited at the right Strouhal number. Once these dynamics are understood the wake mixing control solution, and potentially floating turbine design, can be altered such that wake mixing is maximised with the least amount of input from the wind turbine.

A note should also be made with regard to the blade aerodynamics of the wind turbine. The Helix method's blade pitch input could lead to undesired effects such as aerodynamic stall. This effect is turbine design-specific and should be taken into account when analysing these kind of dynamic pitch methods.

Towards Large Floating Wind Farms

This work focuses on the interaction between two turbines, but within a wind farm, it can easily happen that more than two turbines interact with each other. Using methods optimised for a two-turbine wind farm might not be ideally suited for larger wind farms. A solution to this is to start coordinating or synchronising the actions between several floating turbines that impact each other. One such example is a synchronized deployment of the Helix method, where the second turbine senses how the first turbine is actuated and synchronises its Helix implementation to that [184].

Alternative approaches, unique to floating wind turbines, might bring further trade-offs in the wind farm flow control problem that can be made to mitigate the turbine-to-turbine interaction. One such example is a trade-off between using a wake mixing method or maybe going for turbine displacement, which is impossible for bottom-fixed turbines. Floating turbines can, to a degree, move from their steady-state position by altering their yaw angle and thrust force thereby enabling the option to dynamically change the layout of a wind farm to a new optimal point. Each solution will have its own set of advantages and disadvantages and the ideal wind farm flow control solution will depend on the current conditions, as well as design decisions made during the conceptualisation of the floating wind farm. What this thesis shows is that during the conceptualisation phase, there is a unique opportunity to co-design optimal control solutions for floating wind farm flow control.

Bibliography

References

[1] United Nations. The Paris Agreement. *Accessed: 13 Aug. 2024*. https://unfccc.int/process-and-meetings/the-paris-agreement.

[2] Taejin Park, Hirofumi Hashimoto, Weile Wang, Bridget Thrasher, Andrew R. Michaelis, Tsengdar Lee, Ian G. Brosnan, and Ramakrishna R. Nemani. What does global land climate look like at 2°c warming? *Earth's Future*, 11(5):e2022EF003330, 2023.

[3] NASA/GISS. Global temperature measurements since 1880. *Accessed: 13 Aug. 2024*. https://climate.nasa.gov/vital-signs/global-temperature/?intent=121.

[4] IPCC. Sections. In: Climate Change 2023: Synthesis Report. Contribution of Working Groups I, II and III to the Sixth Assessment Report of the Intergovernmental Panel on Climate Change [Core Writing Team, H. Lee and J. Romero (eds.)]. IPCC, Geneva, Switzerland, pp. 35-115, doi: 10.59327/IPCC/AR6-9789291691647.

[5] IPCC. Grubb, M., C. Okereke, J. Arima, V. Bosetti, Y. Chen, J. Edmonds, S. Gupta, A. Köberle, S. Kverndokk, A. Malik, L. Sulistiawati, 2022: Introduction and Framing. In IPCC, 2022: Climate Change 2022: Mitigation of Climate Change. Contribution of Working Group III to the Sixth Assessment Report of the Intergovernmental Panel on Climate Change. Cambridge University Press, Cambridge, UK and New York, NY, USA. doi: 10.1017/9781009157926.003.

[6] Hannah Ritchie and Pablo Rosado. "Energy Mix" Published online at OurWorldInData.org. Retrieved from: 'https://ourworldindata.org/energy-mix' [Online Resource] Accessed: 21th Aug. 2024.

[7] Kelly Eurek, Patrick Sullivan, Michael Gleason, Dylan Hettinger, Donna Heimiller, and Anthony Lopez. An improved global wind resource estimate for integrated assessment models. *Energy Economics*, 64:552–567, 2017.

[8] European Network of Transmission System Operators for Electricity. Entso-e statistical factsheet. accessed: 14 aug. 2024. https://www.entsoe.eu/data/power-stats/.

[9] European Comission. European wind power action plan. accessed: 14 aug. 2024. https://eur-lex.europa.eu/legal-content/EN/TXT/?uri=CELEX:52023DC0669.

[10] Lisa-Maria Eitler. Sensation: Österreicher baute bereits vor 140 jahren das erste windrad accessed: 14 aug. 2024. https://www.igwindkraft.at/?mdoc_id=1051715.

[11] Unknown Author. Mr. brush's windmill dynamo. *Accessed: 14 Aug. 2024. Scientific American*, 63:389, 1890.

[12] Giuseppe Costanzo, Guy Brindley, Guy Willems, Lizet Ramirez, Phil Cole, and Vasiliki Klonari. Wind energy in europe – 2023 statistics and the outlook for 2024-2030. https://windeurope.org/intelligence-platform/product/wind-energy-in-europe-2023-statistics-and-the-outlook-for-2024-2030/, February 2024.

[13] European Environment Agency, Share of energy consumption from renewable sources in Europe. https://www.eea.europa.eu/en/analysis/indicators/share-of-energy-consumption-from. Accessed: 19th Aug. 2024.

[14] WindEurope, Immediate actions needed to unblock grid capacity for more wind energy. https://windeurope.org/newsroom/press-releases/immediate-actions-needed-to-unblock-grid-capacity-for-more-wind-energy/. Accessed: 21th Aug. 2024.

[15] Energy Storage Colation. https://energystoragecoalition.eu/the-coalition/. Accessed: 21th Aug. 2024.

[16] S. Batel and D. Rudolph. *A critical approach to the social acceptance of renewable energy infrastructures: Going beyond green growth and sustainability.* Springer International Publishing, 2021.

[17] Claire Haggett Mhairi Aitken and David Rudolph. Practices and rationales of community engagement with wind farms: awareness raising, consultation, empowerment. *Planning Theory & Practice*, 17(4):557–576, 2016.

[18] John Glasson, Bridget Durning, Kellie Welch, and Tokunbo Olorundami. The local socio-economic impacts of offshore wind farms. *Environmental Impact Assessment Review*, 95:106783, 2022.

[19] Albert Betz. Das maximum der theoretisch möglichen ausnützung des windes durch windmotoren. *Zeitschrift für das gesamte Turbinenwesen*, 1920.

[20] Ryan Wiser, Eric Lantz, Trieu Mai, Jose Zayas, Edgar DeMeo, Ed Eugeni, Jessica Lin-Powers, and Richard Tusing. Wind vision: A new era for wind power in the united states. *The Electricity Journal*, 28(9):120–132, 2015.

[21] IEA. Offshore wind outlook 2019, distributed under the CC BY 4.0 license, *Last Accessed: 15-June-2023.* https://www.iea.org/reports/offshore-wind-outlook-2019, 2019.

[22] Charlotte Bay Hasager, Nicolai Gayle Nygaard, Patrick J. H. Volker, Ioanna Karagali, Søren Juhl Andersen, and Jake Badger. Wind farm wake: The 2016 horns rev photo case. *Energies*, 10(3), 2017.

[23] Majid Bastankhah and Fernando Porté-Agel. Experimental and theoretical study of wind turbine wakes in yawed conditions. *Journal of Fluid Mechanics*, 806:506–541, 2016.

[24] Michael F Howland, Sanjiva K Lele, and John O Dabiri. Wind farm power optimization through wake steering. *Proceedings of the National Academy of Sciences*, 116(29):14495–14500, 2019.

[25] R. J. Barthelmie, S. C. Pryor, S. T. Frandsen, K. S. Hansen, J. G. Schepers, K. Rados, W. Schlez, A. Neubert, L. E. Jensen, and S. Neckelmann. Quantifying the impact of wind turbine wakes on power output at offshore wind farms. *Journal of Atmospheric and Oceanic Technology*, 27(8):1302 – 1317, 2010.

[26] Siemens Gamesa now able to actively dictate wind flow at offshore wind locations *Last Accessed: 02-June-2023*. `https://www.siemensgamesa.com/en-int/newsroom/2019/11/191126-siemens-gamesa-wake-adapt-en`, 2022-03-03.

[27] E.on and ge: A power up story *Last Accessed: 25-January-2025*. `https://www.gevernova.com/wind-power/stories/eon-power-up`.

[28] J. Meyers, C. Bottasso, K. Dykes, P. Fleming, P. Gebraad, G. Giebel, T. Göçmen, and J.-W. van Wingerden. Wind farm flow control: prospects and challenges. *Wind Energy Science*, 7(6):2271–2306, 2022.

[29] Daniel R Houck. Review of wake management techniques for wind turbines. *Wind Energy*, 25(2):195–220, 2022.

[30] A. Jiménez, A. Crespo, and E. Migoya. Application of a LES technique to characterize the wake deflection of a wind turbine in yaw. *Wind Energy*, 13:559–572, 2010.

[31] Paul A Fleming, Pieter MO Gebraad, Sang Lee, Jan Willem van Wingerden, Kathryn Johnson, Matt Churchfield, John Michalakes, Philippe Spalart, and Patrick Moriarty. Evaluating techniques for redirecting turbine wakes using SOWFA. *Renewable Energy*, 70:211–218, 2014.

[32] P. M. O. Gebraad, F. W. Teeuwisse, J. W. van Wingerden, P. A. Fleming, S. D. Ruben, J. R. Marden, and L. Y. Pao. Wind plant power optimization through yaw control using a parametric model for wake effects—a CFD simulation study. *Wind Energy*, 19:95–114, 2016.

[33] Paul Fleming, Jennifer Annoni, Jigar J. Shah, Linpeng Wang, Shreyas Ananthan, Zhijun Zhang, Kyle Hutchings, Peng Wang, Weiguo Chen, and Lin Chen. Field test of wake steering at an offshore wind farm. *Wind Energy Science*, 2:229–239, 2017.

[34] Michael F Howland, Jesús Bas Quesada, Juan José Pena Martínez, Felipe Palou Larrañaga, Neeraj Yadav, Jasvipul S Chawla, Varun Sivaram, and John O Dabiri. Collective wind farm operation based on a predictive model increases utility-scale energy production. *Nature Energy*, 7(9):818–827, 2022.

[35] Pieter MO Gebraad, Floris W Teeuwisse, Jan Willem van Wingerden, Paul A Fleming, Shalom D Ruben, Jason R Marden, and Lucy Y Pao. A data-driven model for wind plant power optimization by yaw control. In *2014 American Control Conference*, pages 3128–3134. IEEE, 2014.

[36] M. Becker, B. Ritter, B. Doekemeijer, D. van der Hoek, U. Konigorski, D. Allaerts, and Jan Willem van Wingerden. The revised FLORIDyn model: implementation of heterogeneous flow and the Gaussian wake. *Wind Energy Science*, 7(6):2163–2179, 2022.

[37] Nicolas Kirchner-Bossi and Fernando Porté-Agel. Realistic Wind Farm Layout Optimization through Genetic Algorithms Using a Gaussian Wake Model. *Energies*, 11:3268, 2018.

[38] Jason R. Marden, Shalom D. Ruben, and Lucy Y. Pao. A Model-Free Approach to Wind Farm Control Using Game Theoretic Methods. In *IEEE Transactions on Control Systems Technology*, pages 1207–1214, 2013.

[39] Umberto Ciri, Mario A. Rotea, and Stefano Leonardi. Model-free control of wind farms: A comparative study between individual and coordinated extremum seeking. *Renewable Energy*, 113:1033–1045, 2017.

[40] Daan van der Hoek, Stoyan Kanev, Julian Allin, David Bieniek, and Niko Mittelmeier. Effects of axial induction control on wind farm energy production - A field test. *Renewable Energy*, 140:994–1003, 2019.

[41] Ervin Bossanyi, Renzo Ruisi, Gunner Chr. Larsen, and Mads Mølgaard Pedersen. Axial induction control design for a field test at lillgrund wind farm. *Journal of Physics: Conference Series*, 2265(4):042032, may 2022.

[42] Filippo Campagnolo, Vlaho Petrović, Carlo L Bottasso, and Alessandro Croce. Wind tunnel testing of wake control strategies. In *2016 American Control Conference (ACC)*, pages 513–518. IEEE, 2016.

[43] Wim Munters and Johan Meyers. Towards practical dynamic induction control of wind farms: analysis of optimally controlled wind-farm boundary layers and sinusoidal induction control of first-row turbines. *Wind Energy Science*, 3:409–425, 2018.

[44] Joeri A. Frederik, Bart M. Doekemeijer, Sebastiaan P. Mulders, and Jan Willem van Wingerden. The helix approach: Using dynamic individual pitch control to enhance wake mixing in wind farms. *Wind Energy*, 23(8):1739–1751, 2020.

[45] Jay Goit and Johan Meyers. Optimal control of energy extraction in wind-farm boundary layers. *Journal of Fluid Mechanics*, 768:5–50, 2015.

[46] GEBCO Compilation Group. Accessible through: `doi:10.5285/1c44ce99-0a0d-5f4f-e063-7086abc0ea0f`.

[47] European Commission, EMODnet Human Activities Wind farm map. https://emodnet.ec.europa.eu/en/human-activities. Accessed: 16th Aug. 2024.

[48] WindEurope. Floating Offshore Wind Vision Statement. *Last Accessed: 15-May-2023*. https://windeurope.org/about-wind/reports/floating-vision-statement/, 2017.

[49] D. Fraile, A. Vandenberghe, V. Klonari, L. Ramirez, I. Pienda, P. Tardiue, B. Malvault, and I. Komusanac. Getting fit for 55 and set for 2050. *Published: 08-June-2021*. https://windeurope.org/intelligence-platform/product/getting-fit-for-55-and-set-for-2050/.

[50] James, Rhodri and Costa Ros, Marc. https://www.carbontrust.com/our-work-and-impact/guides-reports-and-tools/floating-offshore-wind-market-technology-review. Carbon Trust: Floating Offshore Wind: Market and Technology Review.

[51] Floating wind is making great strides. *Published: 12-May-2023*. https://windeurope.org/newsroom/news/floating-wind-is-making-great-strides/, 2023.

[52] Aegir Insights. Floating wind foundations: Out of more than 50, which concepts will dominate the market? *Last Accessed: 04-July-2023*. https://www.aegirinsights.com/floating-wind-foundations-out-of-more-than-50-which-concepts-will-dominate-the-market.

[53] Morten Thøtt Andersen. Floating foundations for offshore wind turbines, 2016. PhD supervisor: Professor Søren R.K. Nielsen, Aalborg University Assistant PhD supervisor: Associate Professor Peter B. Frigaard, Aalborg University.

[54] G. J. van der Veen, I. J. Couchman, and R. O. Bowyer. Control of floating wind turbines. In *2012 American Control Conference (ACC)*, pages 3148–3153, June 2012. ISSN: 2378-5861.

[55] David Stockhouse, Mandar Phadnis, Aoife Henry, Nikhar Abbas, Michael Sinner, Manuel Pusch, and Lucy Y Pao. Sink or swim: A tutorial on the control of floating wind turbines. In *2023 American Control Conference (ACC)*, pages 2512–2529. IEEE, 2023.

[56] Herbjørn Haslum, Mathias Marley, Sachin Tejwant Navalkar, Bjørn Skaare, Nico Maljaars, and Haakon S Andersen. Roll–yaw lock: Aerodynamic motion instabilities of floating offshore wind turbines. *Journal of Offshore Mechanics and Arctic Engineering*, 144(4):042002, 2022.

[57] S. F. Rodrigues, R. Teixeira Pinto, M. Soleimanzadeh, Peter A. N. Bosman, and P. Bauer. Wake losses optimization of offshore wind farms with moveable floating wind turbines. *Energy Conversion and Management*, 89:933–941, 2015.

[58] Ali C. Kheirabadi and Ryozo Nagamune. Real-time relocation of floating offshore wind turbine platforms for wind farm efficiency maximization: An assessment of feasibility and steady-state potential. *Ocean Engineering*, 208:107445, 2020.

[59] Timothé Jard and Reda Snaiki. Real-time repositioning of floating wind turbines using model predictive control for position and power regulation. *Wind*, 3(2):131–150, 2023.

[60] E. M. Nanos, C. L. Bottasso, S. Tamaro, D. I. Manolas, and V. A. Riziotis. Vertical wake deflection for floating wind turbines by differential ballast control. *Wind Energy Science*, 7(4):1641–1660, 2022.

[61] European Commission. Information on the REPowerEU initiative. Accessed: 15-May-2023. `https://ec.europa.eu/info/strategy/priorities-2019-2024/european-green-deal/repowereu-affordable-secure-and-sustainable-energy-europe_en`, 2022.

[62] N. L. Panwara, S. C. Kaushikb, and S. Kotharia. Role of renewable energy sources in environmental protection: A review. *Renewable and Sustainable Energy Reviews*, 15:1513–1524, 2011.

[63] I. Komusanac, G. Brindley, D. Fraile, and L. Ramirez. Windeurope annual statistics 2021. *Last Accessed: 05-May-2023.* `https://windeurope.org/intelligence-platform/product/wind-energy-in-europe-2021-statistics-and-the-outlook-for-2022-2026/`, 2021.

[64] L. Ramirez, D. Fraille, and G. Brindley. The European offshore wind industry - key trends and statistics 2020. *Last Accessed: 15-May-2023.* `https://windeurope.org/intelligence-platform/product/offshore-wind-in-europe-key-trends-and-statistics-2020/`, 2020.

[65] R. J. Barthelmie, K. Hansen, S. T. Frandsen, O. Rathmann, J. G. Schepers, W. Schlez, J. Phillips, K. Rados, A. Zervos, E. S. Politis, and P. K. Chaviaropoulos. Modelling and measuring flow and wind turbine wakes in large wind farms offshore. *Wind Energy*, 12(5):431–444, 2009.

[66] R. J. Barthelmie, S. C. Pryor, S. T. Frandsen, K. S. Hansen, J. G. Schepers, K. Rados, W. Schlez, A. Neubert, L. E. Jensen, and S. Neckelmann. Quantifying the Impact of Wind Turbine Wakes on Power Output at Offshore Wind Farms. *Journal of Atmospheric and Oceanic Technology*, 27(8):1302–1317, 2010.

[67] N. O. Jensen. *A note on wind generator interaction.* Number 2411 in Risø-M. Risø National Laboratory, 1983.

[68] G. Mosetti, C. Poloni, and B. Diviacco. Optimization of wind turbine positioning in large windfarms by means of a genetic algorithm. *Wind Engineering and Industrial Aerodynamics*, 51:105–116, 1994.

[69] Erik L. Petersen, Niels G. Mortensen, Lars Landberg, Jørgen Højstrup, and Helmut P. Frank. Wind power meteorology. Part I: climate and turbulence. *Wind Energy*, 1:25–45, 1998.

[70] Paul Fleming, Pieter M. O. Gebraad, Sang Lee, Jan Willem van Wingerden, Kathryn Johnson, Matt Churchfield, John Michalakes, Philippe Spalart, and Patrick Moriarty. Simulation comparison of wake mitigation control strategies for a two-turbine case. *Wind Energy*, 18:2135–2143, 2015.

[71] NREL. FLORIS. *Last Accessed: 05-May-2023*, 2023.

[72] Wim Munters and Johan Meyers. Effect of wind turbine response time on optimal dynamic induction control of wind farms. In *Journal of Physics: Conference Series*, volume 753, page 052007, 2016.

[73] Chenlu Han and Ryozo Nagamune. Platform position control of floating wind turbines using aerodynamic force. *Renewable Energy*, 151:896–907, 2020.

[74] Daniel van den Berg, Delphine De Tavernier, and Jan Willem van Wingerden. Using the Helix Mixing Approach on Floating Offshore Wind Turbines. *Journal of Physics: Conference Series*, 2265:042011, 2022.

[75] David Marten. QBlade. *Last Accessed: 15-May-2023*. `http://www.q-blade.org`, 2022.

[76] J. Gordon Leishman, Mahendra J. Bhagwat, and Ashish Bagai. Free-Vortex Filament Methods for the Analysis of Helicopter Rotor Wakes. *Journal of Aircraft*, 39:759–775, 2002.

[77] J. Gordon Leishman, Mahendra J. Bhagwat, and Shreyas Ananthan. The Vortex Ring State as a Spatially and Temporally Developing Wake Instability. *Journal of the American Helicopter Society*, 49:160–175, 2004.

[78] K. Shaler, E. Branlard, A. Platt, and J. Jonkman. Preliminary Introduction of a Free Vortex Wake Method Into OpenFAST. *Journal of Physics: Conference Series*, 1452:012064, 2020.

[79] D. Marten, C. O. Paschereit, X. Huang, M. Meinke, W. Schröder, J. Müller, and K. Oberleithner. Predicting wind turbine wake breakdown using a free vortex wake code. *AIAA Journal*, 58:4672–4685, 2020.

[80] Steven N. Rodriguez, Justin W. Jaworski, and John G. Michopoulos. Stability of helical vortex structures shed from flexible rotors. *Journal of Fluids and Structures*, 104:103279, 2021.

[81] J Jonkman, S Butterfield, W Musial, and G Scott. Definition of a 5-mw reference wind turbine for offshore system development. 2 2009.

[82] J Jonkman. Definition of the floating system for phase IV of OC3. 5 2010.

[83] Floatech. Floatech project website . *Last Accessed: 22-Dec-2023*. `https://www.floatech-project.com`, 2022.

[84] Shreyas Ananthan and J. Gordon Leishman. Role of Filament Strain in the Free-Vortex Modeling of Rotor Wakes. *Journal of the American Helicopter Society*, 49:176–191, 2004.

[85] Tom Berdowski. *Three-Dimensional Free-Wake Vortex Simulations of an Actuator Disc in Yaw and Tilt.* 2018.

[86] J. Leishman, T. S. Beddoes, and Westland Helicopter Ltd. A Generalised Model for Airfoil Unsteady Aerodynamic Behaviour and Dynamic Stall Using the Indicial Method. Accessed 15-May-2023. Presented at the 42nd. Annual Forum of the American Helicopter Society, 1986.

[87] Ricardo Pereira, Gerard Schepers, and Marilena D. Pavel. Validation of the Beddoes–Leishman dynamic stall model for horizontal axis wind turbines using MEXICO data. *Wind Energy*, 16:207–219, 2013.

[88] Karl Johan Astrom and Richard M. Murray. *Feedback Systems: An Introduction for Scientists and Engineers.* Princeton University Press, USA, 2008.

[89] J. A. Frederik, R. Weber, S. Cacciola, F. Campagnolo, A. Croce, C. Bottasso, and Jan Willem van Wingerden. Periodic dynamic induction control of wind farms: proving the potential in simulations and wind tunnel experiments. *Wind Energy Science*, 5(1):245–257, 2020.

[90] Frank Lemmer, Wei Yu, Kolja Müller, and Po Wen Cheng. Semi-submersible wind turbine hull shape design for a favorable system response behavior. *Marine Structures*, 71:102725, 2020.

[91] Maarten J. van den Broek, Daniel van den Berg, Benjamin Sanderse, and Jan W. van Wingerden. Optimal control for wind turbine wake mixing on floating platforms. *IFAC-PapersOnLine*, 56(2):7656–7661, 2023. 22nd IFAC World Congress.

[92] J M J Journée, W W Massie, and R H M Huijsmans. Offshore Hydromechanics Third Edition. Accessed 15-May-2023, 2015.

[93] Joeri A Frederik and Jan Willem van Wingerden. On the load impact of dynamic wind farm wake mixing strategies. *Renewable Energy*, 194:582–595, 2022.

[94] A. A. W. van Vondelen, S. T. Navalkar, D. R. H. Kerssemakers, and J. W. van Wingerden. Enhanced wake mixing in wind farms using the helix approach: A loads sensitivity study. In *2023 American Control Conference (ACC) In Publication.* IEEE, 2023.

[95] G. Costanzo, G. Brindley, and P. Cole. Wind energy in Europe - 2022 statistics and the outlook for 2023-2027 *Last Accessed: 23-Feb-2024.* `https://windeurope.org/intelligence-platform/product/wind-energy-in-europe-2022-statistics-and-the-outlook-for-2023-2027/`.

[96] L. Ramirez. Offshore wind in Europe - key trends and statistics 2022 *Last Accessed: 23-Feb-2024.* `https://windeurope.org/intelligence-platform/product/offshore-wind-in-europe-key-trends-and-statistics-2022/`.

[97] Paul Veers, Katherine Dykes, Eric Lantz, Stephan Barth, Carlo L. Bottasso, Ola Carlson, Andrew Clifton, Johney Green, Peter Green, Hannele Holttinen, Daniel Laird, Ville Lehtomäki, Julie K. Lundquist, James Manwell, Melinda Marquis, Charles Meneveau, Patrick Moriarty, Xabier Munduate, Michael Muskulus, Jonathan Naughton, Lucy Pao, Joshua Paquette, Joachim Peinke, Amy Robertson, Javier Sanz Rodrigo, Anna Maria Sempreviva, J. Charles Smith, Aidan Tuohy, and Ryan Wiser. Grand challenges in the science of wind energy. *Science*, 366(6464):eaau2027, 2019.

[98] BR Clayton and P Filby. Measured effects of oblique flows and change in blade pitch angle on performance and wake development of model wind turbines. In *Proc 4th BWEA Wind Energy Conference*, 1982.

[99] Tuhfe Göçmen, Paul van der Laan, Pierre-Elouan Réthoré, Alfredo Peña Diaz, Gunner Chr. Larsen, and Søren Ott. Wind turbine wake models developed at the technical university of denmark: A review. *Renewable and Sustainable Energy Reviews*, 60:752–769, 2016.

[100] J. J. Thomas, N. F. Baker, P. Malisani, E. Quaeghebeur, S. Sanchez Perez-Moreno, J. Jasa, C. Bay, F. Tilli, D. Bieniek, N. Robinson, A. P. J. Stanley, W. Holt, and A. Ning. A comparison of eight optimization methods applied to a wind farm layout optimization problem. *Wind Energy Science*, 8(5):865–891, 2023.

[101] A. P. J. Stanley, O. Roberts, J. King, and C. J. Bay. Objective and algorithm considerations when optimizing the number and placement of turbines in a wind power plant. *Wind Energy Science*, 6(5):1143–1167, 2021.

[102] E. Quaeghebeur, R. Bos, and M. B. Zaaijer. Wind farm layout optimization using pseudo-gradients. *Wind Energy Science*, 6(3):815–839, 2021.

[103] Roberto Brogna, Ju Feng, Jens Nørkær Sørensen, Wen Zhong Shen, and Fernando Porté-Agel. A new wake model and comparison of eight algorithms for layout optimization of wind farms in complex terrain. *Applied Energy*, 259:114189, 2020.

[104] P Parkin, Richard Holm, and Davide Medici. The application of PIV to the wake of a wind turbine in yaw. In *Particle Image Velocimetry; Gottingen; 17 September 2001 through 19 September 2001*, pages 155–162, 2001.

[105] Davide Medici. *Experimental studies of wind turbine wakes: power optimisation and meandering*. PhD thesis, KTH, 2005.

[106] Paul A Fleming, Andrew Ning, Pieter MO Gebraad, and Katherine Dykes. Wind plant system engineering through optimization of layout and yaw control. *Wind Energy*, 19(2):329–344, 2016.

[107] A. P. J. Stanley, C. J. Bay, and P. Fleming. Enabling control co-design of the next generation of wind power plants. *Wind Energy Science*, 8(8):1341–1350, 2023.

[108] M. J. van den Broek, D. De Tavernier, P. Hulsman, D. van der Hoek, B. Sanderse, and J.-W. van Wingerden. Free-vortex models for wind turbine wakes under yaw misalignment – a validation study on far-wake effects. *Wind Energy Science*, 8(12):1909–1925, 2023.

[109] Carsten Hein Westergaard. Method for improving large array wind park power performance through active wake manipulation reducing shadow effects, December 2017. US Patent 9,835,138.

[110] Joeri Frederik, Bart Doekemeijer, Sebastiaan Mulders, and Jan Willem van Wingerden. On wind farm wake mixing strategies using dynamic individual pitch control. In *Journal of Physics: Conference Series*, volume 1618, page 022050. IOP Publishing, 2020.

[111] Jan Willem van Wingerden, Bart Matthijs Doekemeijer, and Joeri Alexis Frederik. Enhanced wake mixing for floating wind turbines, 2020. US20220412310A1.

[112] D. van den Berg, D. De Tavernier, and J. W. van Wingerden. The dynamic coupling between the pulse wake mixing strategy and floating wind turbines. *Wind Energy Science*, 8(5):849–864, 2023.

[113] Jan Willem van Wingerden and Daniel van den Berg. Enhanced wake mixing for floating wind turbines, November 17 2022. WO2022240292A1.

[114] David Marten. *QBlade: a modern tool for the aeroelastic simulation of wind turbines.* PhD thesis, Technische Universität Berlin, 2020.

[115] Ervin A Bossanyi. Individual blade pitch control for load reduction. *Wind Energy*, 6(2):119–128, 2003.

[116] Ervin A Bossanyi. Further load reductions with individual pitch control. *Wind Energy*, 8(4):481–485, 2005.

[117] Sebastiaan Paul Mulders, Atindriyo Kusumo Pamososuryo, Gianmarco Emilio Disario, and Jan Willem van Wingerden. Analysis and optimal individual pitch control decoupling by inclusion of an azimuth offset in the multiblade coordinate transformation. *Wind Energy*, 22(3):341–359, 2019.

[118] Gunjit Bir. Multi-Blade Coordinate Transformation and its Application to Wind Turbine Analysis. *46th AIAA Aerospace Sciences Meeting and Exhibit*, 2008.

[119] Daan van der Hoek, Bert Van den Abbeele, Carlos Simao Ferreira, and Jan Willem van Wingerden. Maximizing wind farm power output with the helix approach: Experimental validation and wake analysis using tomographic particle image velocimetry, 2024.

[120] F. V. Mühle, F. M. Heckmeier, F. Campagnolo, and C. Breitsamter. Wind tunnel investigations of an individual pitch control strategy for wind farm power optimization. *Wind Energy Science*, 9(5):1251–1271, 2024.

[121] C Muscari, P Schito, A Viré, A Zasso, D van der Hoek, and J W van Wingerden. Physics informed DMD for periodic Dynamic Induction Control of Wind Farms. *Journal of Physics: Conference Series*, 2265(2):022057, may 2022.

[122] E Taschner, A A W van Vondelen, R Verzijlbergh, and J W van Wingerden. On the performance of the helix wind farm control approach in the conventionally neutral atmospheric boundary layer. *Journal of Physics: Conference Series*, 2505(1):012006, May 2023.

[123] H. Korb, H. Asmuth, and S. Ivanell. The characteristics of helically deflected wind turbine wakes. *Journal of Fluid Mechanics*, 965:A2, 2023.

[124] Marion Coquelet. *Numerical investigation of wind turbine control schemes for load alleviation and wake effects mitigation.* PhD thesis, UCL-Université Catholique de Louvain, 2022.

[125] Johan Meyers and Charles Meneveau. Optimal turbine spacing in fully developed wind farm boundary layers. *Wind Energy*, 15(2):305–317, 2012.

[126] Richard J.A.M. Stevens, Dennice F. Gayme, and Charles Meneveau. Effects of turbine spacing on the power output of extended wind-farms. *Wind Energy*, 19(2):359–370, 2016.

[127] Evan Gaertner, Jennifer Rinker, Latha Sethuraman, Frederik Zahle, Benjamin Anderson, Garrett E Barter, Nikhar J Abbas, Fanzhong Meng, Pietro Bortolotti, Witold Skrzypinski, George N Scott, Roland Feil, Henrik Bredmose, Katherine Dykes, Matthew Shields, Christopher Allen, and Anthony Viselli. IEA wind TCP Task 37: Definition of the IEA 15-Megawatt Offshore Reference Wind Turbine. 3 2020.

[128] Christopher Allen, Anthony Viscelli, Habib Dagher, Andrew Goupee, Evan Gaertner, Nikhar Abbas, Matthew Hall, and Garrett Barter. Definition of the UMaine VolturnUS-S reference platform developed for the IEA Wind 15-Megawatt Offshore Reference Wind Turbine. 7 2020.

[129] David Marten, Matthew Lennie, Georgios Pechlivanoglou, Christian Navid Nayeri, and Christian Oliver Paschereit. Implementation, optimization, and validation of a nonlinear lifting line-free vortex wake module within the wind turbine simulation code qblade. *Journal of Engineering for Gas Turbines and Power*, 138(7):072601, 2016.

[130] Minu Jeon, Soogab Lee, Taeseong Kim, and Seunghoon Lee. Wake influence on dynamic load characteristics of offshore floating wind turbines. *Aiaa Journal*, 54(11):3535–3545, 2016.

[131] Carl R Shapiro, Dennice F Gayme, and Charles Meneveau. Modelling yawed wind turbine wakes: a lifting line approach. *Journal of Fluid Mechanics*, 841:R1, 2018.

[132] M.A. Abdullah, A.H.M. Yatim, C.W. Tan, and R. Saidur. A review of maximum power point tracking algorithms for wind energy systems. *Renewable and Sustainable Energy Reviews*, 16(5):3220–3227, 2012.

[133] Ian R Young. *Wind generated ocean waves.* Elsevier, 1999.

[134] IEC 61400-3-1:2019: Wind energy generation systems - Part 3-1: Design requirements for fixed offshore wind turbines. Standard, International Electrotechnical Commission, Geneva, CH, 2019.

[135] Klaus Hasselmann, Tim P Barnett, E Bouws, H Carlson, David E Cartwright, K Enke, JA Ewing, A Gienapp, DE Hasselmann, P Kruseman, et al. Measurements of wind-wave growth and swell decay during the Joint North Sea Wave Project (JONSWAP). *Ergaenzungsheft zur Deutschen Hydrographischen Zeitschrift, Reihe A*, pages 1–95, 01 1973.

[136] Livia Brandetti and Daniel van den Berg. QBlade 2.0.5.2 Matlab Tutorial, 2023.

[137] E A Bossanyi. The design of closed loop controllers for wind turbines. *Wind Energy*, 3(3):149–163, 2000.

[138] Fabio Crameri, Grace E Shephard, and Philip J Heron. The misuse of colour in science communication. *Nature communications*, 11(1):5444, 2020.

[139] J Jonkman, S Butterfield, W Musial, and G Scott. Definition of a 5-MW reference wind turbine for offshore system development. 2 2009.

[140] Dominic Schröder, Thomas Leweke, Ralf Hörnschemeyer, and Eike Stumpf. Generation of a wingtip vortex pair using a pressure-side fin. *Aerospace Science and Technology*, 130:107860, 2022.

[141] Néstor Ramos-García, Aliza Abraham, Thomas Leweke, and Jens Nørkær Sørensen. Multi-fidelity vortex simulations of rotor flows: Validation against detailed wake measurements. *Computers & Fluids*, 255:105790, 2023.

[142] Hugo Umberto Quaranta, Mattias Brynjell-Rahkola, Thomas Leweke, and Dan S. Henningson. Local and global pairing instabilities of two interlaced helical vortices. *Journal of Fluid Mechanics*, 863:927–955, 2019.

[143] S.E. Widnall. The stability of a helical vortex filament. *J. Fl. Mech.*, 54:641–663, 1972.

[144] B. P. Gupta and R. G. Loewy. Theoretical analysis of the aerodynamic stability of multiple, interdigitated helical vortices. *AIAA*, 12(10):1381–1387, 1974.

[145] M. J. Bhagwat and J. Leishman. Stability, consistency and convergence of numerical algorithms for time-marching free-vortex wake analysis. *J. Am. Helicopter Soc.*, 46:59–70, 2001.

[146] G. Leishman, M. J. Bhagwat, and S. Ananthan. The vortex ring state as a spatially and temporally developing wake instability. *J. Am. Helicopter Soc.*, 49(2):160–175, 2004.

[147] Sasan Sarmast, Reza Dadfar, Robert F. Mikkelsen, Philipp Schlatter, Stefan Ivanell, Jens N. Sørensen, and Dan S. Henningson. Mutual inductance instability of the tip vortices behind a wind turbine. *Journal of Fluid Mechanics*, 755:705–731, 2014.

[148] V. G. Kleine, L. Franceschini, B. S. Carmo, A. Hanifi, and D. S. Henningson. The stability of wakes of floating wind turbines. *Physics of Fluids*, 34(7):074106, 07 2022.

[149] P. H. Alfredsson and J. A. Dahlberg. A preliminary wind tunnel study of windmill wake dispersion in various flow conditions. Technical Report AU-1499, 1979.

[150] L.E.M. Lignarolo, D. Ragni, F. Scarano, C.J. Simão Ferreira, and G.J.W. van Bussel. Tip-vortex instability and turbulent mixing in wind-turbine wakes. *Journal of Fluid Mechanics*, 781:467–493, 2015.

[151] T. Leweke, H.U. Quaranta, H. Bolnot, F.J. Blanco-Rodriquez, and L. Le Dizes. Long- and short-wave instabilities in helical vortices. *Journal of Physics: Conference Series*, (524), 2014.

[152] H. Glauert. The elements of aerofoil and airscrew theory. *The Royal Society*, B144(877):73–93, 1935.

[153] A. Tasora, R. Serban, H. Mazhar, A. Pazouki, D. Melanz, J. Fleischmann, M. Taylor, H. Sugiyama, and D. Negrut. Chrono: An open source multi-physics dynamics engine.

[154] James R. Morison, Martin P. O'Brien, John W. Johnson, and Sanford A. Schaaf. The force exerted by surface waves on piles. *Journal of Petroleum Technology*, 2(05):149–154, 1950.

[155] J. N. Newman. *Marine Hydrodynamics*. The MIT Press, 2nd edition, 1977.

[156] C. M. Lee and J. N. Newman. The WAMIT user manual. 2019. Available online: http://www.wamit.com.

[157] Ruddy Kurnia and Guillaume Ducrozet. NEMOH: Open-source boundary element solver for computation of first- and second-order hydrodynamic loads in the frequency domain. *Preprint available at SSRN*, 2023. DOI: http://dx.doi.org/10.2139/ssrn.4396951.

[158] ANSYS. ANSYS AQWA user's manual. 2021. Available online: https://www.ansys.com/products/structures/aqwa.

[159] M. J. van den Broek, M. Becker, B. Sanderse, and J. W. van Wingerden. Dynamic wind farm flow control using free-vortex wake models. *Wind Energy Science Discussions*, 2023:1–28, 2023.

[160] Frank Lemmer, Wei Yu, Po Wen Cheng, Antonio Pegalajar-Jurado, Michael Borg, Robert Mikkelsen, and Henrik Bredmose. The TripleSpar Campaign: Validation of a Reduced-Order Simulation Model for Floating Wind Turbines. In *Ph.D. Thesis Universität Stuttgart*, 2018.

[161] D.G. van den Berg, Delphine De Tavernier, David Marten, Joseph Saverin, and Jan Willem Van Wingerden. Wake mixing control for floating wind farms: Analysis of the implementation of the helix wake mixing strategy on the iea 15-mw floating

wind turbine. *IEEE Control Systems*, 44(5):81–105, 2024. Green Open Access added to TU Delft Institutional Repository 'You share, we take care!' - Taverne project https://www.openaccess.nl/en/you-share-we-take-care Otherwise as indicated in the copyright section: the publisher is the copyright holder of this work and the author uses the Dutch legislation to make this work public.

[162] Amy Robertson, Jason Jonkman, Marco Masciola, Huimin Song, Andrew Goupee, Alexander Coulling, and C Luan. Definition of the semisubmersible floating system for phase II of OC4. Technical report, National Renewable Energy Lab. (NREL), Golden, CO (United States), 2014.

[163] F. Papi, G. Troise, R. Behrens de Luna, J. Saverin, S. Perez-Becker, D. Marten, M.-L. Ducasse, and A. Bianchini. A code-to-code comparison for floating offshore wind turbine simulation in realistic environmental conditions: Quantifying the impact of modeling fidelity on different substructure concepts. *Wind Energy Science Discussions*, 2023:1–34, 2023.

[164] Christian Bak, Frederik Zahle, Robert Bitsche, Taeseong Kim, Anders Yde, Lars Christian Henriksen, Morten Hartvig Hansen, José Pedro Albergaria Amaral Blasques, Mac Gaunaa, and Anand Natarajan. The DTU 10-MW Reference Wind Turbine, 2013.

[165] Vincent Arnal. *Experimental modelling of a floating wind turbine using a «software-in-the-loop» approach.* PhD thesis, École centrale de Nantes, 2020.

[166] G. Lazzerini, D. Coiro, and G. Troise. Optimization of a floating offshore wind turbine platform and mooring lines according to an innovative wind farm wake control technique. 2023:365–375, 2023.

[167] Klaus Hasselmann et al. Measurements of wind-wave growth and swell decay during the Joint North Sea Wave Project (JONSWAP). *Ergaenzungsheft zur Deutschen Hydrographischen Zeitschrift, Reihe A*, pages 1–95, 01 1973.

[168] Gijs Van der Veen, J. W. van Wingerden, Marco Bergamasco, Marco Lovera, and Michel Verhaegen. Closed-loop subspace identification methods: an overview. *IET Control Theory & Applications*, 7(10):1339–1358, 2013.

[169] Evan Gaertner et al. IEA wind TCP Task 37: Definition of the IEA 15-Megawatt Offshore Reference Wind Turbine. 3 2020.

[170] Eric Simley, Paul Fleming, and Jennifer King. Design and analysis of a wake steering controller with wind direction variability. *Wind Energy Science*, 5(2):451–468, 2020.

[171] Ericka Lozon, Matthew Hall, and Mohammad Youssef Mahfouz. Coupled modeling of wake steering and platform offsets for floating wind arrays. *Journal of Physics: Conference Series*, 2767(6):062035, jun 2024.

[172] Daniel van den Berg, Delphine De Tavernier, Jonas Gutknecht, Axelle Viré, and Jan Willem van Wingerden. The influence of floating turbine dynamics on the helix wake mixing method. *Journal of Physics: Conference Series*, 2767(3):032012, jun 2024.

[173] Jannik Schottler, Agnieszka Hölling, Joachim Peinke, and Michael Hölling. Design and implementation of a controllable model wind turbine for experimental studies. In *Journal of Physics: Conference Series*, volume 753, page 072030. IOP Publishing, 2016.

[174] J. Hunt, Alan Wray, and Parviz Moin. Eddies, streams, and convergence zones in turbulent flows. *Studying Turbulence Using Numerical Simulation Databases*, -1:193–208, 11 1988.

[175] R. Soto-Valle, S. Cioni, S. Bartholomay, M. Manolesos, C. N. Nayeri, A. Bianchini, and C. O. Paschereit. Vortex identification methods applied to wind turbine tip vortices. *Wind Energy Science*, 7(2):585–602, 2022.

[176] W. C. Reynolds and A. K. M. F. Hussain. The mechanics of an organized wave in turbulent shear flow. part 3. theoretical models and comparisons with experiments. *Journal of Fluid Mechanics*, 54(2):263–288, 1972.

[177] Raúl Bayoán Cal, José Lebrón, Luciano Castillo, Hyung Suk Kang, and Charles Meneveau. Experimental study of the horizontally averaged flow structure in a model wind-turbine array boundary layer. *Journal of Renewable and Sustainable Energy*, 2(1):013106, 01 2010.

[178] Nicolas Coudou. *Numerical and experimental investigations of the meandering phenomenon in wind turbine wakes.* PhD thesis, UCL-Université Catholique de Louvain, 2021.

[179] N Coudou, M Moens, Y Marichal, J Van Beeck, L Bricteux, and P Chatelain. Development of wake meandering detection algorithms and their application to large eddy simulations of an isolated wind turbine and a wind farm. *Journal of Physics: Conference Series*, 1037(7):072024, jun 2018.

[180] Quanser hexapod web page. *Accessed: 02-Aug-2024*. `https://www.quanser.com/products/hexapod/`.

[181] Fulvio Scarano, Sina Ghaemi, Giuseppe Carlo Alp Caridi, Johannes Bosbach, Uwe Dierksheide, and Andrea Sciacchitano. On the use of helium-filled soap bubbles for large-scale tomographic PIV in wind tunnel experiments. *Experiments in Fluids*, 56(2), 2 2015.

[182] Daniel Schanz, Sebastian Gesemann, and Andreas Schröder. Shake-the-box: Lagrangian particle tracking at high particle image densities. *Experiments in fluids*, 57:1–27, 2016.

[183] R Amaral, F Houtin-Mongrolle, D Von Terzi, and A Viré. Nacelle modeling considerations for wind turbines using large-eddy simulations. *Journal of Physics: Conference Series*, 2767(5):052056, jun 2024.

[184] AAW Van Vondelen, DC Van Der Hoek, ST Navalkar, and JW Van Wingerden. Synchronized dynamic induction control: An experimental investigation. *Journal of Physics: Conference Series*, 2767(3):032027, jun 2024.

Curriculum Vitæ

Daniel Graham van den Berg

1993	Born on the 7th of November 1993 Zwijndrecht, The Netherlands
2006 - 2012	VWO Degree (Pre-university education) Farelcollege Highschool, Ridderkerk, The Netherlands
2009 - 2012	International Baccalaureate in English Farelcollege Highschool, Ridderkerk, The Netherlands
2012 - 2017	Bachelor of Science in Applied Physics Delft University of Technology, The Netherlands
2017 - 2020	Master of Science in Systems and Control Delft University of Technology, The Netherlands MSc Thesis: *A Lateral Control Solution for Cooperative Vehicle Platooning Applications.*
2020 - 2024	Doctoral degree in Control Engineering Delft University of Technology, The Netherlands Doctoral Thesis: *Characterising the Interaction Between Dynamic Wake Mixing Techniques and Floating Wind Turbines.* Promotor: prof. dr. ir. Jan-Willem van Wingerden Copromotor: dr. ir. Delphine De Tavernier

List of Publications

Conferences and Presentations

1. ***Daniel van den Berg*** *and Jan-Willem van Wingerden*: "Enhanced Wake-Mixing with Floating Offshore Wind Turbines." Oral presentation at the Wind Energy Science Conference 2021. Location: Held Online

2. ***Daniel van den Berg***, *Delphine De Tavernier and Jan-Willem van Wingerden*: "Linearized Free Wake Vortex Model for Optimizing Wake Mixing." Oral presentation at EAWA PhD Seminar 2021. Location: Porto, Portugal

✔ 3. ***Daniel van den Berg***, *Delphine De Tavernier and Jan-Willem van Wingerden*: Using The Helix Mixing Approach On Floating Offshore Wind Turbines. Oral Presentation at the Torque 2022 conference, Location: Delft, The Netherlands

4. ***Daniel van den Berg***, *Delphine De Tavernier and Jan-Willem van Wingerden*: Towards Dynamic Floating Windfarms – Using Platform Motion to Enhance Windfarm Power Generation. Oral Presentation at WindEurope 2022 Special Session: Academia and industry: Synergies to boost floating wind. Location: Bilbao, Spain.

5. ***Daniel van den Berg***, *Delphine De Tavernier and Jan-Willem van Wingerden*: The Dynamic Coupling Between Wake Mixing Techniques and Floating Wind Turbines. Oral presentation at the Wind Energy Science Conference 2023. Location: Glasgow, Scotland (UK).

🗎 ✔ 6. ***Daniel van den Berg***, *Delphine de Tavernier, Jonas Gutknecht, Axelle Viré, Jan-Willem van Wingerden* : The Influence of Floating Turbine Dynamics on the Helix Wake Mixing Method. Oral presentation at the Torque Conference 2024. Location: Florence, Italy.

✔ 7. ***Daniel van den Berg***, *Delphine De Tavernier and Jan-Willem van Wingerden*: $\mathcal{H}_\infty$ Phase Locking Control for Wave Induced Wake Mixing. Oral presentation at the American Control Conference 2024. Location: Toronto, Canada.

✔ 8. *Maarten J. van den Broek*, ***Daniel van den Berg***, *Benjamin Sanderse and Jan-Willem van Wingerden*: Optimal control for wind turbine wake mixing on floating platforms. Oral presentation given by **Maarten J. van den Broek** at the IFAC World Congress 2023. Location: Yokohama, Japan.

🗎 Included in this thesis.
✔ Published in conference proceedings

Journal Publications

1. ***Daniel van den Berg**, Delphine De Tavernier and Jan-Willem van Wingerden*: "The dynamic coupling between the pulse wake mixing strategy and floating wind turbines." Wind Energy Science 8.5 (2023): 849-864.

2. ***Daniel van den Berg**, Delphine De Tavernier, David Marten, Joseph Saverin and Jan-Willem van Wingerden*: Wake Mixing Control for Floating Wind Farms - Analysis of the Implementation of the Helix Wake Mixing Strategy on the IEA 15MW Floating Wind Turbine. In Publication: Control Systems Magazine (2024)

3. ***Daniel van den Berg**, Daan van der Hoek, Delphine De Tavernier, Jonas Gutknecht and Jan-Willem van Wingerden*: Phase-controlling the motion of floating wind turbines to reduce wake interactions. In Review: Nature Communications Engineering (2024)

Further Publications

1. *Jan-Willem van Wingerden and **Daniel van den Berg***: Enhanced wake mixing for floating wind turbines, Technische Universiteit Delft, 2024. U.S. Patent Application 18/560,870.

2. *Livia Brandetti and **Daniel van den Berg***: QBlade Version 2.0.5.2: Matlab Tutorial. Published on the 4TU repository under: `https://doi.org/10.4121/22134710.v2`

3. *Josep Saverin, **Daniel van den Berg**, Sebastian Perez-Becker and Jan-Willem van Wingerden*: FLOATECH Deliverable 4.1: Study on the physics underlying the active wake mixing concept.

4. *Guido Lazzerini, Giancarlo Troise, **Daniel van den Berg** and Jan-Willem van Wingerden*: FLOATECH Deliverable 4.2: Initial design report: wind turbine teether hinge, compliant turbine floater, and wind turbine controllers (baseline and IPC).

5. ***Daniel van den Berg** and Jan-Willem van Wingerden*: FLOATECH Deliverable 4.3: Final design report: integrated design optimization

6. ***Daniel van den Berg** and Jan-Willem van Wingerden*: FLOATECH Deliverable 4.4: Validation report: numerical and experimental

Included in this thesis.